UNIVERSITA' DEGLI STUDI DI NAPOLI "FEDERICO II"

PhD thesis in Industrial Products and Process Engineering
(XXX cycle)

"ENGINEERED HYDROGEL-BASED MATERIALS FOR OLIGONUCLEOTIDE DETECTION"

Ing. Alessia Mazzarotta

Supervisors:
Prof. Dr. Paolo Antonio Netti
Prof. Dr. Filippo Causa

Advisor:
Dr. Edmondo Battista

Coordinator:
Prof. Dr. Giuseppe Mensitieri

2014 – 2017

ENGINEERED HYDROGEL-BASED MATERIALS FOR OLIGONUCLEOTIDE DETECTION

A THESIS SUBMITTED IN PARTIAL FULFILLMENT OF THE REQUIREMENT FOR THE DEGREE OF DOCTOR OF PHILOSOPHY IN

INDUSTRIAL PRODUCTS AND PROCESS ENGINEERING

AUTHOR
Ing. Alessia Mazzarotta

SUPERVISORS
Prof. Dr. P.A. Netti
Prof. Dr. F. Causa

ADVISOR
Dr. Edmondo Battista

COORDINATOR
Prof. Dr. Giuseppe Mensitieri

Table of contents

List of Figures IV
List of Tables VIII
List of Abbreviations IX
Abstract XI

Chapter 1:
Introduction 1

1.1 Hydrogels: principal concepts 2
1.2 Hydrogels for biosensing 3
1.3 Biomarkers detection 5
1.4 Classifications of hydrogels 9
1.5 Hydrogels: synthesis procedure 11
1.6 Chemical an physical hydrogel characterization 15
1.6.1 Swelling behavior 15
1.6.2 Equilibrium swelling theory 17
1.6.3 Solute diffusion within hydrogels 22
1.7 Aim and outline of dissertation 23
1.8 References 25

Chapter 2:
Core-shell microgels: synthesis and swelling characterization..... 33

2.1 Introduction 34
2.2 Experimental section 36
2.2.1 Materials 36

2.2.2 Synthesis of core-shell microgels 36
2.2.3 Microgels characterization 37
2.3 Results and discussion 38
2.3.1 Microgels characterization 38
2.3.2 AFM characterization 42
2.3.3 Swelling characterization 45
2.4 Core-shell applications as biosensor 48
2.5 Conclusions 49
2.6 References 51

Chapter 3:
PEGDA hydrogels as potential engineered-based assay 53

3.1 Introduction 54
3.2 Experimental section 57
3.2.1 Materials 57
3.2.2 Synthesis of bulk-hydrogel 57
3.2.3 Bulk-hydrogel characterizations 60
3.3 Results and discussion 63
3.3.1 Swelling characterization 63
3.3.2 NMR: diffusion studies 64
3.3.3 Preliminary study for the assay 73
3.4 Conclusions 80
3.5 Appendix A 81
3.6 Appendix B 82
3.7 References 84

Chapter 4:
Engineered PEGDA-microparticles by microfluidics: oligonucleotide functionalization for selective miRNA 143-3p detection in serum 87

4.1 Introduction 88
4.1.1 Microfluidic technique 88
4.1.2 Biomarkers detection 91
4.2 Experimental section 93
4.2.1 Materials 93
4.2.2 Synthesis of functionalized microparticles 94
4.2.3 Microparticles characterization 96
4.3 Results and discussion 98
4.3.1 Probe design 98
4.3.2 Microparticles: optimization of microfluidic parameters 100
4.3.3 Microparticles: morphological characterization 102
4.3.4 Microparticles: swelling characterization 103
4.3.5 Diffusion studies: CLSM analysis 106
4.3.6 miRNA 143-3p detection 111
4.4 Conclusions 116
4.5 References 117

Chapter 5:
Conclusions and future perspectives 121

List of Figures

Figure 1.1: Hydrogels with tunable control of mesh size 1

Figure 1.2: Histogram showing the increase in publications related to the keyword "hydrogel" during the past 50 years.. 2

Figure 1.3: Schematic illustration of biosensor. 3

Figure 1.4: Chemical structures of PEG and its di(meth)acrylate. 4

Figure 1.5: Most common biomarkers. 5

Figure 1.6: Compartmentalization of circulating miRNAs. 7

Figure 1.7: Conventional techniques for miRNAs detection. 8

Figure 1.8: Principal enviromental factors affecting hydrogels size. 10

Figure 1.9: Different microfluidic techniques 13

Figure 1.10: A crosslinked hydrogel structure with the main swelling parameters 16

Figure 1.11: Parameters which influence diffusion of probe particles in polymeric media. 23

Figure 2.1: Schematic representation of core-shell microgel synthesis obtained combining precipitation and seeded polymerizations. 39

Figure 2.2: DLS analysis: particle size distribution of R1-core..... 40

Figure 2.3: DLS analysis: particle size distribution of 1st shell R_1PEG. 40

Figure 2.4: DLS analysis: particle size distribution of 2nd shell $R_1F_1AA_{100.}$ 41

Figure 2.5: DLS analysis: Zeta potential distribution of 2nd shell $R_1F_1AA_{100.}$ 41

Figure 2.6: (a) AFM images of second shell microgels in dry, relaxed and swollen state. (b) microgels profile taken in three different direction along one microgel in dry, relaxed and swollen state. 43

Figure 2.7: Swelling ratio calculated in both swollen and relaxed state for microgels (Q_s, Q_r) and their crown (Q_s*, Q_r*) 45

Figure 2.8: Focus on the overlap layer between shells. 46

Figure 2.9: Graphical representation of core double shell with mechanism of miRNA detection..... 49

Figure 3.1: Schematic representation of engineered bulk hydrogels. 55

Figure 3.2: UV free radical photopolymerization..... 58

Figure 3.3: UV free radical photopolymerization between PEGDA and methacrylate oligonucleotide. 59

Figure 3.5: DOSY sequence 62

Figure 3.6: Mesh size values for different bulk-PEGDA concentrations. 64

Figure 3.7: ^{1}H-NMR spectrum of PEGDA/darocur solution before polymerization with signal attribution and related peak integration. 65

Figure 3.8: ^{1}H-NMR spectrum of PEGDA/darocur solution after polymerization. 66

Figure 3.9: 2D DOSY of water in hydrogels bulk with different PEGDA concentrations..... 67

Figure 3.10: Diffusion coefficient versus water content for hydrogels sample.... 68

Figure 3.11: Probe diffusion coefficient as function of its molecular weight. 69

Figure 3.12: Diffusion coefficient of several probes in both water and hydrogels with different PEGDA concentrations. 70

Figure 3.13: Effect of the polymer concentration on the reduction of diffusion coefficients (D/D_0). 71

Figure 3.14: Diffusion coefficients of dextrans probes as function of their hydrodynamic radius obtained in water and PEGDA bulk 72

Figure 3.15: Scheme of oligonucleotide detection. 73

Figure 3.16: Quenching percentage in solution for different oligonucleotide concentrations..... 74

Figure 3.17: ATTO 647 response to UV treatment, with and without darocur in solution. 74

Figure 3.18: Fluorescence intensity of ATTO-BHQ in PEGDA 20% and 10% . . 75

Figure 3.19: Quenching percentage with both complementary (C-BHQ) and several not complementary concentrations (N-BHQ). 76

Figure 3.20: Quenching kinetic in PEGDA 10% with several oligonucleotides concentrations..... 77

Figure 3.21: Quenching kinetic in PEGDA 15% with several oligonucleotides concentrations..... 78

Figure 3.22: Quenching kinetic in PEGDA 20% with several oligonucleotides concentrations..... 79

Figure 4.1: Droplet generation in three microfluidic devices: T-junction, flow focusing and co-flowing geometry..... 89

Figure 4.2: Schematic of flow regimes in T-junction microfluidic devices in both dripping (a) and jetting (b) regime. 90

Figure 4.3: Engineered microparticles for specific target detection. 91

Figure 4.4: Histogram showing the increase in publications related to the keyword "microRNA" during the past 20 years. 91

Figure 4.5: The Droplet Junction Chip and its Chip Interface H for fluidic connection. 94

Figure 4.6: Dolomite chip: geometry and size..... 95

Figure 4.7: Set-up for functionalized microparticles generation. 96

Figure 4.8: New scheme showing the mechanism of miRNA detection based on ds displacement assay. 99

Figure 4.9: Diagram as a function of continuous phase flow rate (Qoil) and capillary number (Ca)..... 101

Figure 4.10: Droplet generation in dripping (a) and jetting (b) regimes. 101

Figure 4.11: Diagram as a function of flow rate ratio (Q_{OIL}/Q_{PEGDA}) and dispersed phase flow rate (Q_{PEGDA}) operating in jetting, dripping and unstable regime..... 102

Figure 4.12: Optical image (a) of monodisperse microparticle and relative particle size distribution (b);(c) SEM image of microparticle. 103

Figure 4.13: Effect of both lamp power and darocur concentration on mesh size of microparticles with PEGDA 15%. 104

Figure 4.14: Mesh size values for different microparticle-PEGDA concentrations..... 105

Figure 4.15: Time lapse of fluorescence intensity (I_{IN}/I_{OUT}) of several probes... 107

Figure 4.16: Dextrans molecular weight as function of its hydrodynamic radii. 108

Figure 4.17: Dextrans partition coefficient as function of hydrodynamic radius. 109

Figure 4.18: Time lapse of fluorescence intensity (I/I_{max}) of several probes..... 109

Figure 4.19: Mechanism of Target detection. 111

Figure 4.20: CLSM images of the three fundamental steps of target identification: (a) T-DNA, (b) adding F-DNA, (c) displacement in presence of the Target..... 113

Figure 4.21: Fluorescence intensity of (a) T-DNA, (b) adding F-DNA, (c) displacement in presence of the Target in buffer solution..... 113

Figure 4.22: Displacement percentage for different Target concentrations. CLSM images of microgels..... 114

Figure 4.23: Fluorescence intensity of (a) T-DNA, (b) adding F-DNA, (c) displacement in presence of the Target in buffer solution and (d) in human serum. 114

Figure 4.24: Bead-based microfluidic assays with fluorescent microparticles ... 115

List of Tables

Table 2.1: Microgel recipes. 37

Table 2.2: Characteristic parameters of microgels 46

Table 2.3: Characteristic parameters of spherical-shell 47

Table 2.4: Volumetric fraction calculated by both mesh size values (χ_ξ) and by volume values (χ_V). 48

Table 3.1: Bulk hydrogels recipes. 60

Table 3.2: Properties of bulk hydrogels of PEGDA 64

Table 3.3: Diffusion coefficients (10^{-10} m^2/s) of water in PEGDA hydrogels. 67

Table 3.4: Diffusion coefficient of different probes in D_2O and respective hydrodynamic radii. 69

Table 3.5: Diffusion coefficient (10^{-10} m^2/s) of water different probes in both water and PEGDA hydrogels. 70

Table 3.6: Sequence and thermodynamic parameters of the DNA probes 73

Table 4.1: Sequence, length and thermodynamic parameters of the DNA probes and RNA targets. 100

Table 4.2: Properties of PEGDA microparticles. 105

Table 4.3: Mesh size of PEGDA (15%w/v) microparticles with different T-DNA concentrations. 105

Table 4.4: Extrapolated values of τ for each probes 110

List of Abbreviations

POCT	Point-Of-Care Testing
PEG	PolyEthylene Glycol
UV	Ultra Violet
DNA	Deoxyribose Nucleic Acid
RNA	Ribose Nucleic Acid
miRNAs	Micro RNA
PCR	Polymerase Chain Reaction
qRT-PCR	Quantitative Reverse Transcriptase-PCR
PDMS	PolyDiMethylSiloxane
W/O	Water in Oil
O/W	Oil in Water
HLB	Hydrophilic-Lipophilic Balance
v_2	Polymer Volume Fraction
$\bar{M}_c$	Molecular weight between crosslinks
ξ	Mesh size
$Q_{r/s}$	Swelling ratio (relaxed/swollen state)
AFM	Atomic Force Microscope
PEGDMA	PolyEthylene Glycol DiMethacrylate
AAc	Acrylic Acid
KPS	Potassium PerSulfate
Fluo	Fluoresceine O-methacrylate
PVA	PolyVinyl Alcohol
Rhod	Methacryloxyethyl thiocarbamoyl rhodamine B

DMSO	Dimethyl Sulfoxide
DLS	Dynamic Light Scattering
Dh	Hydrodinamic Diameter
PEGDA	PolyEthylene Glycol DBSAiAcrylate
NMR	Nuclear Magnetic Resonance
BSA	Bovine Serum Albumin
EWC	Equilibrium Water Content
SR-G	Sulforhodamine G
D_0	Diffusion coefficient in water
D	Diffusion coefficient
Rh	Hydrodinamic Radius
nt	Nucleotide
BHQ	Black Hole Quencher
Ca	Capillary Number
LMO	Light Mineral Oil
SPAN 80	Sorbitan monooleate
TWEEN 20	Polyethylene glycol sorbitan monolaurate
IgG	Anti-Human antibody Immunoglobulin G
CLSM	Confocal Laser Scanning Microscope
SEM	Scanning Electron Microscope
λ_{ex}	Excitation wave length
PBS	Phosphate Buffered Saline
$Q_{Oil/PEGDA}$	Flow rate (continuous/dispersed phase)
d_f	Fractal dimension
k	Partition Coefficient
C_{OUT}	Solute concentration of external solution
C_{IN}	Solute concentration in the gel
I	Fluorescence Intensity

Abstract

Biosensors technology growing attention led to the definition of specifically customizable materials to improve the detection in complex fluids. The main focus of this thesis has been devoted to the design of an advanced hydrogel-based tool, properly designed for several features. The study and control of the hydrogel structure is fundamental to achieve an accurate network that allow the transport of selected target and work as molecular filter excluding bigger molecules and repelling unspecific binding.

In particular, in this thesis, are described the engineering, synthesis and characterization of PEG based hydrogel for oligonucleotide detection. Different methods of synthesis are explored applying tagging and filtration effects. The thesis starts with the description of synthesis and characterization of core-shell microgels with controlled structural properties. Core-shell PEG-based microgels, with a size ranging between 0.5 and 1.3 μm, were obtained by combining precipitation and seeded polymerizations. We demonstrated the possibility of tailoring and controlling the bulk and surface properties. Then a structural characterization was attained calculating polymer volumes fraction from AFM images and combined these with equilibrium swelling theory in order to determine the mesh size of the microgels. In such away, we were able to describe the organizations of the different adlayers, highlighting the possibility of some overlap of the adlayers representing physical barriers at the boundaries of each shell. These multifunctional microgels were used in multiplex assays for their favorable capability to accommodate encoding systems and anchoring groups for probes to capture circulating targets.

In the second part of the work, we described PEGDA bulk hydrogels, synthesized by UV radical photopolymerization and characterized by their swelling parameters.

Results show a mesh size values between 2.6-1.6 nm. Moreover, diffusion studies of several probes with different hydrodynamic radii were accomplished using NMR technique. Results showed that diffusion of small molecules, as sulforhodamine G was not affected by decrease of mesh size values, which, by the contrast, slow down the diffusion of bigger molecules as dextrans. All these characterizations were preliminarily done on bulk hydrogels in order to customize the network to obtain a specific structure and desired final properties. Then same recipes were scaled-down to synthetize microparticles by microfluidic device improving the shape and size control and to reduce both production time and costs. Microparticles so obtained were characterized by swelling parameters showing the same trend of ξ obtained for bulk. Finally, we focused on the probe design to achieve our customized platform for biomarkers detection, in particular for miRNA143-3p which play an important role in the function and formation of the cardiac chamber. Our double strand probe consisted of a short methacrylate DNA-Tail, covalently bound to the polymer networks, and a longer fluorescent DNA sequence. The latter was partially complementary to DNA-Tail and totally complementary to a specific target. Target identification occurred by double strand displacement assay. Using this probe scheme, we included, directly in flow, the capture element of the target to accomplish functionalized particles. Then were characterized in term of their swelling behavior, using confocal light microscopy. Moreover, the CLSM images allowed to evaluate the fluorescence intensity of our hydrogels for each step to determine displacement percentage and efficiency of our detection system. Results showed a 93% of displacement proving the good efficiency of our detection system in both buffer solution and in complex fluids such as the human serum.

To sum up, in this thesis is shown the importance of the choice of materials and their characterization to modulate and predict final properties. In this way, it is possible to synthetize materials with specific features and capture elements to combine both molecular filter capability and target detection. These engineered hydrogels represent in fact a tunable, fast, costless and easy platform for biomarkers detection.

Chapter 1

Introduction

In biosensor field, no-wash assay have been found to be particularly attractive due to their extraordinary potentiality. In fact, these analytical devices represent a new generation assay, easily performed mixing the signal generator probes with the sample solution. Compared with conventional biosensor, the highest advantages of no-wash assay are correlated to their user-friendly and time saving properties, portability and low costs. All these features make them suitable for point-of-care testing (POCT) development.

These biosensors can be developed using different materials and, among these, polymers are the common choice. In particular, hydrogels are suitable for this purpose due to their tunable chemistry and possibility to modulate their network structure.

Therefore, in this work we show the possibility to synthesize functionalized hydrogels with a flexible chemistry, tunable control of the network and specific capture molecules. In such a way, we are able to accomplish a bead-based assay merging both molecular filter and detection capabilities (Figure 1.1).

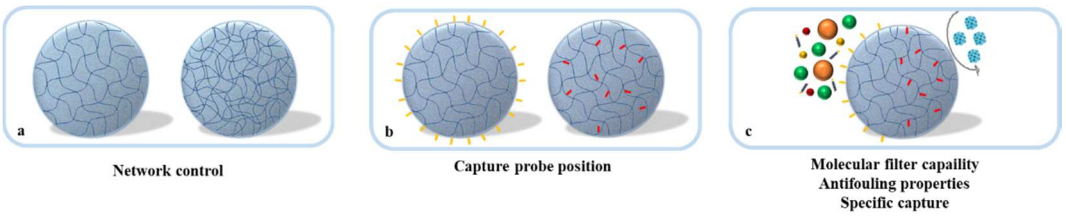

Figure 1.1: Hydrogels with (a) tunable control of mesh size (b) versatile chemistry to allow the conjugation of capture molecule in different position; and (c) molecular filter capability, with antifouling properties and specific capture of a given target.

1.1 Hydrogels: principal concepts

Hydrogels are a class of polymer networks which, due to their hydrophilic nature, may absorb large amount of water[1] and physiological fluids while remaining insoluble in aqueous solutions. The large water content lends them a high flexibility comparable with natural tissue. Due to their good ability in wide range of applications, they are widely studied for the past 50 years[2-3] and there is an increasingly interest of the scientific community on the hydrogel topic (Figure 1.2).

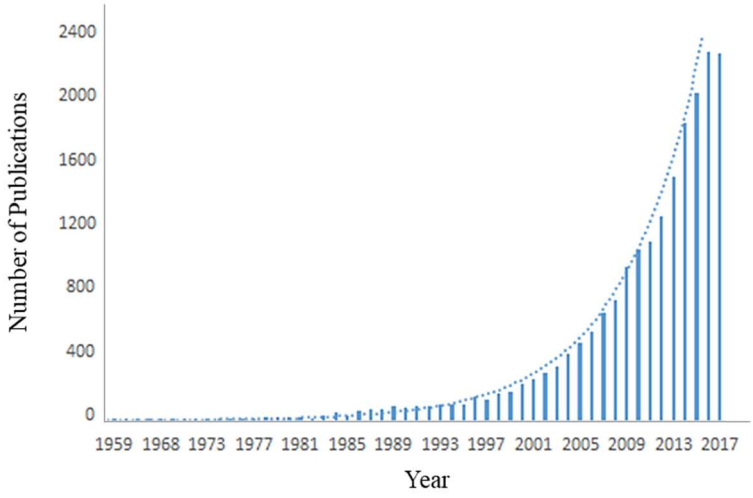

Figure 1.2: Histogram showing the increase in publications related to the keyword "*hydrogel*" during the past 50 years. PubMed data.

In particular, they can be used in several biomedical applications including diagnostic,[4-5] drug delivery,[6-7] tissue engineering[8-9] and pharmaceutical applications.[10] The structure of a hydrogel is usually an elastic and porous mesh where biological molecules can be incorporated or entrapped within. These networks are composed of homopolymers or copolymers, based on the method of preparation. Modifying the density of the network, the mechanical properties of the material and their mesh can be properly modulated to suit specific applications.

Hydrogels are generally characterized by several parameters such as the final capability to absorb liquids (swelling thermodynamics), the rate at which the liquid

is absorbed into their structure (swelling kinetics), as well as their mechanical property in wet or hydrated state (wet strength).

Chemical functionalization of this polymeric hydrogels is widely studied with the aim of adding on the surface or in the network, several molecules as peptide, enzyme or oligonucleotide to allow the detection of different target.[11-13]

1.2 Hydrogels for biosensing

As defined 1999 by the IUPAC, "a biosensor is a self-contained integrated device which is capable of providing specific quantitative or semi-quantitative analytical information using a biological recognition element (biochemical receptor) which is in direct spatial contact with a transducer element. A biosensor should be clearly distinguished from a bioanalytical system, which requires additional processing steps, such as reagent addition. Furthermore, a biosensor should be distinguished from a bioprobe which is either disposable after one measurement, i.e. single use, or unable to continuously monitor the analyte concentration" (Figure 1.3).[14]

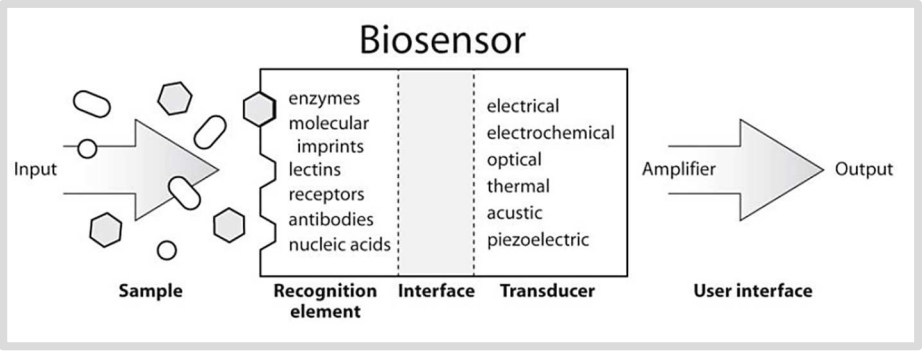

Figure 1.3: Schematic illustration of biosensor.

The first biosensor was described in 1962 by Clark and Lyons who immobilized glucose oxidase (GOD) on an amperometric oxygen electrode surface in order to quantify directly the glucose concentration in a sample.[15-16]

Biosensors represent an advanced platforms for biomarker analysis with the advantages of being easy to use, inexpensive and rapid as well as offering multi-analyte testing capability.[17]

Hydrogels for biosensor can be prepared in aqueous solutions by different synthesis procedure as thermo-initiated[18] or UV[19] radical polymerization. Moreover, adding recognition motifs such as peptides, enzyme or oligonucleotides, is possible to use hydrogels for detection applications. Polymer network and hydrophilic environment allow the diffusion of different molecules through the hydrogel matrix. However, diffusion of larger analytes, such as proteins, can be prevented by an increasing crosslinking density and an appropriate choice of materials.[20]

These biosensors can be developed using different materials. In particular, polymers are widely used and, among these, polyethylene glycol (PEG) hydrogels results to be the suitable monomer to attain low-fouling properties, enhancing the specificity of the capture elements. Moreover, PEG derivatives (Figure 1.4) are extensively adopted for their good solubility in aqueous solution, low-cost production at different molecular weights and chemical functionalities.[21]

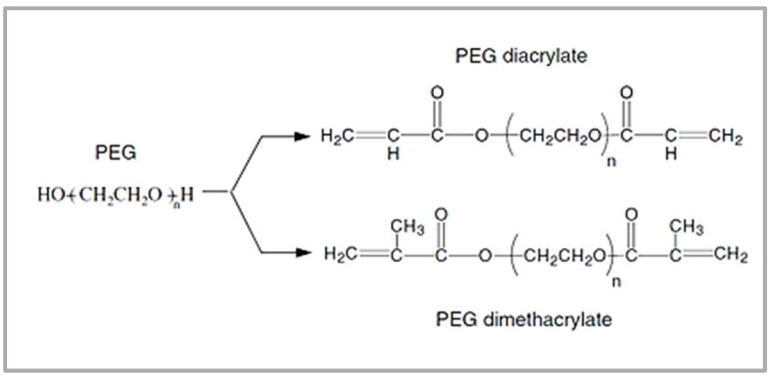

Figure 1.4: Chemical structures of PEG and its di(meth)acrylate.

These materials are usually prepared using the free-radical polymerization of reactive methacrylate PEG derivatives or polyethylene glycol di-acrylates (PEGDA) in the presence of a UV or thermal initiator. The light or temperature induce the

photoinitiator activation generating a benzoyl free radical through a homolytic scission of a C–C bond, subsequently triggering the covalent crosslinking of the gel.

1.3 Biomarkers detection

Biomarkers cover a broad range of biochemical entities, such as proteins, nucleic acids, small metabolites, sugars and tumor cells found in the body fluid (Figure 1.5). They are widely used for risk assessment, diagnosis, prognosis, and for the prediction of treatment efficacy and toxicity.[22-23]

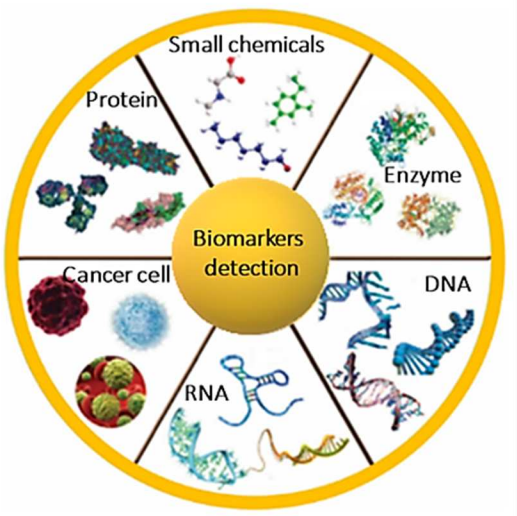

Figure 1.5: Most common biomarkers.

In particular, nucleic acids (DNA and RNA), due to their high specificity, can be amplified to increase abundance in most applications, and can be labelled (for detection) using different approaches, resulting extremely attractive targets for diagnostics. The assessment of both nucleic acid sequence and relative expression level is extremely important for diagnostics applications. In fact, both mutations (changes in nucleic acid sequence) and abundance of nucleic acid target can indicate disease. Their up- or down- regulation is an important indicator for applications like

drug discovery and cancer diagnostics.[24] In biomarkers context, miRNAs have attracted high attention due to their immense regulatory power so that the variation of their levels can be utilized as potential biomarkers for the diagnosis and prognosis of a variety of diseases.[25-29] MicroRNAs (miRNAs) are a class of small non-coding, highly conserved, single stranded RNAs. According to the current database (http://www.mirbase.org), there are total 1881 annotated human miRNA precursor genes that processes 2588 mature miRNAs. Although miRNAs abound in tissues, it has been shown that there are also circulating miRNAs in body fluids such as plasma, urine, saliva, seminal fluid, amniotic fluid, breast milk, bronchial lavage and cerebrospinal fluid.[30] Mature miRNAs are approximately 21 nucleotides in length, with a good stability in a wide range of biological contexts, and play important roles in the development and cellular process with regulatory tasks on the genome expression.[31-33] In addition to these vital processes, miRNAs are implicated in diverse cellular activities, such as immune response,[34] insulin secretion, neurotransmitter synthesis, circadian rhythm,[35] and viral replication. Recent genome-wide analyses have also identified deregulated miRNA expression in human malignancies. MiRNAs can modulate oncogenic or tumor suppressor pathways, whereas miRNAs themselves can be regulated by oncogenes or tumor suppressors.[36] MiRNAs have been reported to associate with a number of pathological conditions of the central nervous system, such as Alzheimer's and Parkinson's.[37] In addition, the roles of miRNAs in the pathological processes of heart, vascular tissue, and blood have been popularly studied. Among these, several researches are focused on the role of miRNAs in cardiovascular pathologies[38-39] such as arrhythmias,[40] fibrosis,[41] pressure overload-induced remodeling,[42] and metabolic disorders.[43] Correlation between disease state and expression level of these circulating species suggest that miRNAs can be strong candidates for the development of non-invasive biomarker screens, for the early and asymptomatic detection of disease and for the monitoring of the treatment response.[44]

Extracellular miRNAs circulating in the blood of both healthy and diseased people showed extreme stability, and resistance to degradation from RNases activity. Most of the circulating miRNAs are well protected from RNases because they can reside in membrane structure of microvesicles such as exosomes, microparticles, and apoptotic bodies.[29]

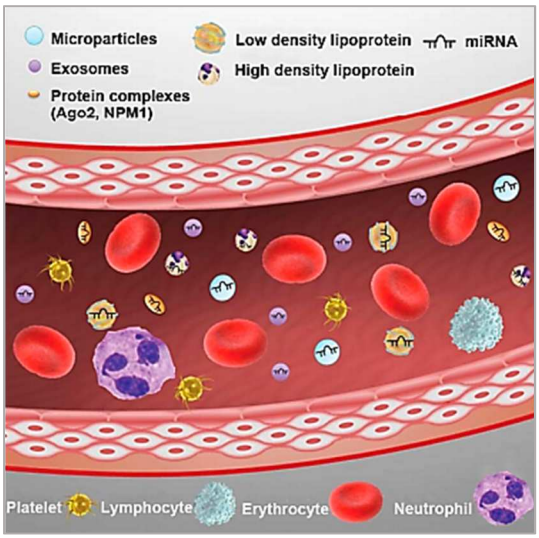

Figure 1.6: Compartmentalization of circulating miRNAs.
Circulating miRNAs are contained within vesicles, in protein complexes, and in lipoprotein complexes. Adapted with permission form Ref [29] Copyright 2013, American Chemical Society.

In any given diagnostic test, the targets must be manipulated, captured, or detected. For a test to be meaningful, it must be specific for the target of interest and sensitive enough to detect entities at physiologically relevant quantities. For this purpose, nucleic acids results an ideal choice due to their intrinsic molecular base pairing ability, offering a high degree of selectivity and stability. Oligonucleotide detection is based on specific hybridization between a probe that is a single-stranded nucleic acid oligonucleotide and the target, the sequence to be detected.

Well-known conventional technologies for the detection of oligonucleotides, based on hybridization to complementary probes, are represented by microarray analysis,[45-46] polymerase chain reaction (PCR, qRT-PCR)[47] and oligonucleotide probes such as molecular beacons[48] and double strands (Figure 1.7).[49]

However, for all these techniques, extraction, amplification, and calibration steps are needed resulting time-consuming. Moreover, preliminary amplification step may compromise the assay accuracy.[17, 30, 47]

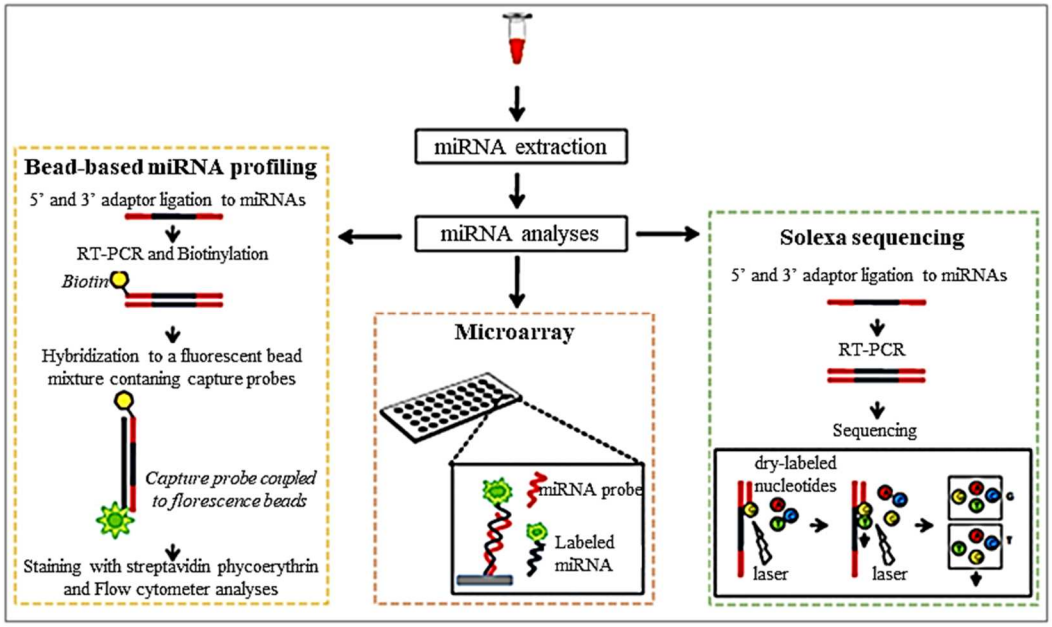

Figure 1.7: Conventional techniques for miRNAs detection.

Novel suspension arrays offer several advantages such as the high flexibility (obtained by simply changing/adding probe particles), enhanced reaction kinetics due to radial diffusion, lower costs and sample consumption and shorter incubation.[50-54] Suspension arrays involving polystyrene beads doped with combinations of dyes for optical coding have been carried out by Luminex.[55] In order to improve the multiplexed readout, suspension array technologies with barcodes, silica nanotubes, Au/Ag nano-barcodes, and dot-coded polymer particles have been developed.[53-55] Then, particle-based suspension arrays have been attracting increasing interest for the multiplexed detection of nucleic acids, offering high flexibility, easy probe-set modification, and high degrees of reproducibility.[56]

A direct and absolute quantification of circulating miRNAs in body fluids is particularly needed even though challenges are represented by their small size, high level of sequences homology, demand of high sensitivity and specificity.

1.4 Classifications of hydrogels

The classification of hydrogels depends on many factors such as their physical properties, nature of swelling, method of preparation, ionic charges, and nature of crosslinking.[57] A first classification can be based on gel dimensions. Typically, hydrogels can be categorized as microgels, microparticles and macrogels. The first ones are defined as colloidal stable system, with a water swellable polymeric networks whose diameter typically ranges from 100 nm to 1 μm. Hydrogels microparticles, instead, show a range from tens to hundreds of microns and can be considered a sort of macrogels. These are bulk, monolithic networks with a typical range in size from hundreds of microns or greater.

Microgels are physically different from macrogels even though internally have the same gel structure. Indeed, as the high surface to volume ratios are several orders of magnitude larger than those in macrogels, microgels can present a non-uniform distribution of polymer chains throughout the network.[58-59] The synthesis of microgels particles typically involves a nucleation, aggregation and growth mechanism that ultimately results in a non-uniform distribution of polymer chains throughout the network.[60-61]

Hydrogels can be also classified into different categories based on their crosslinking chemistry.[62] The first one involves physical gels, which are defined as polymeric networks that are bound together via polymer chain entanglement and/or non-covalent interactions that exist between polymer chains.[1, 63-65] The attractive forces holding these networks together are typically based on hydrogen bonding, electrostatic or hydrophobic interactions and thus, the gels can be reversibly

dissolved under certain conditions that would weaken these attractive forces, i.e. a change in pH. In contrast to these weak physically crosslinked networks, the other general class of hydrogels consist of the chemical crosslinked gels. These hydrogels exhibit improved stability due to the formation of covalent bonds between different polymer chains throughout the networks and display endurance with respect to network structure.[1, 66-67] These gels are usually formed through monomer polymerization in the presence of a crosslinking agent, which is typically a monomer with at least two polymerizable functional moieties.

Moreover, hydrogels can be also categorized as neutral or ionic, based on the nature of side groups. In neutral ones, the driving force for swelling is due to the water-polymer thermodynamic mixing contribution to the overall free energy, along with elastic polymer contribution.[10] The swelling of ionic hydrogels is also affected by the ionic interactions between charged polymers and free ions.[68] This kind of gel, containing ionic groups (such as carboxylic acid) can imbibe larger amount of water because of its increased hydrophilicity.

Finally, hydrogel can also be grouped in terms of their interaction with the surrounding environment. Non-responsive gels are simple polymeric networks that dramatically swell upon exposure to water. Depending on its structure, hydrogel can respond to environmental changes by changing its size or shape. Most important factors that trigger a hydrogel response are temperature,[64, 69-70] pH,[71-72] ionic strength,[73-74] light,[63, 75-76] and electric field[77] (Figure 1.8).

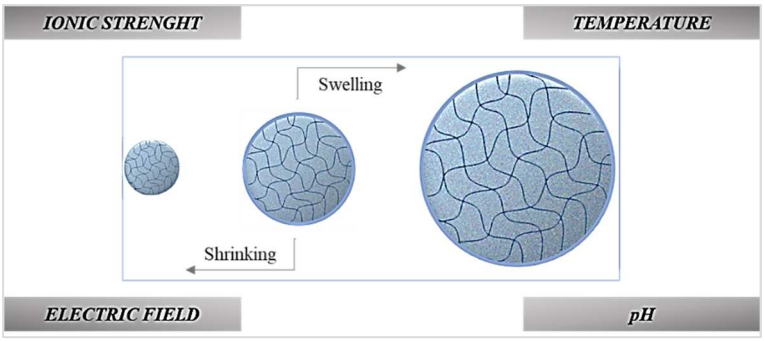

Figure 1.8: Principal environmental factors affecting hydrogels size.

As far as the temperature is concerned, hydrogels containing hydrophobic groups, or those susceptible to chain aggregation, respond to the temperature change with a great extent. Because of both solubility and swelling are driven by the same forces, the response of the hydrogel to temperature change can be either direct or inverse. The solubility and swelling of the hydrogel can increase with increase in temperature, while an opposite trend is observed with inverse thermo-responsive hydrogels. Hydrogels can also change their size with the change in the composition of the swelling medium. The hydrogel response is deeply affected by the presence of salt and non-solvent in the swelling solution.

Because hydrogels are tunable, responsive, and chemically versatile, they are suitable platform in the design of many biomaterials,[78] where the properties of the polymer may be engineered to suit specific medical applications.

1.5 Hydrogels: synthesis procedure

Hydrogels may be synthesized in a several ‘‘classical’’ chemical ways. These include one-step procedures like polymerization and parallel crosslinking of multifunctional monomers, as well as multiple step procedures involving synthesis of polymer molecules with reactive groups and their subsequent crosslinking. One of the most common technique is synthesis in batch.[79] This procedure is usually radical photo or thermal-initiated by using appropriate initiators or, for complex architecture, the synthesis can be performed via living controlled radical polymerizations. It is possible to identify three different preparation strategies, based on the particle formation mechanism: homogeneous nucleation, emulsification and complexation. In the first one microgels are generated from an initially homogeneous solutions. On the other hand, during the emulsification, aqueous droplets of a pre-gel solution are formed in an oil phase and, then, the droplets are polymerized becoming microgels. Finally, microgels can be synthesized by mixing two dilute

water-soluble polymers that form complexes in water. The new generation of polymer materials are designed and synthesized with an high control of the structure (crosslinking density) and with tailored properties such as swelling behavior and chemical and biological response to stimuli.[80-81]

In order to obtain a good control on the size, shape and chemistry, hydrogels can be produced using miniaturized devices such as microfluidic. In fact the recent years, advance of microfabrication methods, allow to synthesize tunable microparticles with a significant reduction in terms of time, costs and reagent needed.[82] Microfluidic assisted methods are usually based on formation of a stable emulsion of an oil phase (as continuous phase) and a water phase constituted by a mix of monomers and biomolecules. The synthesis occurs in a miniaturized devices made in glass or polydimethylsiloxane (PDMS).[83] The crosslinking of polymeric monomers is performed by shining UV/Vis light on the flowing liquids in-situ or in specialized compartments activating a suitable photoinitiator based on hydroxyalkylphenone species (i.e., Darocur, Irgacure). Benzoyl free radical is produced upon the homolytic scission of C–C bonds in the photosensitive molecules that allows the cross-links formation in the gel.[84] The intensity of light, the exposure time and the concentration of photoinitiator are determinant on the double bond conversion and in turn on the mechanical rigidity and the pores of the gels. Microfluidic techniques can be divided in droplet generation based methods and flow lithography (Figure 1.9). Droplet forming micro-devices have been described since 2005 as continuous on-chip production of water-in-oil emulsions based on the break-off of droplets in two-phases at T-junction or in flow-focusing geometries.[85-86] An innovative approach has been developed by Doyle et al.[11, 87] that reported an innovative method for the continuous production of hydrogel particles under flow in a PDMS microfluidic device with high throughput. With this technique, they were able to obtaining a high number codes by combining the graphical and spectral encoding.[87-88] This approach has been defined as continuous flow lithography and it relies on rectangular microfluidic

channel where multiple co-flowing streams pass over a pulsing UV light, that is projected through a mask from the objective, to give complex shapes. Multiple shapes and sizes have been obtained as well as differential chemistries, such as Janus particles, are possible. An evolution of this technology is represented by stop-flow lithography where the pumping system is actuated so that the flow is stopped for few milliseconds allowing the polymerization through a mask. In such a way Doyle's group obtained particles with graphical and spectral encoding as well as with multiple capture probes positioned in different regions.[89]

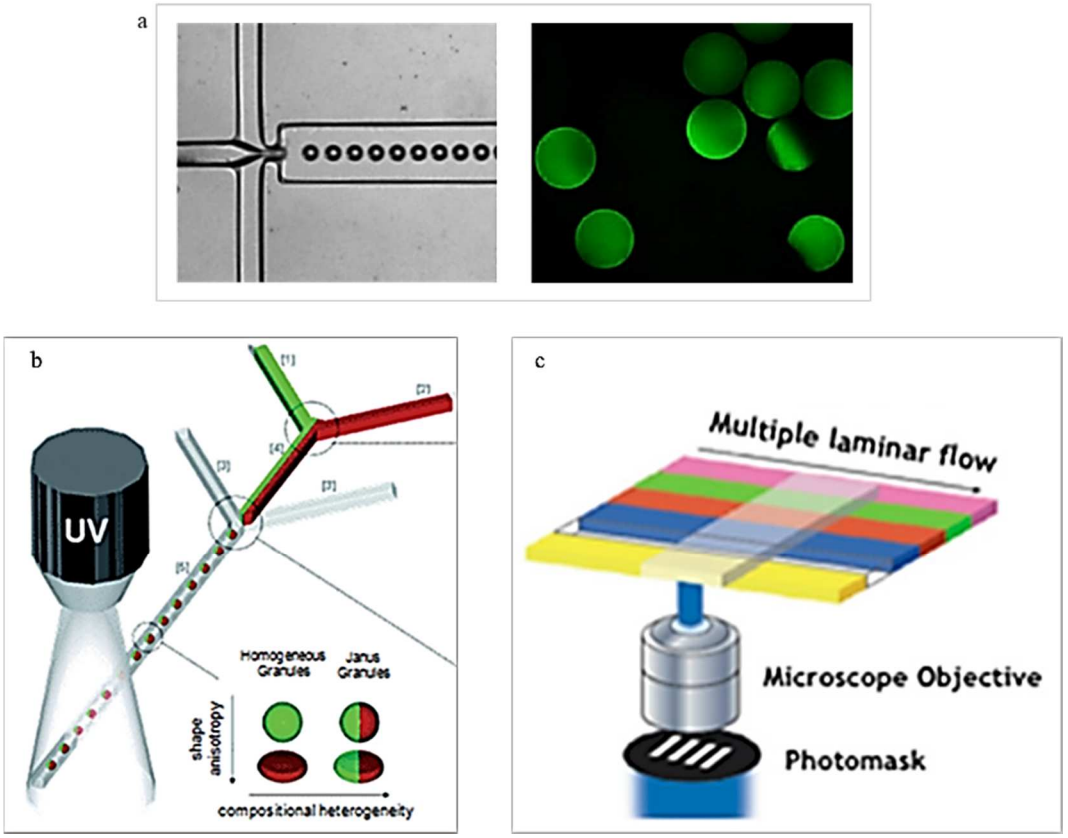

Figure 1.9: Different microfluidic techniques: (a) Flow focusing device for functionalized microparticles; (b) Droplet microfluidics for functional Janus microparticles production; (c) Continuous flow lithography for complex shaped hydrogel microparticles. Respectively adapted with permission from : Ref.[90] Copyright 2016, Elsevier B.V.; Ref. [91] Copyright 2011, Royal Society of Chemistry; Ref. [89] Copyright 2014, Rights Managed by Nature Publishing Group.

Regarding polymerization techniques, exist several kind of strategies, such as bulk polymerization, solution polymerization/crosslinking and suspension polymerization or inverse-suspension polymerization. Polymerized hydrogels may be produced in a wide variety of forms including films and membranes, rods, particles, and emulsions. High rate of polymerization and degree of polymerization occur because of the high concentration of monomer. The bulk polymerization of monomers, to make a homogeneous hydrogel, produces a glassy and transparent polymer matrix, which is very hard. When immersed in water, the glassy matrix swells to become soft and flexible. In solution copolymerization/crosslinking reactions, monomers are mixed with the multifunctional crosslinking agent. The polymerization starts by UV-irradiation or by a redox initiator system. Hydrogels so obtained need to be washed to remove the monomers, crosslinking agent, the initiator, and other impurities. Phase separation occurs and the heterogeneous hydrogel is formed when the amount of water during polymerization is more than the water content corresponding to the equilibrium swelling. Typical solvents used for solution polymerization of hydrogels include water, ethanol, water–ethanol mixtures, and benzyl alcohol. Then the synthesis solvent may be removed after formation of the gel by swelling the hydrogels in water. Suspension polymerization is an advantageous method since the products are obtained as microspheres and thus, grinding is not required. Since water-in-oil (W/O) process is chosen instead of the more common oil-in-water (O/W), the polymerization is referred to as ‘‘inverse-suspension’’. In this procedure, the monomers and initiator are dispersed as homogenous mixture. The viscosity of the monomer solution, agitation speed, rotor design, and dispersant type mainly governs the resin particle size and shape. The dispersion is thermodynamically unstable and requires both continuous agitation and addition of a low hydrophilic–lipophilic-balance (HLB) suspending agent.

1.6 Chemical an physical hydrogel characterization

In this section, we report on the chemical and physical properties of hydrogels that affect primarily their behavior. The three-dimensional and potentially responsive nature of the polymer networks plays a key role in bead-based assays and, when considering hydrogel materials in biosensing applications, a number of concerns has to be take into account. Particularly important are the issues related to the capability of capturing the given target and to the mass transport inside the network closely connected to the swelling behavior and diffusion of solutes.

1.6.1 Swelling behavior

Hydrogels are crosslinked polymer networks swollen in a liquid medium. They are able to absorb from 10-20% up to thousands of times their dry weight in water. When a dry hydrogel begins to absorb water, the first water molecules entering the matrix will hydrate the most polar, hydrophilic groups, leading to primary bound water. Once the polar groups are hydrated, the network swells, and exposes hydrophobic groups, which also interact with water molecules, leading to hydrophobically-bound water, or secondary bound water. Primary and secondary bound water are often grouped in the so-called total bound water.

After the polar and hydrophobic sites have interacted with and bound water molecules, the network will imbibe additional water, due to the osmotic driving force of the network chains towards infinite dilution. This additional swelling is hindered by the covalent or physical crosslink, leading to an elastic network retraction force. Thus, the hydrogel will reach an equilibrium swelling level. The additional swelling water that is imbibed after the ionic, polar and hydrophobic groups become saturated with bound water is called free water or bulk water and is assumed to fill the space between the network chains, and-or the center of larger pores, macropores or voids.[1, 92] The hydrogels biocompatibility and crosslinked structure are responsible for their different applications. The nature of monomers, method of preparation,

and nature of crosslinking agent determine the crosslinked structure of the gel. This can be characterized studying the gel swelling behavior. Several theories have been proposed to explain the network structure of the gel, as well as the mechanism of their swelling. Some theories examine the real network structure with its defects, while others, for analysis simplicity, consider the network as an ideal structure. For biomedical purposes, the hydrogel network is considered ideal.

The most important parameters used to characterize network structure are the polymer volume fraction (ν_2), molecular weight of the polymer chain between two neighboring crosslinks ($\bar{M}_c$), and the corresponding mesh size (ξ).[10] These three parameters, which are correlated to one another, describes the nanostructure of the crosslinked hydrogels and can be determined theoretically or using many experimental techniques. In particular two prominent theory are frequently used to elucidate the structure of hydrogels: equilibrium-swelling theory[93] and rubber-elasticity (Figure 1.10).[94]

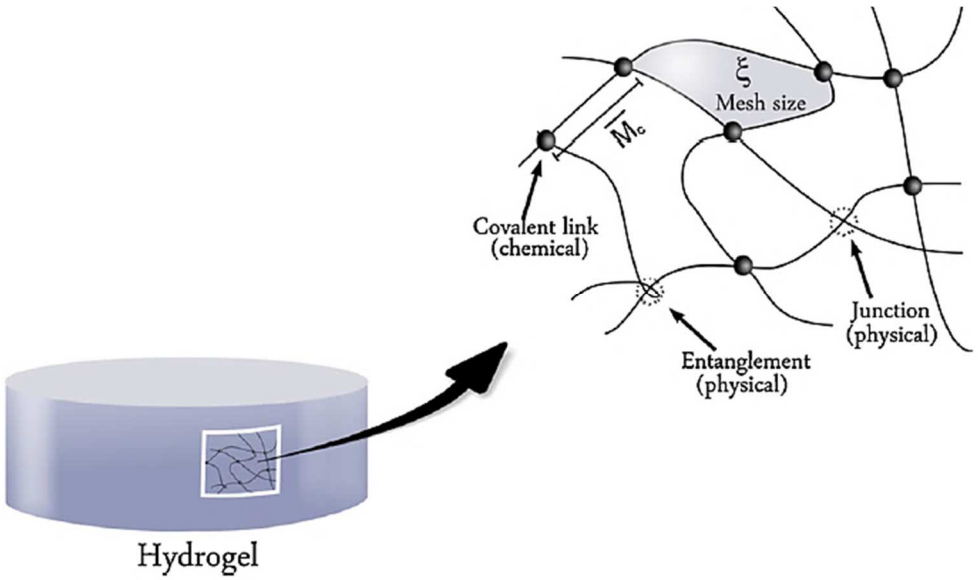

Figure 1.10: A crosslinked hydrogel structure with the main swelling parameters: mesh size (ξ) and the average molecular weight between crosslinks($\bar{M}_c$). Reproduced with permission from Ref.[20], Copyright 2012 Elsevier Ltd.

1.6.2 Equilibrium swelling theory

The structure of hydrogels that do not contain ionic moieties, can be analyzed by the Flory–Rehner theory.[95] It states that a crosslinked polymer gel, that is immersed in a fluid and allowed to reach equilibrium with its surroundings, is subject only to two opposing forces: the thermodynamic force of mixing and the retroactive force of the polymer chains. At equilibrium, these two forces are equal. This physical situation is defined in terms of the Gibbs free energy (Equation 1.1).

$$\Delta G_{tot} = \Delta G_{elastic} + \Delta G_{mixing} \qquad \text{Equation 1.1}$$

Here, $\Delta G_{elastic}$ is the contribution due to the elastic retroactive forces developed inside the gel, and ΔG_{mixing} is the result of the spontaneous mixing of the fluid molecules with the polymer chains. The term ΔG_{mixing} is a measure of the compatibility of the polymer with the molecules of the surrounding fluid. This compatibility is usually expressed by the polymer-solvent interaction parameter, χ. Differentiation of Equation 1.1 with respect to the number of solvent molecules while keeping temperature and pressure constant results in Equation 1.2:

$$\mu_1 - \mu_{1,0} = \Delta\mu_{elastic} + \Delta\mu_{mixing} \qquad \text{Equation 1.2}$$

Where μ_1 is the chemical potential of the solvent in the polymer gel and $\mu_{1,0}$ is the chemical potential of the pure solvent. At equilibrium, the difference between the chemical potentials of the solvent outside and inside the gel must be zero. Therefore, changes in the chemical potential due to mixing and elastic forces must balance each other. The change of chemical potential due to mixing can be expressed using heat and the entropy of mixing. By the contrast, the change in chemical potential due to the elastic retroactive forces of the polymer chains can be determined from the theory of rubber elasticity.[96-97] Upon equaling these two contributions, an expression for determining the molecular weight between two adjacent crosslinks of a neutral hydrogel prepared in the absence of a solvent can be obtained.[10, 98-100] The molecular

weight between two consecutive crosslinks, which can be either chemical or physical in nature, is a measure of the degree of crosslinking of the polymer and can be related to physical properties including swelling behavior and stiffness. It is important to note that due to the random nature of the polymerization process itself only average values of $\bar{M}_c$ can be calculated Equation 1.3

$$\frac{1}{\bar{M}_c} = \frac{2}{\bar{M}_n} - \frac{\left(\frac{\bar{\nu}}{V_1}\right)\left[\ln\left(1-v_{2,s}\right)+v_{2,s}+\chi_1 v_{2,s}^2\right]}{\left(v_{2,s}^{1/3}-\frac{v_{2,s}}{2}\right)} \qquad \text{Equation 1.3}$$

In this equation $\bar{M}_n$ is the molecular weight of the polymer chains prepared in the absence of a crosslinking agent, $v_{2,s}$ is the polymer fraction in the swollen state, $\chi_{1,2}$ is the polymer-solvent interaction parameter, $\bar{\nu}$ is the specific volume of the polymer, and V_1 is the molar volume of water.

In particular, polymer volume fraction in the swollen state characterizes how well the polymer absorbs water. It can be expressed as the ratio of the volume of dry polymer, V_d, to the volume of the swollen polymer gel, V_s, and is the reciprocal of the degree of swelling, Q.[101] The polymer fraction in the swollen state can easily be determined with equilibrium swelling and lyophilization experiments using Equation 1.4 above.

$$v_{2,s} = \frac{V_d}{V_s} = \frac{1}{Q} \qquad \text{Equation 1.4}$$

If the volume of the polymer and solute can be assumed additive, Equation 1.5 can be considered:

$$V_{gel} = V_{polymer} + V_{solvent} \qquad \text{Equation 1.5}$$

Then the dry and swollen mass of the gel can be used to find the polymer volume fraction in the swollen state, applying Equation 1.6, where $\rho_{solvent}$ is the density of

the solvent, $\rho_{polymer}$ is the density of the polymer, $m_{swollen}$ is the mass of the swollen hydrogel, and m_{dry} is the mass of the dry hydrogel after lyophilization.

$$v_{2,s} = \frac{1}{1+\frac{\rho_{polymer}}{\rho_{solvent}}\left(\frac{m_{swollen}}{m_{dry}}-1\right)} \quad \text{Equation 1.6}$$

Regarding molecular weight between crosslink, Peppas and Merrill[102] modified the original Flory-Rehner theory for hydrogels prepared in the presence of the water. The presence of the water effectively modifies the change of chemical potential due to the elastic forces. Equation 1.7 predict the molecular weight between crosslinks in a neutral hydrogel prepared in the presence of water; $v_{2,r}$ is the polymer volume fraction in the relaxed state, which is defined as the state of the polymer after crosslinking, but before swelling.

$$\frac{1}{\overline{M}_c} = \frac{2}{\overline{M}_n} - \frac{\left(\frac{\bar{v}}{V_1}\right)\left[\ln(1-v_{2,s})+v_{2,s}+\chi_1 v_{2,s}^2\right]}{v_{2,r}\left[\left(\frac{v_{2,s}}{v_{2,r}}\right)^{1/3}-\left(\frac{v_{2,s}}{2v_{2,r}}\right)\right]} \quad \text{Equation 1.7}$$

The presence of ionic moieties in hydrogels makes the theoretical treatment of swelling much more complex. In addition to the contributions of ΔG_{mixing} and $\Delta G_{elastic}$ in Equation 1.1, there is an additional contribution to the total change in Gibbs free energy due to the ionic nature of the polymer network, ΔG_{ionic} (Equation 1.8):

$$\Delta G_{tot} = \Delta G_{elastic} + \Delta G_{mixing} + \Delta G_{ionic} \quad \text{Equation 1.8}$$

Upon differentiating Equation 1.8 with respect to the number of moles of solvent, keeping T and P constant, an expression similar to Equation 1.2 for the chemical potential can be derived (Equation 1.9):

$$\mu_1 - \mu_{1,0} = \Delta\mu_{elastic} + \Delta\mu_{mixing} + \Delta\mu_{ionic} \quad \text{Equation 1.9}$$

Here, the $\Delta\mu_{ionic}$ is the change in chemical potential due to the ionic character of the hydrogel.

1.6.2.1 Rubber elasticity theory

Hydrogels resemble natural rubbers in their remarkable property to elastically respond to applied stresses. A hydrogel subjected to a relatively small deformation (less than 20%) will fully recover to its original dimension rapidly. This elastic behavior of hydrogels can be used to explain their structure applying the rubber-elasticity theory originally developed by Treloar[97] and Flory[94] for vulcanized rubbers and then modified by Flory for polymers.[96] An expression (Equation 1.10) has also been developed for relating the molecular weight between crosslinks and the elastic, or Young's, modulus E,

$$\frac{1}{\bar{M}_c} = \frac{3\rho RT}{E} \qquad \text{Equation 1.10}$$

The relationship should be taken as a rough estimation which often underestimates $\bar{M}_c$ since it does not take into account physical crosslinks or chain ends.[103] Another important parameter used to describe hydrogels is the mesh size, or characteristic length, ξ, which represent the characteristic distance between crosslinks, provides a measure of the space available between the macromolecular chains and it is an important factor in solute transport in hydrogels. The mesh size also affects properties such as mechanical strength, degradability, and diffusivity within a hydrogel. If a solute molecule is larger than the mesh size, it is theoretically impossible for the solute molecule to move through the hydrogel. The mesh size of a hydrogel is affected by the degree of crosslinking, chemical structure of the monomer, and other external stimuli, such as pH, temperature, and the presence of ions. Again, it can be reported only as an average value. The mesh size can be related to other parameters discussed above

via scaling relationships, which produce the Equation 1.11, where $(\bar{r}_0^2)^{1/2}$ is the root-mean-squared, unperturbed, end to end distance of the polymer chain between two adjacent crosslinks.

$$\xi = v_{2,s}^{-1/3}(r_0^2)^{1/2} \qquad \text{Equation 1.11}$$

This statistical parameter can be found via a relationship first developed by Flory, Equation 1.12:

$$(r_0^2)^{1/2} = C_n N l^2 \qquad \text{Equation 1.12}$$

where C_n is the Flory characteristic ratio, l is the length of each link and N, the number of links in the chain, is given by Equation 1.13:

$$N = \frac{2\,\bar{M}_c}{M_r} \qquad \text{Equation 1.13}$$

Where M_r is the molecular weight of the repeating unit of the polymer.

1.6.2.2 Factors affecting swelling of hydrogels

One of the most important factors that affects the swelling of hydrogels is the crosslinking ratio. It is defined as the ratio of the moles of crosslinking agent to the moles of polymer repeating units. The presence of crosslinks represent a hindrance to the mobility of the polymer chain.[10] In fact, a high value of crosslinking ratio is associated with a tighter structure that consequently will swell less compared to the same hydrogels with lower crosslinking ratio. Moreover, the chemical structure of the polymer may also affect the swelling ratio. For example, hydrogels containing hydrophilic groups swell more than hydrogels containing hydrophobic one. The latter, in fact, collapse in the presence of water in order to minimize their exposure to the water molecules.[10] Finally, as described previously, there are environmentally

sensitive-hydrogels. For these materials, there are many specific stimuli, as pH, temperature, light, that can affect their swelling.

1.6.3 Solute diffusion within hydrogels

The diffusion of solutes in hydrogels is widely studied in several fields. Hydrogels are in fact used in separation processes such as chromatography,[104] for the encapsulation of cells for both biomedical and fermentation purposes, in biosensors and as biomaterials for the delivery of drug and prosthetic applications.[105-106]

The one feature of hydrogels that all these applications capitalize upon is their ability to restrict the diffusive movement of a solute. Solute transport within hydrogels occurs primarily within the water-filled regions in the space delineated by the polymer chains.

Any factor, which reduces the size of these spaces, will have an effect on the movement of the solute. Several factors such as the size of the solute related with the size of the openings between polymer chains, the fractal dimension of the diffusing species, polymer chain mobility and the existence of charged groups on the polymer, might influence the solute mobility.

In particular, the polymer chain mobility is an important factor governing solute movement within the hydrogel. In general, the diffusivity of a solute through a physically crosslinked hydrogel decreases as crosslinking density increases, as the size of the solute increases and as the volume fraction of water within the gel decreases.[107] The fractal dimension of the diffusing species d_f is dependent from rigidity of the molecule, in particular for a rigid sphere, $d_f = 3.0$, for a linear Gaussian polymer coil (random walk) $d_f = 2.0$ and $d_f < 2$ for polymers with excluded-volume interactions.[108]

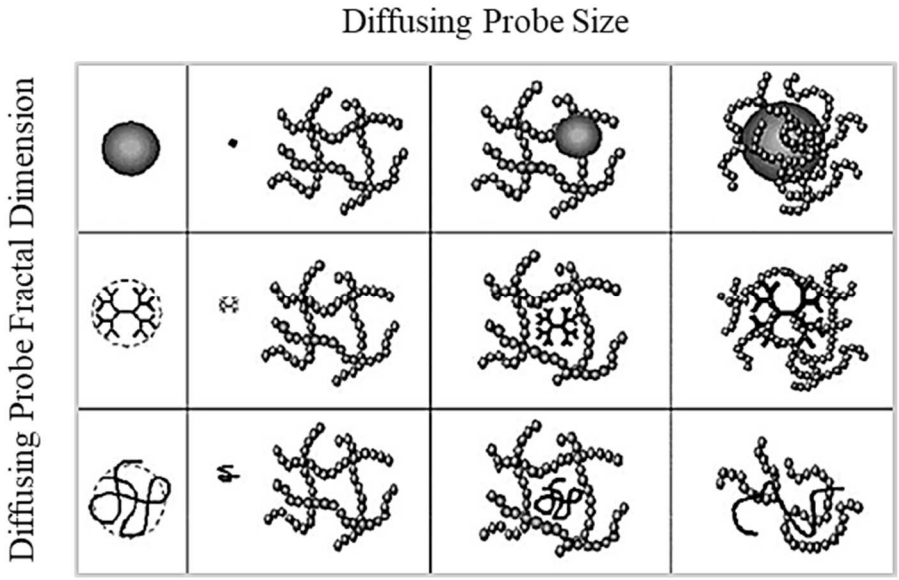

Figure 1.11: Parameters that influence diffusion of probe particles in polymeric media. Adapted with permission from Ref.[108], Copyright 2002, American Chemical Society.

For all these reasons, the understanding of the parameters governing solute diffusion within hydrogels as well as the means by which they affect diffusion are important to be studied. Therefore, a number of mathematical expressions have been developed in an effort to model solute diffusion in hydrogels.[109]

1.7 Aim and outline of dissertation

The growing interest in biosensor field has driven us to study novel materials, to improve the detection in complex fluids.

Although different types of microparticles are already on the market (e.g., fluorescent labeled and magnetic), there is a need for materials with high flexibility to introduce the right functionalities for the encoding and for the capture elements with enhanced properties. A direct and absolute quantification of circulating miRNAs in body fluids is challenging, due to the high level of sequences homology, small size and demand of high sensitivity and specificity.

In order achieve this, we focused on the research, synthesis and optimization of materials, which combine features of biocompatibility, stability and low interaction with proteins. This work is, in fact, focused on the challenge to combine these properties with flexible chemistry and tunable control of the network.

Therefore, we synthesized engineered PEG-based materials, properly functionalized, with versatile chemistry and tunable control of mesh size allow to obtain a customized molecular filter for a simple detection of oligonucleotides in complex fluids. Our particle-based assay allow to overcome limitations of conventional techniques, previously described. This kind of assay is based on optical detection scheme for oligonucleotide. Capture element can be added on the hydrogel surface or inside in order to achieve smart materials for specific detection.

In **Chapter 2**, we focused on the synthesis and characterization of core-shell PEGMA-microgels, obtained by combining precipitation and seeded polymerizations, with controlled structural properties. AFM images, combined with equilibrium swelling theory, allowed to describe the organizations of the different adlayers highlighting the possibility of some overlap representing physical barriers at the boundaries of each shell.

In **Chapter 3**, synthesis and characterization of PEGDA-bulk hydrogels, properly functionalized with capture element, were done. Swelling studies, combined with both NMR and fluorimetric analysis for probes diffusion, allow to optimize the network structure to combine both molecular filter and capture element capabilities.

Finally, in **Chapter 4**, this knowledge were scaled down to synthetize microparticles by microfluidic device improving the shape and size control and to reduce both production time and costs. Moreover, adding directly in flow a probe, properly designed for the detection of miRNA143-3p (responsible of cardiovascular diseases) we were able to detect, also in complex fluids the presence of the interest target.

Conclusions and future perspectives are synthetically presented and discussed in **Chapter 5**.

1.8 References

1. Hoffman, A. S., Hydrogels for biomedical applications. *Advanced drug delivery reviews* **2012,** *64*, 18-23.
2. Brannon-Peppas, L.; Harland, R. S., *Absorbent polymer technology*. Elsevier: 2012; Vol. 8.
3. Buchholz, F. L.; Graham, A. T., Modern superabsorbent polymer technology. *John! Wiley & Sons, Inc, 605 Third Ave, New York, NY 10016, USA, 1998. 279* **1998**.
4. Helgeson, M. E.; Chapin, S. C.; Doyle, P. S., Hydrogel microparticles from lithographic processes: Novel materials for fundamental and applied colloid science. *Current opinion in colloid & interface science* **2011,** *16* (2), 106-117.
5. Rubina, A. Y.; Kolchinsky, A.; Makarov, A. A.; Zasedatelev, A. S., Why 3-D? Gel-based microarrays in proteomics. *Proteomics* **2008,** *8* (4), 817-831.
6. Peppas, N. A.; Hilt, J. Z.; Khademhosseini, A.; Langer, R., Hydrogels in biology and medicine: from molecular principles to bionanotechnology. *Advanced materials* **2006,** *18* (11), 1345-1360.
7. Peppas, N. A.; Keys, K. B.; Torres-Lugo, M.; Lowman, A. M., Poly (ethylene glycol)-containing hydrogels in drug delivery. *Journal of controlled release* **1999,** *62* (1), 81-87.
8. Lee, K. Y.; Mooney, D. J., Hydrogels for tissue engineering. *Chemical reviews* **2001,** *101* (7), 1869-1880.
9. Sannino, A.; Netti, P.; Madaghiele, M.; Coccoli, V.; Luciani, A.; Maffezzoli, A.; Nicolais, L., Synthesis and characterization of macroporous poly (ethylene glycol)-based hydrogels for tissue engineering application. *Journal of Biomedical Materials Research Part A* **2006,** *79* (2), 229-236.
10. Peppas, N.; Bures, P.; Leobandung, W.; Ichikawa, H., Hydrogels in pharmaceutical formulations. *European journal of pharmaceutics and biopharmaceutics* **2000,** *50* (1), 27-46.
11. Chapin, S. C.; Appleyard, D. C.; Pregibon, D. C.; Doyle, P. S., Rapid microRNA profiling on encoded gel microparticles. *Angewandte Chemie International Edition* **2011,** *50* (10), 2289-2293.
12. Choi, N. W.; Kim, J.; Chapin, S. C.; Duong, T.; Donohue, E.; Pandey, P.; Broom, W.; Hill, W. A.; Doyle, P. S., Multiplexed detection of mRNA using porosity-tuned hydrogel microparticles. *Analytical chemistry* **2012,** *84* (21), 9370-9378.
13. Causa, F.; Aliberti, A.; Cusano, A. M.; Battista, E.; Netti, P. A., Supramolecular spectrally encoded microgels with double strand probes for absolute and direct miRNA fluorescence detection at high sensitivity. *Journal of the American Chemical Society* **2015,** *137* (5), 1758-1761.

14. Thévenot, D. R.; Toth, K.; Durst, R. A.; Wilson, G. S., Electrochemical biosensors: recommended definitions and classification. *Biosensors and Bioelectronics* **2001,** *16* (1), 121-131.
15. Sassolas, A.; Blum, L. J.; Leca-Bouvier, B. D., Immobilization strategies to develop enzymatic biosensors. *Biotechnology advances* **2012,** *30* (3), 489-511.
16. Nambiar, S.; Yeow, J. T., Conductive polymer-based sensors for biomedical applications. *Biosensors and Bioelectronics* **2011,** *26* (5), 1825-1832.
17. Tothill, I. E. In *Biosensors for cancer markers diagnosis*, Seminars in cell & developmental biology, Elsevier: 2009; pp 55-62.
18. Biswal, D.; Hilt, J. Z., Microscale analysis of patterning reactions via FTIR imaging: Application to intelligent hydrogel systems. *Polymer* **2006,** *47* (21), 7355-7360.
19. Nguyen, K. T.; West, J. L., Photopolymerizable hydrogels for tissue engineering applications. *Biomaterials* **2002,** *23* (22), 4307-4314.
20. Buenger, D.; Topuz, F.; Groll, J., Hydrogels in sensing applications. *Progress in Polymer Science* **2012,** *37* (12), 1678-1719.
21. Le Goff, G. C.; Srinivas, R. L.; Hill, W. A.; Doyle, P. S., Hydrogel microparticles for biosensing. *European polymer journal* **2015,** *72*, 386-412.
22. Wu, L.; Qu, X., Cancer biomarker detection: recent achievements and challenges. *Chemical Society Reviews* **2015,** *44* (10), 2963-2997.
23. Kosaka, N.; Iguchi, H.; Ochiya, T., Circulating microRNA in body fluid: a new potential biomarker for cancer diagnosis and prognosis. *Cancer science* **2010,** *101* (10), 2087-2092.
24. Segal, E.; Friedman, N.; Koller, D.; Regev, A., Extracting condition-specific modules from cancer microarray data. *NATURE GENETICS* **2004,** *36* (10), 1090-1098.
25. Condorelli, G.; Latronico, M. V.; Cavarretta, E., microRNAs in cardiovascular diseases: current knowledge and the road ahead. *Journal of the American College of Cardiology* **2014,** *63* (21), 2177-2187.
26. Hébert, S. S.; Horré, K.; Nicolaï, L.; Bergmans, B.; Papadopoulou, A. S.; Delacourte, A.; De Strooper, B., MicroRNA regulation of Alzheimer's Amyloid precursor protein expression. *Neurobiology of disease* **2009,** *33* (3), 422-428.
27. Hitachi, K.; Nakatani, M.; Tsuchida, K., Myostatin signaling regulates Akt activity via the regulation of miR-486 expression. *The international journal of biochemistry & cell biology* **2014,** *47*, 93-103.
28. Kjaer-Frifeldt, S.; Hansen, T.; Nielsen, B.; Joergensen, S.; Lindebjerg, J.; Soerensen, F.; dePont Christensen, R.; Jakobsen, A., The prognostic importance of miR-21 in stage II colon cancer: a population-based study. *British journal of cancer* **2012,** *107* (7), 1169.

29. Dong, H.; Lei, J.; Ding, L.; Wen, Y.; Ju, H.; Zhang, X., MicroRNA: function, detection, and bioanalysis. *Chemical reviews* **2013,** *113* (8), 6207-6233.

30. Kilic, T.; Erdem, A.; Ozsoz, M.; Carrara, S., microRNA biosensors: Opportunities and challenges among conventional and commercially available techniques. *Biosensors and Bioelectronics* **2018,** *99*, 525-546.

31. Chen, X.; Ba, Y.; Ma, L.; Cai, X.; Yin, Y.; Wang, K.; Guo, J.; Zhang, Y.; Chen, J.; Guo, X., Characterization of microRNAs in serum: a novel class of biomarkers for diagnosis of cancer and other diseases. *Cell research* **2008,** *18* (10), 997.

32. Ambros, V., The functions of animal microRNAs. *Nature* **2004,** *431* (7006), 350.

33. Stefani, G.; Slack, F. J., Small non-coding RNAs in animal development. *Nature reviews. Molecular cell biology* **2008,** *9* (3), 219.

34. O'connell, R. M.; Rao, D. S.; Chaudhuri, A. A.; Baltimore, D., Physiological and pathological roles for microRNAs in the immune system. *Nature reviews. Immunology* **2010,** *10* (2), 111.

35. Cheng, H.-Y. M.; Papp, J. W.; Varlamova, O.; Dziema, H.; Russell, B.; Curfman, J. P.; Nakazawa, T.; Shimizu, K.; Okamura, H.; Impey, S., microRNA modulation of circadian-clock period and entrainment. *Neuron* **2007,** *54* (5), 813-829.

36. Di Leva, G.; Croce, C. M., Roles of small RNAs in tumor formation. *Trends in molecular medicine* **2010,** *16* (6), 257-267.

37. Fiore, R.; Siegel, G.; Schratt, G., MicroRNA function in neuronal development, plasticity and disease. *Biochimica et Biophysica Acta (BBA)-Gene Regulatory Mechanisms* **2008,** *1779* (8), 471-478.

38. Rangrez, A. Y.; Massy, Z. A.; Metzinger-Le Meuth, V.; Metzinger, L., MiR-143 and MiR-145. *Circulation: Cardiovascular Genetics* **2011,** *4* (2), 197-205.

39. Zhao, W.; Zhao, S.-P.; Zhao, Y.-H., MicroRNA-143/-145 in cardiovascular diseases. *BioMed research international* **2015,** *2015*.

40. Yang, B.; Lin, H.; Xiao, J.; Lu, Y.; Luo, X.; Li, B.; Zhang, Y.; Xu, C.; Bai, Y.; Wang, H., The muscle-specific microRNA miR-1 regulates cardiac arrhythmogenic potential by targeting GJA1 and KCNJ2. *Nature medicine* **2007,** *13* (4), 486.

41. Thum, T.; Gross, C.; Fiedler, J.; Fischer, T.; Kissler, S.; Bussen, M.; Galuppo, P.; Just, S.; Rottbauer, W.; Frantz, S., MicroRNA-21 contributes to myocardial disease by stimulating MAP kinase signalling in fibroblasts. *Nature* **2008,** *456* (7224), 980.

42. van Rooij, E.; Sutherland, L. B.; Qi, X.; Richardson, J. A.; Hill, J.; Olson, E. N., Control of stress-dependent cardiac growth and gene expression by a microRNA. *Science* **2007,** *316* (5824), 575-579.

43. Najafi-Shoushtari, S. H.; Kristo, F.; Li, Y.; Shioda, T.; Cohen, D. E.; Gerszten, R. E.; Näär, A. M., MicroRNA-33 and the SREBP host genes cooperate to control cholesterol homeostasis. *Science* **2010,** *328* (5985), 1566-1569.

44. Mitchell, P. S.; Parkin, R. K.; Kroh, E. M.; Fritz, B. R.; Wyman, S. K.; Pogosova-Agadjanyan, E. L.; Peterson, A.; Noteboom, J.; O'Briant, K. C.; Allen, A., Circulating microRNAs as stable blood-based markers for cancer detection. *Proceedings of the National Academy of Sciences* **2008,** *105* (30), 10513-10518.

45. Garcia-Schwarz, G.; Santiago, J. G., Integration of on-chip isotachophoresis and functionalized hydrogels for enhanced-sensitivity nucleic acid detection. *Analytical chemistry* **2012,** *84* (15), 6366-6369.

46. Wark, A. W.; Lee, H. J.; Corn, R. M., Multiplexed detection methods for profiling microRNA expression in biological samples. *Angewandte Chemie International Edition* **2008,** *47* (4), 644-652.

47. Chen, C.; Tan, R.; Wong, L.; Fekete, R.; Halsey, J., Quantitation of microRNAs by real-time RT-qPCR. *PCR Protocols* **2011**, 113-134.

48. Li, Y.; Zhou, X.; Ye, D., Molecular beacons: an optimal multifunctional biological probe. *Biochemical and biophysical research communications* **2008,** *373* (4), 457-461.

49. Zhang, D. Y.; Seelig, G., Dynamic DNA nanotechnology using strand-displacement reactions. *Nature chemistry* **2011,** *3* (2), 103-113.

50. Evans, M.; Sewter, C.; Hill, E., An encoded particle array tool for multiplex bioassays. *Assay and drug development technologies* **2003,** *1* (1, Supplement 2), 199-207.

51. Nolan, J. P.; Sklar, L. A., Suspension array technology: evolution of the flat-array paradigm. *TRENDS in Biotechnology* **2002,** *20* (1), 9-12.

52. Al-Ameen, M. A.; Ghosh, G., Sensitive quantification of vascular endothelial growth factor (VEGF) using porosity induced hydrogel microspheres. *Biosensors and Bioelectronics* **2013,** *49*, 105-110.

53. Wang, L.; Yang, C.; Tan, W., Dual-luminophore-doped silica nanoparticles for multiplexed signaling. *Nano letters* **2005,** *5* (1), 37-43.

54. Chapin, S. C.; Pregibon, D. C.; Doyle, P. S., High-throughput flow alignment of barcoded hydrogel microparticles. *Lab on a Chip* **2009,** *9* (21), 3100-3109.

55. Birtwell, S.; Morgan, H., Microparticle encoding technologies for high-throughput multiplexed suspension assays. *Integrative Biology* **2009,** *1* (5-6), 345-362.

56. Wilson, R.; Cossins, A. R.; Spiller, D. G., Encoded microcarriers for high-throughput multiplexed detection. *Angewandte Chemie International Edition* **2006,** *45* (37), 6104-6117.

57. Qiu, Y.; Park, K., Environment-sensitive hydrogels for drug delivery. *Advanced drug delivery reviews* **2001,** *53* (3), 321-339.

58. Smith, M. H.; Herman, E. S.; Lyon, L. A., Network deconstruction reveals network structure in responsive microgels. *The Journal of Physical Chemistry B* **2011,** *115* (14), 3761-3764.

59. Hoare, T.; Pelton, R., Dimensionless plot analysis: A new way to analyze functionalized microgels. *Journal of colloid and interface science* **2006,** *303* (1), 109-116.

60. Saunders, B. R., On the structure of poly (N-isopropylacrylamide) microgel particles. *Langmuir* **2004,** *20* (10), 3925-3932.

61. Wu, X.; Pelton, R.; Hamielec, A.; Woods, D.; McPhee, W., The kinetics of poly (N-isopropylacrylamide) microgel latex formation. *Colloid & Polymer Science* **1994,** *272* (4), 467-477.

62. Langer, R.; Tirrell, D. A., Designing materials for biology and medicine. *Nature* **2004,** *428* (6982), 487-492.

63. Collier, J. H.; Hu, B. H.; Ruberti, J. W.; Zhang, J.; Shum, P.; Thompson, D. H.; Messersmith, P. B., Thermally and photochemically triggered self-assembly of peptide hydrogels. *Journal of the American Chemical Society* **2001,** *123* (38), 9463-9464.

64. Akiyoshi, K.; Kang, E.-C.; Kurumada, S.; Sunamoto, J.; Principi, T.; Winnik, F. M., Controlled association of amphiphilic polymers in water: thermosensitive nanoparticles formed by self-assembly of hydrophobically modified pullulans and poly (N-isopropylacrylamides). *Macromolecules* **2000,** *33* (9), 3244-3249.

65. De Rossi, D.; Kajiwara, K.; Osada, Y.; Yamauchi, A., Polymer gels. *Plenum Press, New York* **1991,** *2*, 297.

66. Hennink, W.; Van Nostrum, C. F., Novel crosslinking methods to design hydrogels. *Advanced drug delivery reviews* **2012,** *64*, 223-236.

67. Eddington, D. T.; Beebe, D. J., Flow control with hydrogels. *Advanced drug delivery reviews* **2004,** *56* (2), 199-210.

68. Peppas, N. A.; Khare, A. R., Preparation, structure and diffusional behavior of hydrogels in controlled release. *Advanced drug delivery reviews* **1993,** *11* (1-2), 1-35.

69. Tanaka, T.; Fillmore, D.; Sun, S.-T.; Nishio, I.; Swislow, G.; Shah, A., Phase transitions in ionic gels. *Physical Review Letters* **1980,** *45* (20), 1636.

70. Ghugare, S. V.; Mozetic, P.; Paradossi, G., Temperature-sensitive poly (vinyl alcohol)/poly (methacrylate-co-N-isopropyl acrylamide) microgels for doxorubicin delivery. *Biomacromolecules* **2009,** *10* (6), 1589-1596.

71. Jones, C. D.; Lyon, L. A., Synthesis and characterization of multiresponsive core− shell microgels. *Macromolecules* **2000,** *33* (22), 8301-8306.

72. Moselhy, J.; Wu, X. Y.; Nicholov, R.; Kodaria, K., In vitro studies of the interaction of poly (NIPAm/MAA) nanoparticles with proteins and cells. *Journal of Biomaterials Science, Polymer Edition* **2000,** *11* (2), 123-147.

73. Duracher, D.; Sauzedde, F.; Elaissari, A.; Perrin, A.; Pichot, C., Cationic amino-containing N-isopropyl-acrylamide–styrene copolymer latex particles: 1-Particle size and morphology vs. polymerization process. *Colloid & Polymer Science* **1998,** *276* (3), 219-231.

74. Snowden, M. J.; Chowdhry, B. Z.; Vincent, B.; Morris, G. E., Colloidal copolymer microgels of N-isopropylacrylamide and acrylic acid: pH, ionic strength and temperature effects. *Journal of the Chemical Society, Faraday Transactions* **1996,** *92* (24), 5013-5016.

75. Sershen, S.; Westcott, S.; Halas, N.; West, J., Temperature-sensitive polymer–nanoshell composites for photothermally modulated drug delivery. *Journal of Biomedical Materials Research Part A* **2000,** *51* (3), 293-298.

76. Suzuki, A.; Tanaka, T., Phase transition in polymer gels induced by visible light. *Nature* **1990,** *346* (6282), 345-347.

77. Tanaka, T.; Nishio, I.; Sun, S.-T.; Ueno-Nishio, S., Collapse of gels in an electric field. *Science* **1982,** *218* (4571), 467-469.

78. Kishi, R.; Miura, T.; Kihara, H.; Asano, T.; Shibata, M.; Yosomiya, R., Fast pH-thermo-responsive copolymer hydrogels with micro-porous structures. *Journal of applied polymer science* **2003,** *89* (1), 75-84.

79. Amalvy, J.; Wanless, E.; Li, Y.; Michailidou, V.; Armes, S.; Duccini, Y., Synthesis and characterization of novel pH-responsive microgels based on tertiary amine methacrylates. *Langmuir* **2004,** *20* (21), 8992-8999.

80. Burkert, S.; Schmidt, T.; Gohs, U.; Dorschner, H.; Arndt, K.-F., Crosslinking of poly (N-vinyl pyrrolidone) films by electron beam irradiation. *Radiation Physics and Chemistry* **2007,** *76* (8), 1324-1328.

81. Ahmed, E. M., Hydrogel: Preparation, characterization, and applications: A review. *Journal of advanced research* **2015,** *6* (2), 105-121.

82. Wang, J. T.; Wang, J.; Han, J. J., Fabrication of Advanced Particles and Particle-Based Materials Assisted by Droplet-Based Microfluidics. *small* **2011,** *7* (13), 1728-1754.

83. Serra, C. A.; Chang, Z., Microfluidic-assisted synthesis of polymer particles. *Chemical engineering & technology* **2008,** *31* (8), 1099-1115.

84. Lewis, C. L.; Choi, C.-H.; Lin, Y.; Lee, C.-S.; Yi, H., Fabrication of uniform DNA-conjugated hydrogel microparticles via replica molding for facile nucleic acid hybridization assays. *Analytical chemistry* **2010,** *82* (13), 5851-5858.

85. Heida, T.; Neubauer, J. W.; Seuss, M.; Hauck, N.; Thiele, J.; Fery, A., Mechanically defined microgels by droplet microfluidics. *Macromolecular Chemistry and Physics* **2017,** *218* (2).

86. Zhu, P.; Wang, L., Passive and active droplet generation with microfluidics: a review. *Lab on a Chip* **2017,** *17* (1), 34-75.

87. Pregibon, D. C.; Toner, M.; Doyle, P. S., Multifunctional encoded particles for high-throughput biomolecule analysis. *Science* **2007,** *315* (5817), 1393-1396.

88. Appleyard, D. C.; Chapin, S. C.; Srinivas, R. L.; Doyle, P. S., Bar-coded hydrogel microparticles for protein detection: synthesis, assay and scanning. *Nature protocols* **2011,** *6* (11), 1761.

89. Lee, J.; Bisso, P. W.; Srinivas, R. L.; Kim, J. J.; Swiston, A. J.; Doyle, P. S., Universal process-inert encoding architecture for polymer microparticles. *Nature materials* **2014,** *13* (5), 524-529.

90. Celetti, G.; Di Natale, C.; Causa, F.; Battista, E.; Netti, P. A., Functionalized poly (ethylene glycol) diacrylate microgels by microfluidics: In situ peptide encapsulation for in serum selective protein detection. *Colloids and Surfaces B: Biointerfaces* **2016,** *145*, 21-29.

91. Chung, B. G.; Lee, K.-H.; Khademhosseini, A.; Lee, S.-H., Microfluidic fabrication of microengineered hydrogels and their application in tissue engineering. *Lab on a Chip* **2012,** *12* (1), 45-59.

92. Yahia, L.; Chirani, N.; Gritsch, L.; Motta, F. L.; Fare, S., History and applications of hydrogels. *Journal of biomedical sciences* **2015,** *4* (2).

93. Flory, P. J.; Rehner Jr, J., Statistical mechanics of cross-linked polymer networks II. Swelling. *The Journal of Chemical Physics* **1943,** *11* (11), 521-526.

94. Flory, P. J.; Rabjohn, N.; Shaffer, M. C., Dependence of elastic properties of vulcanized rubber on the degree of cross linking. *Journal of Polymer Science Part A: Polymer Chemistry* **1949,** *4* (3), 225-245.

95. Langer, R.; Peppas, N. A., Advances in biomaterials, drug delivery, and bionanotechnology. *AIChE Journal* **2003,** *49* (12), 2990-3006.

96. Flory, P. J., *Principles of polymer chemistry*. Cornell University Press: 1953.

97. Treloar, L., *Physics of Rubber Elasticity (Oxford classic texts in the physical sciences)*. Oxford University Press: 2005.

98. Lin, C.-C.; Metters, A. T., Hydrogels in controlled release formulations: network design and mathematical modeling. *Advanced drug delivery reviews* **2006,** *58* (12), 1379-1408.

99. Moorthy, J., Hydrogels in microfluidics. *SMART POLYMERS: Application in biotechnology and biomedicine, Taylor & Francis* **2007**, 437-457.

100. Peppas, N.; Huang, Y.; Torres-Lugo, M.; Ward, J.; Zhang, J., Physicochemical foundations and structural design of hydrogels in medicine and biology. *Annual review of biomedical engineering* **2000,** *2* (1), 9-29.

101. Thakur, A.; Wanchoo, R.; Singh, P., Structural parameters and swelling behavior of pH sensitive poly (acrylamide-co-acrylic acid) hydrogels. *Chemical and Biochemical Engineering Quarterly* **2011,** *25* (2), 181-194.

102. Peppas, N. A.; Merrill, E. W., Crosslinked poly (vinyl alcohol) hydrogels as swollen elastic networks. *Journal of Applied Polymer Science* **1977,** *21* (7), 1763-1770.

103. Lin, H.; Kai, T.; Freeman, B. D.; Kalakkunnath, S.; Kalika, D. S., The effect of crosslinking on gas permeability in crosslinked poly (ethylene glycol diacrylate). *Macromolecules* **2005,** *38* (20), 8381-8393.

104. Moussaoui, M.; Benlyas, M.; Wahl, P., Diffusion of proteins in the chromatographic gel AcA-34. *Journal of Chromatography A* **1991,** *558* (1), 71-80.

105. Jen, A. C.; Wake, M. C.; Mikos, A. G., Hydrogels for cell immobilization. *Biotechnology and bioengineering* **1996,** *50* (4), 357-364.

106. Lee, P. I., Kinetics of drug release from hydrogel matrices. *Journal of Controlled Release* **1985,** *2*, 277-288.

107. Yasuda, H.; Peterlin, A.; Colton, C.; Smith, K.; Merrill, E., Permeability of solutes through hydrated polymer membranes. Part III. Theoretical background for the selectivity of dialysis membranes. *Macromolecular Chemistry and Physics* **1969,** *126* (1), 177-186.

108. Cheng, Y.; Prud'Homme, R. K.; Thomas, J. L., Diffusion of mesoscopic probes in aqueous polymer solutions measured by fluorescence recovery after photobleaching. *Macromolecules* **2002,** *35* (21), 8111-8121.

109. Pluen, A.; Netti, P. A.; Jain, R. K.; Berk, D. A., Diffusion of macromolecules in agarose gels: comparison of linear and globular configurations. *Biophysical journal* **1999,** *77* (1), 542-552.

Chapter 2

Core-shell microgels: synthesis and swelling characterization

Abstract. Due to their versatility and their modulating properties, microgels have been largely studied in biomedical field for their wide application in diagnostic. In particular, multifunctional core-shell microgels, with complex architectures, have been used for multiplex assays. Changing synthesis parameters was possible to accommodate encoding system and anchoring group for specific probes in order to capture circulating targets. In this chapter, we focused on the synthesis and characterization of a fluorescent encoded poly(ethyleneglycol)-based microgels with a core-shell architecture obtained combining precipitation and seeded polymerizations. Structural characterization was done combining AFM images with equilibrium swelling theory. In such a way, we were able to describe the organizations of each single shell, evaluating the presence and effects of the overlaps as physical barriers.

The work described in this chapter is part of a manuscript published: E. Battista, **A. Mazzarotta**, F. Causa, A.M. Cusano, P. A. Netti. **"Core−shell microgels with controlled structural properties"**. Polymer International, (2016). 65(7), 747-755.[1]
Part of this work is reproduced or adapted with permission from [1], Copyright 2016 Wiley.

2.1 Introduction

Hydrogels are three-dimensional, and potentially responsive, polymer networks that, due to their customizable physical and chemical properties, has been widely used in biomedical field. In particular, recent studies have focused on multifunctional hydrogel particles as materials platforms to attain the new generation of diagnostic tools.[2-5] Multifunctional microgels require that the chemistries of the surface and the bulk could be independently modified to include the appropriate molecules for the desired purpose. The flexible chemistry, in fact, allow to functionalize these materials with several capture elements able for the detection of different targets as biomarkers[6-7] or pollutants.[8]

In the diagnostic field, microgels have been extensively applied in bead-based multiplex assays, an evolution of traditional immunoassays. For this purpose, the recognition motif was directly mounted on the surface of encoded microgels to test panels of targets in a single reaction vessel.[2]

Conventional technique for the synthesis of microgels, based on a single-step polymerization, involves a nucleation, aggregation and growth mechanism that ultimately results in a non-uniform distribution of polymer chains throughout the network. Therefore, new strategies has been studied to attain a high control of the particle size distribution, the colloidal stability, and the distribution of specific functional groups.

To do this, core-shell architecture by two-step "seed–feed" polymerization were synthesized.[7] The core-shell architecture resulted was very interesting having hydrogel compartmentalization with differentiated proprieties in both core and the shells and almost all kinds of functional groups could be incorporated into microgel particles by one-pot copolymerization, two-step "seed-feed" polymerization, and post-functionalization.[9] Moreover, changing the recipe, is possible to achieve different phase-transition behavior with temperature or pH.

Several techniques have been used so far to investigate the structural and chemical properties of microgels either directed to the bulk and of surface. On the other hand, not enough studies has been already done for the study of swelling parameters of microgels.

The traditional technique used for macrogels structural characterization is based on the equilibrium swelling theory developed by Flory and Rehner[10] and then modified by Peppas and Merrill.[11] This theory has not been frequently applied to microgels, as difficulties arisen in the measurements of swelling of such micro-objects in the canonical way. Peppas et al. developed a method for the direct determination of mesh size and molecular weight between crosslinks of microgels by applying an equilibrium swelling theory through atomic force microscopy (AFM).

In particular, in their work, particle volume size was determined by average diameter of spherical microgel measured by AFM.[11] Possible deformations due to collapse of microgels on the surface were not considered. In order to overcome the mistake associated with this possible collapse, we propose in this chapter an innovative swelling characterization obtaining by the measure of the volume of each particle directly form AFM images by “Laplacian volume”.

For this characterization, multifunctional microgels with core-shell architecture were synthesized and provided by a wide range of fluorescence-based codes. In particular core double shell microgels, made of poly(ethyleneglycol) dimethacrylate (PEGDMA), were obtained by copolymerization of two different dyes and acrylic acid, all positioned in a spatially controlled manner with the aim to accomplish an encoding system and provide carboxyls as anchoring groups for subsequent conjugations.

2.2 Experimental section

2.2.1 Materials

Poly(ethylene glycol) dimethacrylate (PEGDMA-550 Da), Acrylic acid (AAc), Potassium persulfate (KPS), Fluorescein *O*-methacrylate (Fluo), Polyvinyl alcohol 40-88 (PVA), Dimethyl Sulfoxide (DMSO) were all purchased from Sigma-Aldrich (St. Gallen, CH) and used as received. The dye Methacryloxyethyl Thiocarbamoyl rhodamine B (Rhod) was obtained from Polysciences Inc.

2.2.2 Synthesis of core-shell microgels

Core-shell microgels were prepared first by free-radical precipitation polymerization. Reaction was carried out in a three-neck, 100 mL round-bottom flask to which a filtered aqueous solution of 1% (w/v) total monomer concentration and 1% (w/v) of PVA were added. This solution was heated to ~ 65 ºC while being purged with N_2 gas and stirred vigorously for ~ 1 h. Then initiator, a KPS aqueous solution (to make a final KPS concentration of 0.06 w/v), was added and solution turned turbid, indicating successful initiation. Rhod dissolved in dimethyl sulfoxide (DMSO) (0.1 mL) and diluted with water (1.9 mL), was then added to the stirred mixture at final concentration ranging from 0.1 mM (Table 2.1). The solution was allowed to heat and stir for an additional 7 h while being purged with nitrogen gas. To remove unreacted monomers, oligomers and surfactants microgels were dialyzed for 15 days against distilled water, centrifuged several times, re-suspended in 25 mL of deionized water and stored at 4 °C until further use. The rhodamine-labelled core microgels (R_1) were re-suspended in deionized water to a concentration of 10 mg/mL and used as seeds for subsequent polymerization of additional PEGDMA cross-linked. For the second reaction step, a solution of R_1 microgels (10 mg/mL) in deionized water (25 mL) was heated to 65 ºC under a gentle stream of N_2. Then a PEGDMA solution (0.5% w/v), previously purged with N_2, was slowly

added. Finally, after the temperature remained stable at 65 ºC for ~ 1 h, KPS (final concentration of 1mM) was added to initiate the polymerization (Table 2.1). The reaction was allowed to proceed for 6 h. Microgels (R_1-PEG) so obtained were purified by analogues procedure already described and re-suspended in deionized water. Finally, for the outer shell synthesis, a solution of R_1-PEG microgels (10mg/ml) was heated to 65 ºC, followed by the slow addition of 10 mL of aqueous monomer solution containing PEGDMA (250 mg).

To obtain double shell microgels with different content of Fluo and AAc (R_1-$F_x$$AAc_x$), AAc was added in concentration ranging from 3.6-36 mM. After the temperature remained stable at 70 ºC for ~ 1 h, 2 mL of aqueous solution of KPS (final concentration of 1mM) was added to initiate the polymerization. Fluorescein O-methacrylate diluted in water (2 mL) was then added to the stirred mixture at final concentration ranging from 0.1-0.3 mM to obtain different dye amount (Table 2.1). The reaction was allowed to proceed for 6 h. Again, also double shell microgels were washed, re-suspended in deionized water and then stored at 4 °C prior to use until further use.

Table 2.1: Microgel recipes.
All numbers are reported as mM concentrations of the final solution.

	PEGDMA	RHOD	FLUO	AAC	KPS	PVA
R_1	18.2	0.1	--	--	2.2	48
R_1PEG	9.1	--	--	--	1.1	48
$R_1F_1AAC_{100}$	9.1	--	0.1	36	1.1	48
$R_1F_3AAC_{10}$	9.1	--	0.3	3.6	1.1	48
$R_1F_3AAC_{100}$	9.1	--	0.3	36	1.1	48

2.2.3 Microgels characterization

Particle size of microgels was evaluated by DLS measurements using Dynamic light scattering (Malvern Zetasizer Nano ZS instrument, λ: 633 nm He-Ne laser, 173° scattering angle).

The hydrodynamic diameter (Dh) was determined in the presence of 10^{-3} M KCl as the background electrolyte using a dilute microgels solution 0.1% w/v. A total of 5 runs (each comprised of 3 cumulant cycles) were conducted; the experimental uncertainties represent the standard error of the mean of 5 replicate runs.

2.2.3.1 Swelling characterization

To visualize the morphology and volumes of the microgels in the dried and swollen state, *in-situ* Atomic Force Microscopy (AFM, ScanasystBruker, Germany, GmbH) measurements were performed. In particular, for our experiments "ScanAsyst Fluid+" (Brukerprobes) probes were chosen in order to obtain high-resolution imaging in fluid. About thirty particles were examined for triplicate of each sample, in both dry and wet conditions. A drop of 50 µL of microgel dispersion (~1 µg/mL) was deposited on a glass wafer and dried in a vacuum oven at 40 °C, until weight remains constant. For wet analysis, a solution of phosphate saline buffer (PBS) 10 mM at different pH was added and, for correct measurement, we waited until microgels deposition on the surface. Images were analyzed by Gwyddion-Free SPM (Scanning Probe Microscopy) data analysis software, applying a polynomial surface leveling of first order and afterward particles were selected through a mask to calculate Laplacian volume.

2.3 Results and discussion

2.3.1 Microgels characterization

Multifunctional microgels were obtained through a multistep procedure combining free-radical precipitation polymerization and seeding polymerization, PEGDMA as the main crosslinker. Such particles were designed to respond to the requisites of a multiplex assay having a unique encoding system for each particle, through the

placement of two fluorescent dyes with emission not overlapped, and accommodating an anchoring group on the outmost shell for subsequent conjugations, in this case carboxyl groups (Figure 2.1).

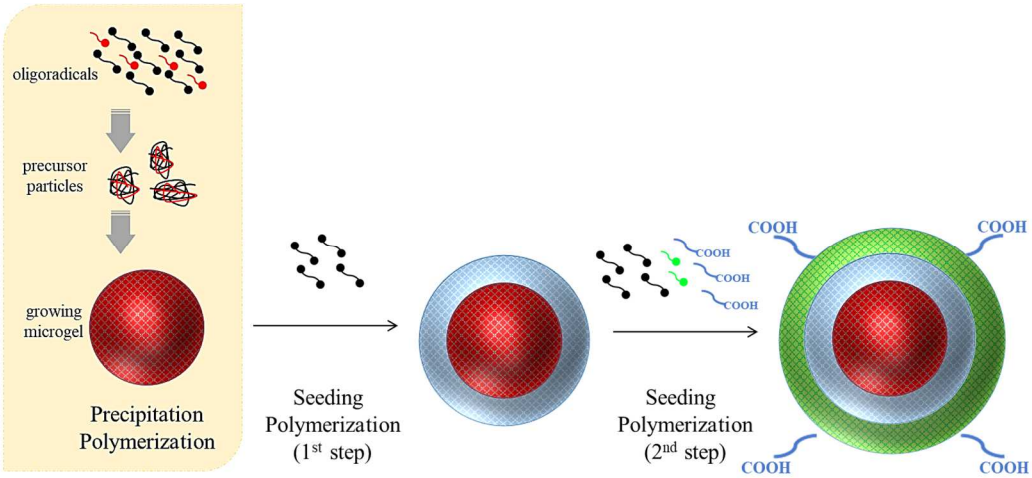

Figure 2.1: Schematic representation of core-shell microgel synthesis obtained combining precipitation and seeded polymerizations.

Microgels obtained by each reaction step were properly characterized by DLS analysis to determine the size distribution and evaluate the effective monodispersity. It is known that DLS on fluorescent microparticles can be, in principle, a problem caused by the possibility of absorption of light by the fluorophores at the wavelength of laser. In order to minimize this undesirable effect, several dilute solutions of our microgels were prepared and tested in order to find the best measurement conditions. In particular, a 0.1% w/v microgels solutions were finally chosen for size measurement. As shown in Figure 2.2, we were able to synthetize monodisperse core microgels (R_1) with a narrow size distribution (549 ± 7 nm), that can be used as seeds for the other layers.

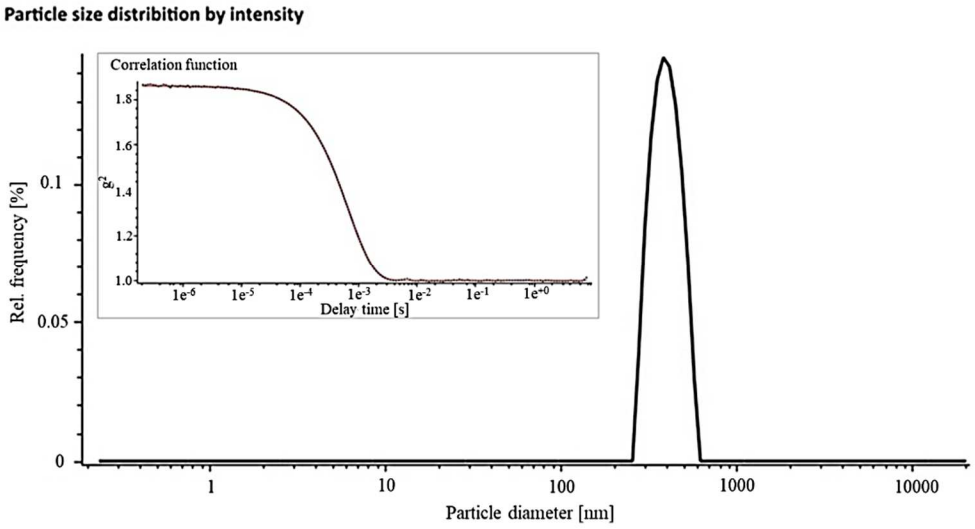

Figure 2.2: DLS analysis: particle size distribution of R1-core.

Similarly, DLS analysis of the first-shell were done, confirming monodisperse microgels with a narrow size distribution (724 ± 16 nm) (Figure 2.3).

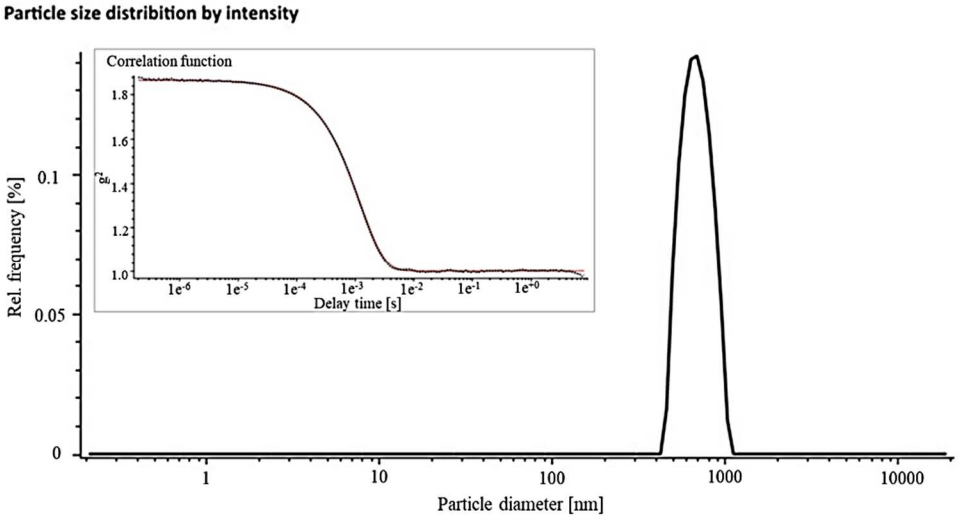

Figure 2.3: DLS analysis: particle size distribution of 1st shell R_1PEG.

Finally, particle size distribution (Figure 2.4) and zeta potential (Figure 2.5) of a second-shell sample ($R_1F_1AA_{100}$) were analyzed. Final core-double shell microgels resulted monodispersed with a narrow size distribution (976 ± 16) and Zeta potential

distribution of -15.4 ± 9 mV. The measurement of charge properties is clearly important in any attempt to estimate electrostatic interactions between microgel particles.

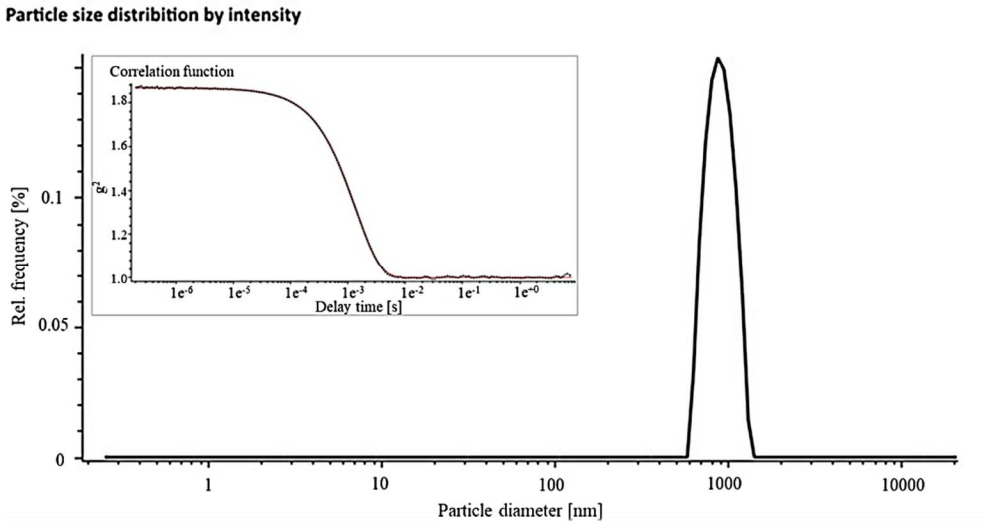

Figure 2.4: DLS analysis: particle size distribution of 2nd shell $R_1F_1AA_{100}$.

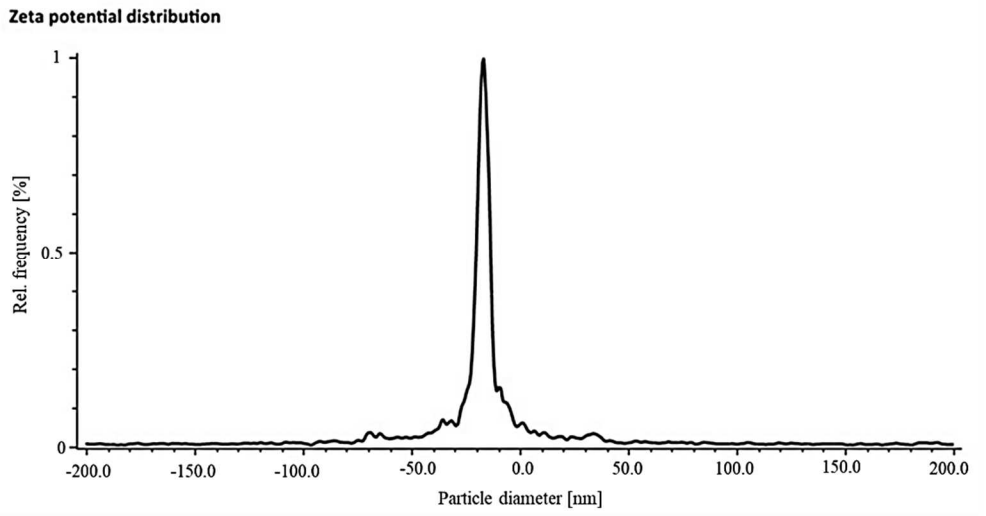

Figure 2.5: DLS analysis: Zeta potential distribution of 2nd shell $R_1F_1AA_{100}$.

2.3.2 AFM characterization

AFM measurements were performed in order to determine morphological features and swelling parameters useful to probe the inside structure of microgels. In-situ AFM measurements were conducted on all samples in dried form and at different pH. First, we measured dried microgels, then an amount of PBS 10 mM pH>8 was added submerging all the microgels. The system was allowed to swell for at least 30 min and images were acquired. Afterwards, measurements in acid conditions were performed on the same regions by exchanging the medium (PBS 10mM at pH<3) allowing microgels to equilibrate for a period of time (about 30 min). Polyelectrolyte hydrogels usually exhibit a variation of their equilibrium swelling as a function of pH according to the acid–base equilibrium for a weak acid: in acidic solution, most of the acidic units remain in the protonated form while they are ionized under basic conditions. Indeed our microgels respond to the different pH collapsing in acid and swelling to their maximum size in base above their pKa (pH>8).

From a morphological point of view, R_1 and R_1-PEG microgels resulted fairly spherical while all the double shell microgels assumed an irregular shape upon the drying process. Indeed, during the drying process, microgels were dried in vacuum at 40 °C producing an alteration of their original shape due to their softness. Moreover, microgels in the swollen state tended to lose their spherical structure remaining stuck on the substrate reaching on average a height far from the original one measured by DLS in solution.

Double shell microgels resulted to be uniform in size, as reported in Figure 2.6, where are shown example of 2D images of $R_1F_3AAc_{100}$ in dry, swollen and relaxed state. From those images, is possible to see more regular and spherical shape in dry with respect to the same wet particles. The resulting profiles, in Figure 2.6-b, revealed an irregular shape in each conditions considered (dry and wet).

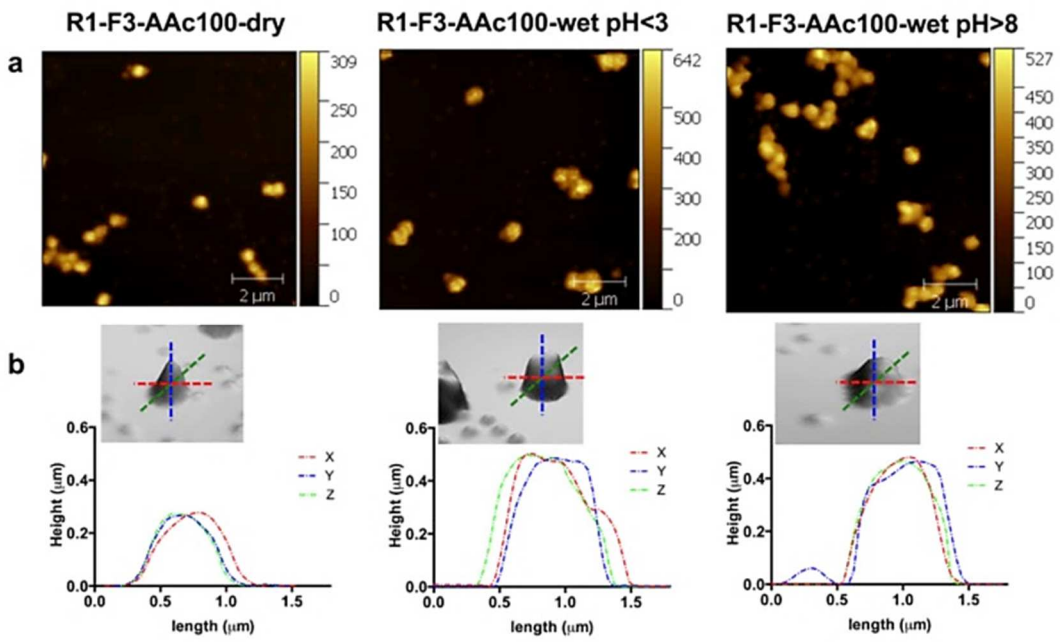

Figure 2.6: (a) AFM images of second shell microgels in dry, relaxed and swollen state. (b) microgels profile taken in three different direction along one microgel in dry, relaxed and swollen state. Reproduced with permission from Ref. [1], Copyright 2016 Wiley.

The measure of particle volume simply through the diameter resulted difficult and unreliable. In the case of $R_1F_3AAc_{100}$ microgels, the profiles taken in three different directions along the center of a microgel were completely different in shape, describing three different areas/volumes and bringing to a misinterpretation of the real volume simply by the diameter. For these reasons we calculated the volume of each particle directly form AFM images by "Laplacian volume".

The images were leveled applying a polynomial surface leveling of first order and creating a mask on the region of particles. In that way we were able to calculate "Laplacian volume" that represents the volume between grain surface and the basis surface formed by Laplacian interpolation of surrounding values. Once volumes were calculated, swelling ratio (Q) was obtained for both swollen (Q_s) and relaxed state (Equation 2.1):

$$Q_s = \frac{V_s}{V_d} \qquad Q_r = \frac{V_r}{V_d} \qquad \text{Equation 2.1}$$

where V_d represents the dry volume, V_s the volume in the swollen state and V_r in the relaxed state. Here we consider microgels in the swollen state when the polymer chains are completely extended (i.e. at pH > 8 for double shell microgels and in PBS at pH 7.4 for not responsive R1 and R1-PEG microparticles). The relaxed state is intended the volume of microgels obtained in acid condition at pH < 3, where the acid groups in the un-dissociated form bring to a partial collapse of the polymer chains.

In Figure 2.7 is reported the graph of swelling ratio that shows a different trend of Q_s and Q_r. As regards Q_s, we can find a constant increase from R_1 to R_1-PEG and the double shell microgels. Indeed the core result to have a higher density with respect to the adlayers: indeed, in this case we reduce the concentration of crosslinker (PEGDA) in the synthesis of the additional layers for 1% to 0.5% w/v. On the other hand, while we were not able to calculate Q_r for the not pH-responsive microgels (R_1 and R_1PEG), the swelling behavior in the relaxed state of double shell microgels showed an increasing trend that basically follows the increase of the monofunctional monomers (Fluo and AAc). Indeed, they represent chain extenders as the relative ratio crosslinker/monomer increase.

Furthermore considering the swelling ratio for each single spherical shell (Q_s*, Q_r*) (taken as separated from the adjacent inner shell) we showed greater differences already in the first shell, which is around 15 times higher than the one calculated for the R_1PEG. In the case of double shell microgels, the swelling behavior of the spherical and the whole microgels followed the same trend ($Q_{s/r}$ vs $Q^*_{s/r}$): we observed here the double contribution due to the different species of monomers and their concentration. Indeed the $R_1F_1AAc_{100}$ resulted more swollen than the other double shell microgels in basic conditions wile in the relaxed state a high degree of collapse is registered (about 4 times). In the series at higher content of Fluo (R_1F_3), the swelling is decreased and the contribution of acid groups seems negligible for both AAc_{100} and AAc_{10} samples.

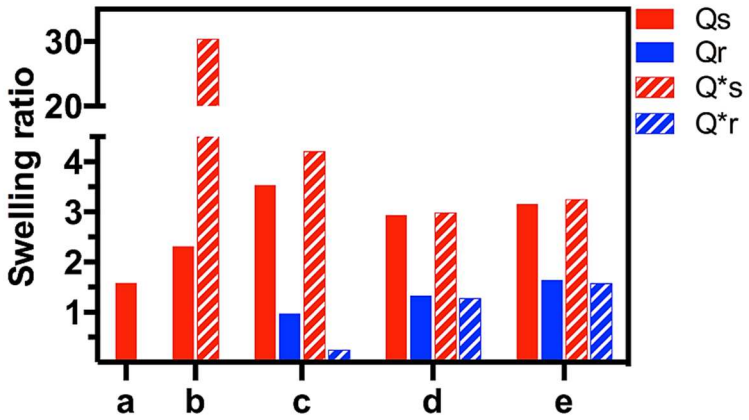

Figure 2.7: Swelling ratio calculated in both swollen and relaxed state for microgels (Q_s, Q_r) and their crown (Q_s*, Q_r*). *a*: core microgel (R_1); *b*: first shell (R_1 PEG); *c*: second shell (R_1-F_1 AA_c100); *d*: second shell (R_1-F_3-AAc_{10}); *e*: second shell (R_1-F_3-AAc_{100}). Reproduced with permission from Ref. [1], Copyright 2016 Wiley.

2.3.3 Swelling characterization

The equilibrium swelling theory allow analyzing the structure of hydrogels that do not contain ionic moieties. As described in chapter 1, for hydrogels prepared in the presence of water is possible to apply Peppas and Merril (Equation 1.7). For our microgels, only in 2nd shell was possible to recognize different value of $v_{2,s}$ and $v_{2,r}$ because of the presence of AAc that produce a pH response. For this reason, in core and 1st shell microgels we applied the simpler Flory-Rehner equation (Equation 1.3). Here we reported characteristic parameters used: interaction parameter PEG/water, χ = 0.426;[12] specific volume, v = 0.91 ml/g; molar volume of water, V_1 = 18.1 ml/mol;[12] uncrosslinked molecular weight of PEG, M_n = 550 Da. Mesh size of a gel is strongly influenced by the degree of crosslinking and by the interaction of the network forming polymer with the solvent. Once $\bar{M}_c$ was calculated, the mesh size (ξ) can be determined applying Equation 1.11. In particular, we used these values: C_n = 4,[12] the molecular weight of the repeating unit of the polymer M_r = 44[12] and the C–C bond length l = 0.146 Å.[12]

Table 2.2: Characteristic parameters of microgels: volume (dry, relaxed and swollen (μm^3)), molecular weight between crosslinks calculated respectively by the Flory-Rehner ($\bar{M}_c$ (Da)) and by Peppas-Merrill ($\bar{M}_c$ * (Da)) formula and mesh size (ξ (nm)).

	V_D	V_R	V_S	$\bar{M}_C$	$\bar{M}_C$ *	ξ
R_1	$5.40 \cdot 10^{-3}$	--	$8.55 \cdot 10^{-3}$	46	--	1.05
R_1PEG	$5.54 \cdot 10^{-3}$	--	$1.28 \cdot 10^{-2}$	115	--	1.94
$R_1F_1AAC_{100}$	$1.57 \cdot 10^{-2}$	$1.53 \cdot 10^{-2}$	$5.55 \cdot 10^{-2}$	194	196	3.55
$R_1F_3AAC_{10}$	$9.45 \cdot 10^{-2}$	$1.26 \cdot 10^{-1}$	$2.78 \cdot 10^{-1}$	163	145	2.70
$R_1F_3AAC_{100}$	$5.98 \cdot 10^{-2}$	$9.82 \cdot 10^{-2}$	$1.89 \cdot 10^{-2}$	176	146	2.64

We observed that from core to first shell $\bar{M}_c$ value increases from 46 Da to 115 Da while ξ passes from 1 nm to 1.9 nm. For double shell microgels instead the $\bar{M}_c$ is 194 Da, 163 Da and 176 Da while ξ is 3.5 nm, 3 nm and 3.2 nm respectively for $R_1F_1AAc_{100}$, $R_1F_3AAc_{10}$ and $R_1F_3AAc_{100}$. Then, in order to remark the AAc effect, we applied Peppas-Merril formula to pH responsive shells (double shell microgels) considering the relaxed state at pH < 3. In this case, we noticed that $\bar{M}_c$ is 196 Da, 145 Da and 146 Da and ξ is 3.5 nm, 2.7 nm and 2.6 nm respectively for $R_1F_1AAc_{100}$, $R_1F_3AAc_{10}$ and $R_1F_3AAc_{100}$. Furthermore, in order to evaluate the presence of eventual overlap region, we did a similar characterization considering only the spherical layers (Figure 2.8).

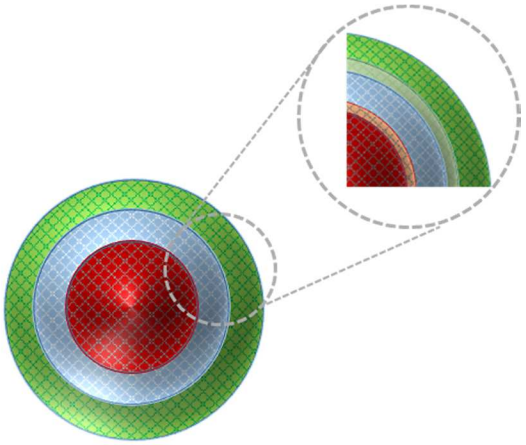

Figure 2.8: Focus on the overlap layer between shells.

Results were summarized in Table 2.3. Comparing results so obtained with previous one, we noticed a significant increase of both $\bar{M}_c$ and ξ calculated only for the spherical shell. Similarly appended also for $R_1F_1AAc_{100}$ while, as regard the series R_1F_3, the differences are minimal.

Table 2.3: Characteristic parameters of spherical-shell: volume (dry, relaxed and swollen (μm^3)), molecular weight between crosslinks calculated respectively by the Flory-Rehner ($\bar{M}_c$ (Da)) and by Peppas-Merrill (Mc* (Da)) formula and mesh size (ξ (nm)).

	$\bar{M}_C$	$\bar{M}_C$ *	ξ
R_1	46	--	1.05
R_1PEG	274	--	4.61
$R_1F_1AAC_{100}$	214	252	4.57
$R_1F_3AAC_{10}$	165	151	2.80
$R_1F_3AAC_{100}$	181	154	2.77

Overall, the discrepancies observed in the swelling behavior could be explained considering the presence of overlapping regions at boundaries between adjacent layers and a certain degree of interpenetration of the shells. In order to evaluate this overlap, we calculated volumetric fraction (χ) of single shell, considered separated from each other in two different ways: the first one (χ_ξ) by mesh size value (Equation 2.2 – Equation 2.3) and the second one (χ_V) by volume values obtained by AFM measurement (Equation 2.4 – Equation 2.5)

$$\xi_{core/1°shell} = \xi_{core}\chi_{core} + \xi_{1°shell}\chi_{1°shell} \quad \text{Equation 2.2}$$

$$\xi_{core/2°shell} = \xi_{core/1°shell}\chi_{core/1°shell} + \xi_{2°shell}\chi_{2°shell} \quad \text{Equation 2.3}$$

$$\chi_{core} = \frac{V_{core}}{V_{core/1°shell}} \quad \text{Equation 2.4}$$

$$\chi_{core/1°shell} = \frac{V_{core/1°shell}}{V_{core/2°shell}} \quad \text{Equation 2.5}$$

Table 2.4: Volumetric fraction calculated by both mesh size values (χ_ξ) and by volume values (χ_V).

	χ_ξ core	χ_ξ 1°shell	χ_ξ 2°shell	χ_V core	χ_V 1°shell	χ_V 2°shell
R_1/R_1PEG	0.75	0.25	--	0.67	0.33	--
R_1PEG/$R_1F_1AAC_{100}$	--	0.21	0.79	--	0.23	0.77
R_1PEG/$R_1F_3AAC_{10}$	--	0.035	0.965	--	0.046	0.954
R_1PEG/$R_1F_3AAC_{100}$	--	0.038	0.962	--	0.068	0.932

When volumetric fraction calculated by mesh size showed different values from the component obtained by volume, probably an overlap occurred and its fraction can be estimated.

Our results showed this discrepancy suggesting the evaluation of the volumetric fraction of overlap. Therefore, we firstly focalized on the core/1stshell layer and, proceeding in similar way described before, we calculated the volumetric fraction of the overlap. It resulted to be ~0.08 so we concluded that it represented a very thin layer. Likewise, 1st/2nd shell overlap was estimated and values were approximately the same. To sum up we can conclude that the overlap between all these three shells exist but it is minimal.

2.4 Core-shell applications as biosensor

Core-shell microparticles so described represent an ideal support for multiplexed bead-based assay. In particular, these microgels were used by Netti's group[13-14] as bioassay based on optical detection (Figure 2.9).

In particular, microgels were used for direct and absolute set of miRNAs properly chosen as cancer biomarkers. After a multistep synthesis, microgels were functionalized with fluorescent DNA-tail, properly modified with –NH_2 group that have to react with the –COOH moiety on the microgels outer shell.

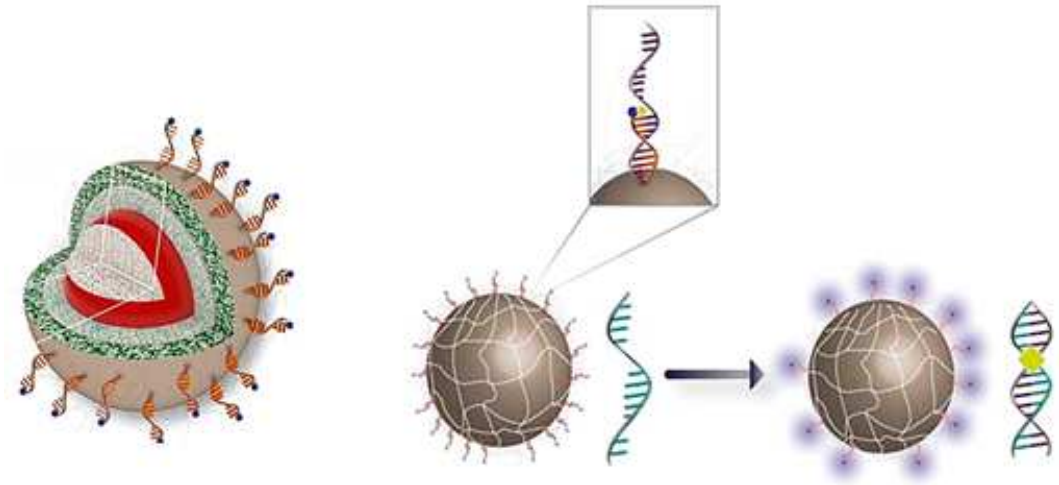

Figure 2.9: Graphical representation of core double shell with mechanism of miRNA detection. Adapted with permission from Ref[13]. Copyright (2015) American Chemical Society.

Moreover, our recent studies, showed the possibility to use these microparticles for an innovative, versatile, specific and sensible assay that combine a new class of biomarkers, the endogenous viral hCMV microRNAs, with a promising technology based on encoded microgel beads.

Microgels so functionalized offer important advantages: first, little changes can be followed by dynamic light scattering, which is sensitive to both swelling and surface charge; second, microgels can be centrifuged and readily re-dispersed, which facilitates cleaning;[14-15] third, flexibility of manipulation in 3D and, finally, microgels are generally more colloidal stable than other nanosized support particles. This kind of microgels are continuously evolving the concepts of the liquid assays representing a material platform with enhanced capability to overcome specific needs.

2.5 Conclusions

In conclusion, here we report a flexible synthesis of fluorescent encoded double-shell microgels. We successfully synthetized multifunctional microgels in a combination

of precipitation and seeded polymerizations demonstrating the ability of the process to obtain well defined particles in terms of inner and outer shell chemistry. We included carboxyl groups on the outer layer that give rise responsivity to pH changes and the potential anchoring group for a capture molecule. The swelling characterization, done combining AFM images and equilibrium-swelling theory, allowed obtaining a detailed characterization of each single layer. The presence of overlap layers was evaluated and estimated negligible. To sum up, the results presented here, and in very recent studies of our group,[7-15] suggest that such microgels represent a valuable tool for the realization of highly hydrated multifunctional particles with extreme flexibility and reproducibility to be used as carrier in diagnostics.

2.6 References

1. Battista, E.; Mazzarotta, A.; Causa, F.; Cusano, A. M.; Netti, P. A., Core− shell microgels with controlled structural properties. *Polymer International* **2016,** *65* (7), 747-755.
2. Birtwell, S.; Morgan, H., Microparticle encoding technologies for high-throughput multiplexed suspension assays. *Integrative Biology* **2009,** *1* (5-6), 345-362.
3. Ulijn, R. V.; Bibi, N.; Jayawarna, V.; Thornton, P. D.; Todd, S. J.; Mart, R. J.; Smith, A. M.; Gough, J. E., Bioresponsive hydrogels. *Mater Today* **2007,** *10* (4), 40-48.
4. Pregibon, D. C.; Toner, M.; Doyle, P. S., Multifunctional encoded particles for high-throughput biomolecule analysis. *Science* **2007,** *315* (5817), 1393-1396.
5. Cusano, A. M.; Causa, F.; Moglie, R. D.; Falco, N.; Scognamiglio, P. L.; Aliberti, A.; Vecchione, R.; Battista, E.; Marasco, D.; Savarese, M.; Raucci, U.; Rega, N.; Netti, P. A., Integration of binding peptide selection and multifunctional particles as tool-box for capture of soluble proteins in serum. *J R Soc Interface* **2014,** *11* (99).
6. Chapin, S. C.; Appleyard, D. C.; Pregibon, D. C.; Doyle, P. S., Rapid microRNA Profiling on Encoded Gel Microparticles. *Angewandte Chemie-International Edition* **2011,** *50* (10), 2289-2293.
7. Causa, F.; Aliberti, A.; Cusano, A. M.; Battista, E.; Netti, P. A., Supramolecular spectrally encoded microgels with double strand probes for absolute and direct miRNA fluorescence detection at high sensitivity. *J Am Chem Soc* **2015,** *137* (5), 1758-61.
8. Manikas, A. C.; Aliberti, A.; Causa, F.; Battista, E.; Netti, P. A., Thermoresponsive PNIPAAm hydrogel scaffolds with encapsulated AuNPs show high analyte-trapping ability and tailored plasmonic properties for high sensing efficiency. *J Mater Chem B* **2015,** *3* (1), 53-58.
9. Jones, C. D.; Lyon, L. A., Synthesis and characterization of multiresponsive core-shell microgels. *Macromolecules* **2000,** *33* (22), 8301-8306.
10. Langer, R.; Peppas, N. A., Advances in biomaterials, drug delivery, and bionanotechnology. *AIChE Journal* **2003,** *49* (12), 2990-3006.
11. Peppas, N. A.; Merrill, E. W. Crosslinked poly(vinyl alcohol) hydrogels as swollen elastic networks Journal of Applied Polymer Science Volume 21, Issue 7 *Journal of Applied Polymer Science* [Online], 1977, p. 1763-1770. http://onlinelibrary.wiley.com/doi/10.1002/app.1977.070210704/abstract (accessed 01).

12. Zustiak, S. P.; Leach, J. B., Hydrolytically Degradable Poly(Ethylene Glycol) Hydrogel Scaffolds with Tunable Degradation and Mechanical Properties. *Biomacromolecules* **2010,** *11* (5), 1348-1357.
13. Causa, F.; Aliberti, A.; Cusano, A. M.; Battista, E.; Netti, P. A., Supramolecular spectrally encoded microgels with double strand probes for absolute and direct miRNA fluorescence detection at high sensitivity. *Journal of the American Chemical Society* **2015,** *137* (5), 1758-1761.
14. Aliberti, A.; Cusano, A. M.; Battista, E.; Causa, F.; Netti, P. A., High sensitive and direct fluorescence detection of single viral DNA sequences by integration of double strand probes onto microgels particles. *Analyst* **2016,** *141* (4), 1250-1256.
15. Causa, F.; Aliberti, A.; Cusano, A. M.; Battista, E.; Netti, P. A. In *Microgels for multiplex and direct fluorescence detection*, 2015; pp 952919-952919-7.

Chapter 3

PEGDA hydrogels as potential engineered-based assay

Abstract. In recent years, development of new detection system, in several fields, has rapidly increased and so there is a growing interest in the research of novel customizable materials. The possibility to control the network structure as well as the swelling behavior is important in the synthesis of materials with tunable final properties. The aim of this chapter is to define a set-up to attain a tailored hydrogel-based material that combine both molecular filter and capture element capability. PEGDA-bulk hydrogels were synthetized by UV radical photopolymerization using different polymer concentrations (10-15-20% w/v). In order to test the molecular filter capability, diffusion studies of several probes (sulforhodamine G and dextrans) with different hydrodynamic radii, were carried out using NMR technique. This analysis showed that only 10%-15% polymer allow obtaining appropriate network for our purposes. Moreover, fluorimetric analysis were fulfilled using functionalized PEGDA-hydrogels, properly obtained polymerizing PEGDA with a methacrylate oligonucleotide. These studies were carried out to evaluate the oligonucleotide diffusion, probe density, efficiency and kinetic of hybridization. Results confirmed that only 10-15% allow probe diffusion. Furthermore, we demonstrated that high probe density obstructs the hybridization. Therefore, we developed a set-up for functionalized hydrogels that merge the best condition of probe density and diffusion transport to allow oligonucleotide capture.

This chapter is part of an article in preparation: **A. Mazzarotta,** T.M. Caputo, L. Raiola, E. Battista, F. Causa, P.A. Netti.- ***"PEGDA hydrogels as potential engineered-based assay."***

3.1 Introduction

In order to accomplish an engineered device useful for molecular recognition is important to find a suitable material and investigate the critical parameters that affect the efficiency of recognition. Because of the concentration of molecules represent an obstacle for recognition, the possibility to use hydrogels as molecular filter is important in order to reduce crowding effects within the hydrogels. Therefore the modulation of both the network structure and capture element concentration allow to obtain a tunable material for efficient molecule capture.

Hydrogels, due to their potentiality such as biocompatibility and high water content, have been of great interest as biomaterials for many years.[1-3] The network is crosslinked by chemical bond or physical entanglements, which give them the ability to swell or shrink, altering the overall structure.[4-8] The most common characterization of this material is based on three parameters: the polymer volume fraction in the swollen state, $v_{2,s}$, the molecular weight between crosslinks, $\bar{M}c$, and the mesh size ξ. The study of these parameters and the suitable modulation to obtain an engineered material, results to be fundamental to understand the network structure that allow us to predict the final properties of our materials.

In this chapter, we focus on the chemical and physical properties of hydrogels that primarily affect the final properties of materials. Particularly we evaluate the parameters that play an important role in the probe diffusion inside the network. The performances of a hydrogel are dependent to a large extent on its bulk structure and on the interaction with solvent molecules.[9] The knowledge and the control at molecular level of hydrogel structure is then a crucial issue in the network customization to permit the diffusion of selected target, based on the size and the chemical content. In fact, hydrogels can work as molecular filter representing a physical barrier for large molecules and repelling unspecific

binding (antifouling property) (Figure 3.1). By the contrast, a specific binding can be achieved adding, during polymerization or in a post modification step, a molecular catcher inside the bulk or on the surface.

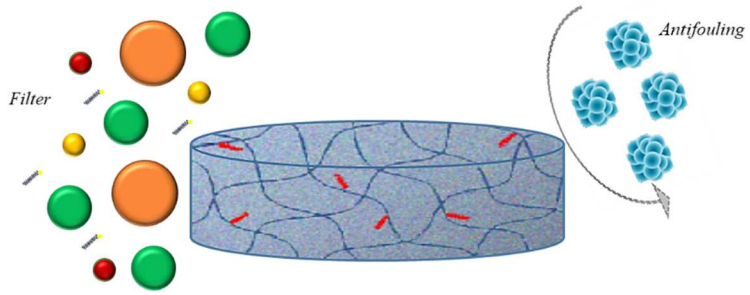

Figure 3.1: Schematic representation of engineered bulk hydrogels.

Several methods for evaluating bulk hydrogel properties are well studied in the last years.[4-7, 9-11] In particular, the swelling ratio and polymer volume fraction in the swollen state can be measured through equilibrium swelling experiment.[7] Then the molecular weight and the mesh size can then be obtained by a theoretical model for swelling of polymer hydrogels.[12]

The structure of hydrogels can be analyzed by the Flory-Rehner theory, subsequently modified by Peppas and Merrill, which developed a theoretical framework that has significant success in describing the hydrogel swelling behaviour.[4, 11]

In addition to these parameters, for many applications, diffusion into the network, controlled by the mesh size of the gel, is important to be investigated. Several information, in fact, can be gained by studying the diffusion of probe molecules through hydrogel networks.[13-14] In the absence of any specific interactions between the probe and the network, the diffusivity of the probe reflects the network structure.[14-16]

Common techniques used to study probe diffusion include source–sink techniques,[17] fluorescence recovery after photobleaching (FRAP),[14, 18] and pulsed

field gradient-NMR (PFG-NMR).[13, 16, 19-21] The key for PFG-NMR analysis is the fact that NMR data render information on the chemical nature as well as on the molecular mobility of an observed component. Nuclear magnetic resonance spectroscopy, most commonly known as NMR spectroscopy, is a technique that exploits the magnetic properties of certain atomic nuclei. It determines the physical and chemical properties of atoms or the molecules in which they are contained. It relies on the phenomenon of nuclear magnetic resonance and can provide detailed information about the structure, dynamics, reaction state, and chemical environment of molecules.

The advantage of this analysis is that works in the absence of concentration gradients, studying instead the chaotic motion of molecules driven by intermolecular collisions.[13] Diffusion times over a large range, usually from few milliseconds up to seconds, are available via PFG-NMR techniques and can be chosen arbitrarily by selecting the correct attenuation parameters.[13]

The study of the probe diffusion on these short timescales, allow obtaining much information on the microscopic structure of materials.[13, 22-26] Furthermore, this technique has the potential to characterize water binding and mobility in a directly quantifiable manner, and has been commonly used in studies of the water–polymer interaction. In particular, it is possible to measure the water self-diffusion coefficient (D) that is directly related to the potential for water to leave a hydrogel.[27]

The identification and study of critical parameters that affect the efficiency of recognition result to be fundamental for the application of these hydrogels for assay. For this application, in fact, not only the network structure affect the adequacy of the assay but also the concentration of molecules, representing an obstacle for recognition. Appropriate diffusion studies are fundamental to evaluate the molecules crowding effect and avoid the unwanted obstruction.

3.2 Experimental section

3.2.1 Materials

Poly(ethylene glycol)diacrylate (PEGDA-700 Da), Deuterium oxide (D_2O), Sulforhodamine G, Albumin-fluorescein isothiocyanate conjugate (BSA), Ethanol and Diethyl ether were purchased from Sigma-Aldrich (St. Gallen, CH) and used as received. Crosslinking reagent 2-Hydroxy-2-methylpropiophenone (DAROCUR 1173) was provided from Ciba. Texas Red labelled dextrans with different molecular weight (3 kDa, 10 kDa and 40 kDa) were supplied by Thermo Fisher Scientific. DNA oligonucleotides were purchased from Metabion with HPLC purification. NMR tubes, properly designed for gel samples, were supplied by New Era Enterprises, Inc and OptiPlate-96 F HB were purchased by PerkinElmer.

3.2.2 Synthesis of bulk-hydrogel

The bulk-hydrogels were synthesized using a UV free radical photopolymerization. The process involves three basic steps (Figure 3.2). First, a free radical must be formed through the initiation step. For the PEGDA system used in this work, the initiator is darocur, which forms a free radical under UV light (Figure 3.2 a). The next step is known as propagation, where the free radical from the initiator comes into contact with the end of a PEGDA molecule and reacts with the carbon-carbon double bond in the acrylate functional group (Figure 3.2 b). This step produces a second free radical species, which can go on to react with more PEGDA polymers propagating the crosslink. The final step in the process of this polymerization is termination, which occurs when two radical species meet and a bond forms between them. A general reaction scheme for a difunctional polymer forming a network is reported in (Figure 3.2 c).

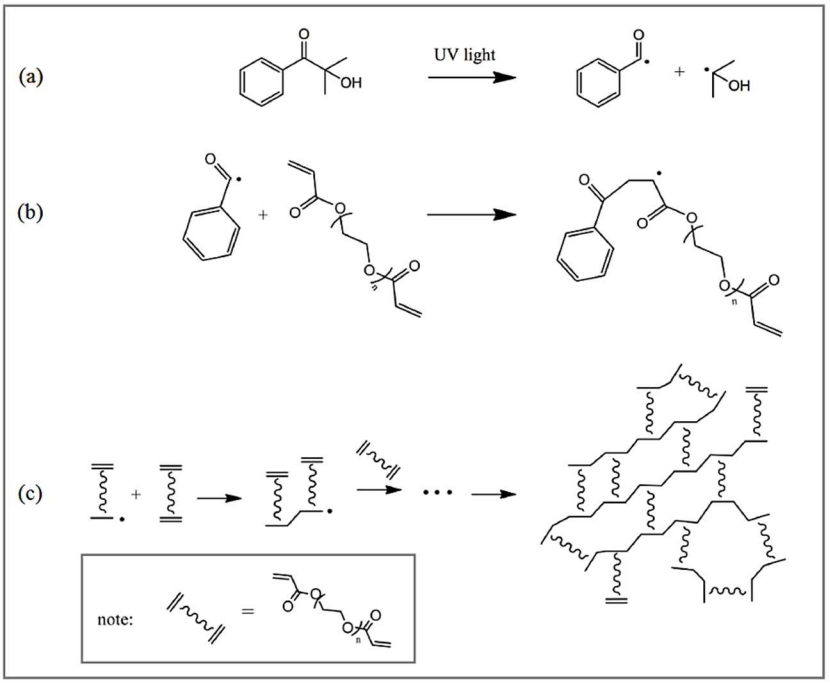

Figure 3.2: UV free radical photopolymerization: (a) Initiation mechanism, (b) Propagation mechanism, (c) Formation of a crosslinked polymer network.

Our mixture was composed of poly(ethylene glycol) diacrylate (PEGDA, 700 Da), at different concentrations in Milli-Q water and darocur used as initiator. Each hydrogel sample was prepared dissolving photoinitiator in 10 mL of polymer solution, obtaining a darocur final concentration of ~0.1% v/v (Table 3.1). The reaction mixture was strongly mixed and then purged with high purity nitrogen for 5 minutes to remove the excess of oxygen that may interfere with the free radical polymerization. The reaction mixture was then carried out in 10 mL test tubes and illuminated with UV lamp (λ = 365 nm and power-lamp = 10 W) for 5 minutes leading to complete polymerization. For NMR studies, we reduced the total reaction volume to 1 mL of deuterated water (Table 3.1). Polymerization was performed directly in special NMR tubes designed for gel samples. Hydrogel samples were than expelled from the NMR tube and put in a solution of D_2O for the next 24h to remove all the unreacted materials. Hydrogels were dried in oven at 30°C for few hours, swelled with 1 mL of probe solution and finally put in the NMR tube for the

measurement. In particular, different probes, sulforhodamine G and several dextrans (3 kDa, 10 kDa and 40 kDa) were dissolved in D_2O to reach a final concentration of 1 mg/mL.

Moreover, functionalized bulk were synthesized using UV free radical photopolymerization between PEGDA and oligonucleotide, properly modified with methacrylamide moieties. Propagation step of the reaction between polymer and methacrylate oligonucleotide is highlighted in Figure 3.3.

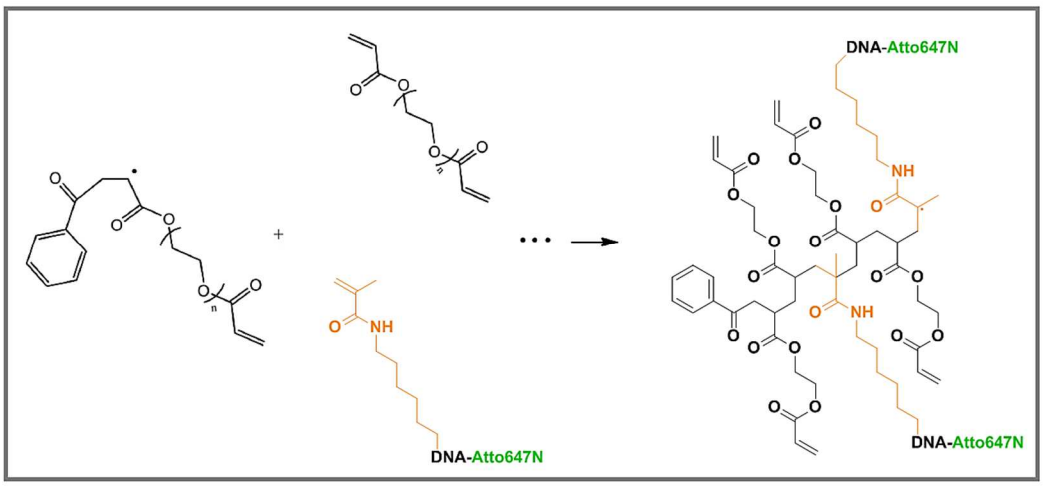

Figure 3.3: UV free radical photopolymerization between PEGDA and methacrylate oligonucleotide.

Several recipes with different PEGDA and oligonucleotide concentrations were prepared and tested. The mixture was composed of PEGDA (MW 700 Da) at different concentrations (10-15-20% w/v) in buffer solution, darocur as initiator and fluorescent oligonucleotide methacrylate (F-DNA-Tail) at different concentrations (1µM-5µM) (Table 3.1). Our buffer solution was obtained adding 1 x PBS and NaCl 200 mM in milliQ water. The reaction mixture was strongly mixed and then purged with high purity nitrogen for 5 minutes to remove the excess of oxygen that may interfere with the free radical polymerization. Then, 100µL of the mixture was carried out in 96-optiplate, illuminated with the same UV lamp used before for 5 minutes leading to complete polymerization.

Table 3.1: Bulk hydrogels recipes.

	PEGDA (% w/v)	SOLVENT	DAROCUR (% v/v)	OLIGONUCLEOTIDE
B-10%	10%	H_2O	0.1%	--
B-15%	15%	H_2O	0.1%	--
B-20%	20%	H_2O	0.1%	--
B-25%	25%	H_2O	0.1%	--
B-30%	30%	H_2O	0.1%	--
N-10%	10%	D_2O	0.1%	--
N-15%	15%	D_2O	0.1%	--
N-20%	20%	D_2O	0.1%	--
F_1-10%	10%	Buffer solution	0.1%	1 μM
F_1-15%	15%	Buffer solution	0.1%	1 μM
F_1-20%	20%	Buffer solution	0.1%	1 μM
F_2-10%	10%	Buffer solution	0.1%	5 μM
F_2-15%	15%	Buffer solution	0.1%	5 μM
F_2-20%	20%	Buffer solution	0.1%	5 μM

3.2.3 Bulk-hydrogel characterizations

Several characterization, attained due to NMR and fluorometer measurements, were accomplished on different bulk samples to define the structural and diffusion properties of these materials in both PEG-bulk and functionalized-hydrogels.

3.2.3.1 Swelling characterization

Swelling characterization of hydrogels were carried out in order to calculate polymer volume fraction in swollen state ($v_{2,s}$). It was evaluated starting from the mass of hydrogel measured in both swollen and dry conditions. Once polymerized, hydrogels were removed from the glass tubes, uniformly cut into samples of short cylindrical

shape and then immersed in an excess of milli-Q water in order to remove the unreacted reagents. Water was changed several times for the next 24 h and samples were then swollen overnight in water at room temperature. Then cylindrical parts were gently wiped with a filter paper and weighted to obtain the mass of swollen hydrogel (m_s). For dried measurement, in order to obtain a total dehydration, hydrogels were properly grinded and lyophilized overnight, so the mass of dry samples were recovered (m_d). Therefore, we were able to determined hydrogel volume in both swollen and dry state, using Equation 3.1:[28]

$$v_{2,s} = \frac{1}{1+\frac{\rho_{polymer}}{\rho_{solvent}}\left(\frac{m_s}{m_d}-1\right)} \qquad \text{Equation 3.1}$$

were $\rho_{polymer}$ = 1.12 g/ml and $\rho_{polymer}$ = 1 g/ml. Moreover, the water contents of the gels, which represent the mass fraction of water (F_{water}) in the swollen condition, were calculated using Equation 3.2:

$$F_{water} = \frac{m_{swollen}-m_{dry}}{m_{swollen}} \qquad \text{Equation 3.2}$$

where $m_{swollen}$ and m_{dry} are, respectively, the weight of the swollen and dry hydrogels. Then, using equations described in chapter 1, polymer volume fraction (Equation 1.6), molecular weight between crosslinks (Equation 1.3) and mesh size (Equation 1.11) were calculated.

3.2.3.2 NMR measurement

NMR analysis was performed using an Agilent 600 MHz (14 Tesla) spectrometer equipped with a DD2 console. ^{1}H-1D-NMR spectra were recorded at 300 K with 64 scans to obtain a good signal to noise ratio. Diffusion spectra were recorded at 300 K using a Dbppste (DOSY bipolar pulse pair stimulated echo) pulse sequence Figure 3.4.

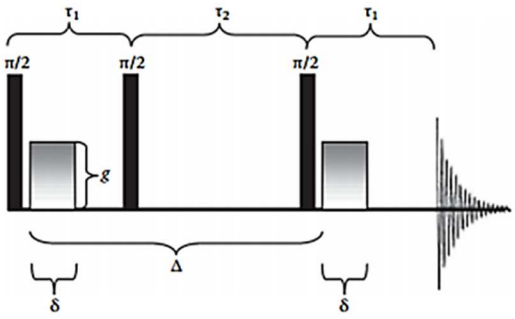

Figure 3.4: DOSY sequence[29].

An array of 15 pulse field gradient values from 0:98 to 63:7 Gauss/cm were used with a gradient pulse length (δ) of 2 ms. Diffusion delay (Δ) in ms was optimized for each sample to obtain a ratio of 1:0.2 between I(Gmin) and I(Gmax), where I(Gmin) is the intensity of the NMR peak at the minimum gradient value and I(Gmax) is the intensity of the NMR peak at the maximum gradient value. Diffusion coefficients were calculated using the formula reported in Equation 3.3:

$$I(\delta, \Delta) = I_0 \, exp\left[-D\gamma^2 g^2 \delta^2 \left(\Delta - \frac{\delta}{3}\right)\right] \qquad \text{Equation 3.3}$$

where I and I_0 are the spin echo amplitudes in the presence and in the absence of a magnetic field gradient pulse, respectively; γ is the gyromagnetic ratio of the given nucleus, Hz/T, and g is the magnetic gradient, T/m. NMR data were processed and analyzed using VNMRJ4 software.

3.2.3.3 Fluorescent measurement

In order to evaluate the best concentration of both polymer and oligonucleotide and to check the effective hybridization of Fluorescent-DNA-Tail and BHQ-strand, fluorescence analysis were done. Fluorescence spectra of fixed amount of labelled oligonucleotides were collected in a 1 cm path length cuvette with a Horiba JobinYvon model FluoroMax-4 fluorometer equipped with a Peltier temperature

controller. The conjugated and unconjugated sequences were excited at 647 nm with a slit width of 5 nm, and emission spectra were collected from 667 to 750 nm with a slit width of 5 nm. Then, using a 2300 EnSpire multilabel reader (Perkin-Elmer, Waltham, MA) several tests on the functionalized hydrogel samples were done. Fluorescence was measured from the top of the plate, with excitation wavelength of 647 nm, and emission wavelength at 667nm, height 9mm and 500 number of flash.

3.3 Results and discussion

3.3.1 Swelling characterization

The bulk-hydrogels were synthesized using a UV free radical photopolymerization. Several recipes, using different polymer concentration (10-15-20-25-30 % w/v), were tasted in order to obtain various network structure with different molecular filter capability. In Table 3.2 are summarized water content (F_{water}) and all fundamental swelling parameters ($v_{2,s}$, Q, $\bar{M}_c$, ξ) for each preparation. Firstly, we noticed a range of water content from 91% up to 73% with increasing of polymer concentration. Moreover, changing the PEGDA concentration, polymer volume fraction in the range of 0.08-0.24 was obtained. As expected, Q, $\bar{M}_c$ and ξ decreased with increase of polymer concentration. In fact, the equilibrium-swelling ratio decreased from 12.6 to 4.1 as the crosslink density increased. The molecular weight between crosslinks decreased from 340 to 259 Da as the percent polymer fraction increased from 10 to 30% (w/v). Mesh size were achieved in the range of 2.6-1.6 nm, as reported in Figure 3.5. All these results are attributable to the fact that as the amount of polymer present for crosslinking in the hydrogel increases, the degree of crosslinking increases and thereby decrease both the average molecular weight between crosslinks, the equilibrium-swelling ratio and mesh size.

Table 3.2: Properties of bulk hydrogels of PEGDA.
All values were calculated from averaged measured values.

	PEGDA 10%	PEGDA 15%	PEGDA 20%	PEGDA 25%	PEGDA 30%
F_{water}	91.2% ± 0.1%	87.2% ± 0.1%	82.7% ± 0.1%	78.2% ± 0.1%	73.5% ± 0.1%
$v_{2,s}$ ($\cdot 10^{-3}$)	79.2 ± 0.9	116.2 ± 1.8	157.5 ± 0.5	199.3 ± 0. 5	243.4 ± 0.4
Q	12.63 ± 0.14	8.61 ± 0.14	6.349 ± 0.018	5.017 ± 0.012	4.109 ± 0.008
$\bar{M}_c$ (Da)	340.43 ± 0.21	329.35 ± 0.66	311.62 ± 0.23	288.24 ± 0.30	259.06 ± 0.31
ξ (nm)	2.652 ± 0.011	2.299 ± 0.014	2.022 ± 0.003	1.800 ± 0.002	1.597 ± 0.002

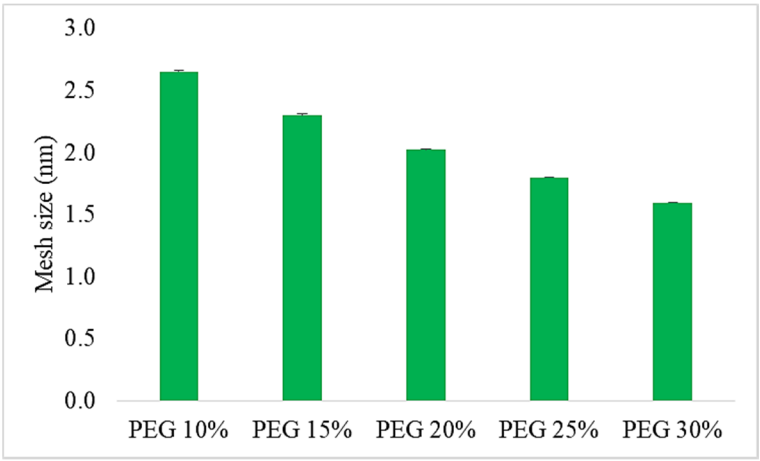

Figure 3.5: Mesh size values for different bulk-PEGDA concentrations.

These results confirm that the polymer concentration permit to optimize the network density for the specific purpose.

3.3.2 NMR: diffusion studies

3.3.2.1 Hydrogels polymerization

One-dimensional ^{1}H-NMR spectra of PEGDA/darocur solution were recorded before and after UV treatment to confirm that polymerization was completed. In Figure 3.6 ^{1}H-NMR spectra of PEGDA/darocur solution before polymerization is

shown. Very intense peaks at 3.73 (*f*), 3.85 (*e*) and 4.38 (*d*) ppm are typical of PEG main chain methylene group while peaks *a*, *b* and *c* in the olefinic region (6.0 to 6.6 ppm) refer to PEGDA terminals acrylic protons. Peaks in the aromatic region (*a'*, *b'* and *c'* from 7.5 to 8.2 ppm) and singlet at 1.45 ppm (*d'*) become, respectively, from aromatic and methyl groups protons of darocur. Broad peak at 4.65 ppm is the H_2O residual signal. Peak integrations demonstrate chemical structures of solution components and their related amount in the mixture. Moreover, signals attribution was confirmed by ^{1}H-NMR spectra of individual components, reported in Appendix A.

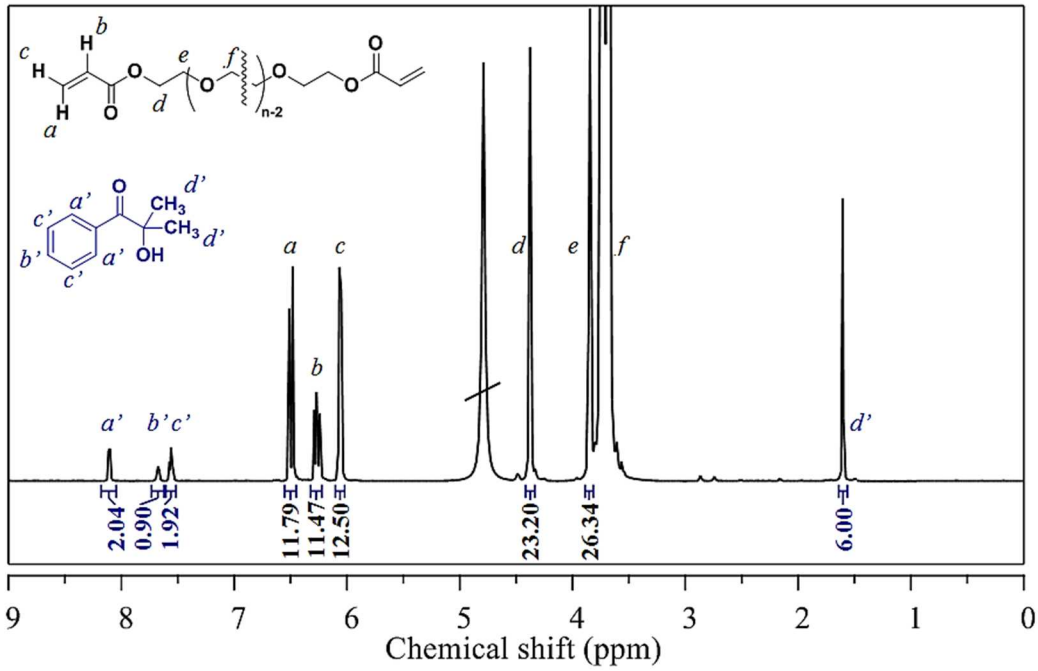

Figure 3.6: ^{1}H-NMR spectrum of PEGDA/darocur solution before polymerization with signal attribution and related peak integration.

In Figure 3.7 is shown H^1-NMR spectra of the same PEGDA/darocur solution after polymerization. Complete polymerization was confirmed by the disappearing of the PEGDA acrylic signals. In addition, the very broad peak from 4.5 to 3.5 ppm showed the transition of PEG chains from a very flexible situation (solution) to a less flexible

state (hydrogel). Relative decrease of the darocur peak intensities also confirmed that a large amount of the initiator was consumed in the polymerization reaction. Again, the broad peak at 4.65 ppm is the H_2O residual signal.

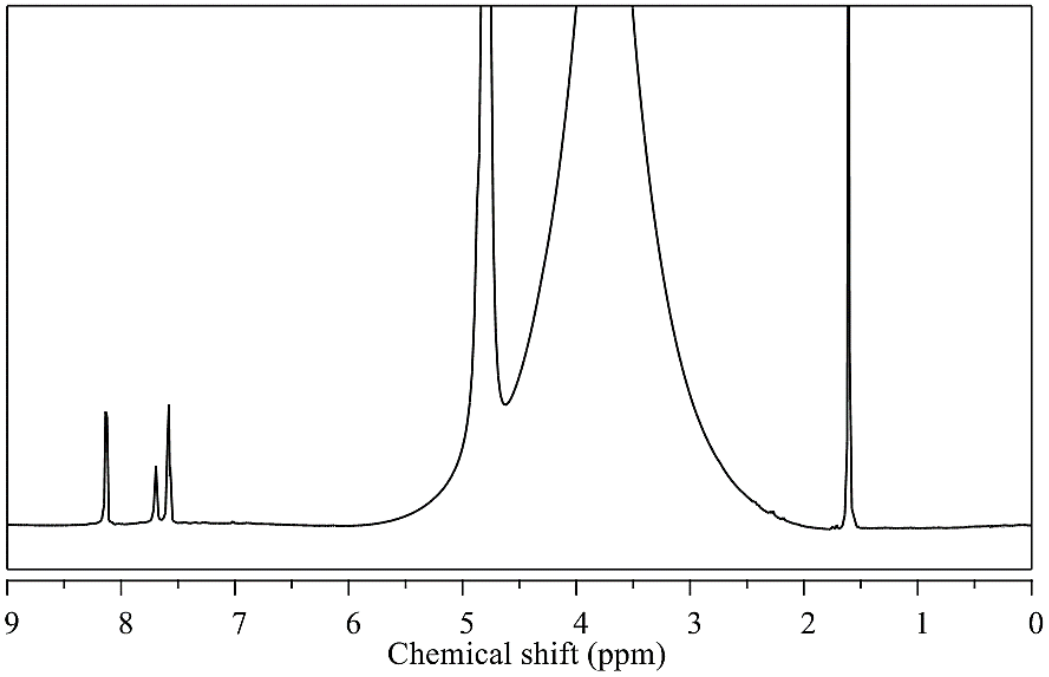

Figure 3.7: ^{1}H-NMR spectrum of PEGDA/darocur solution after polymerization.

3.3.2.2 Water diffusion

DOSY experiments were used to study the diffusion of molecules, with different size, in hydrogels samples prepared with a PEGDA concentration of 10%, 15% and 20% (w/v). Firstly, we evaluated the water self-diffusion coefficient. Measurement resulted to be 24.55 ± 0.11 ($\cdot 10^{-10}$ m^2/s), in agreement with literature data.[30] Furthermore, diffusion coefficient of solvent in the first hydration shell of hydrogels sample was calculated. Results indicated that water diffusion coefficient was affected by the PEGDA concentrations as shown in Table 3.3 and Figure 3.8. (Fitting curve reported in Appendix B).

Table 3.3: Diffusion coefficients (10^{-10} m^2/s) of water in PEGDA hydrogels.

	PEGDA 10%	PEGDA 15%	PEGDA 20%
Water	18.84 ± 0.03	16.05 ± 0.02	15.08 ± 0.13

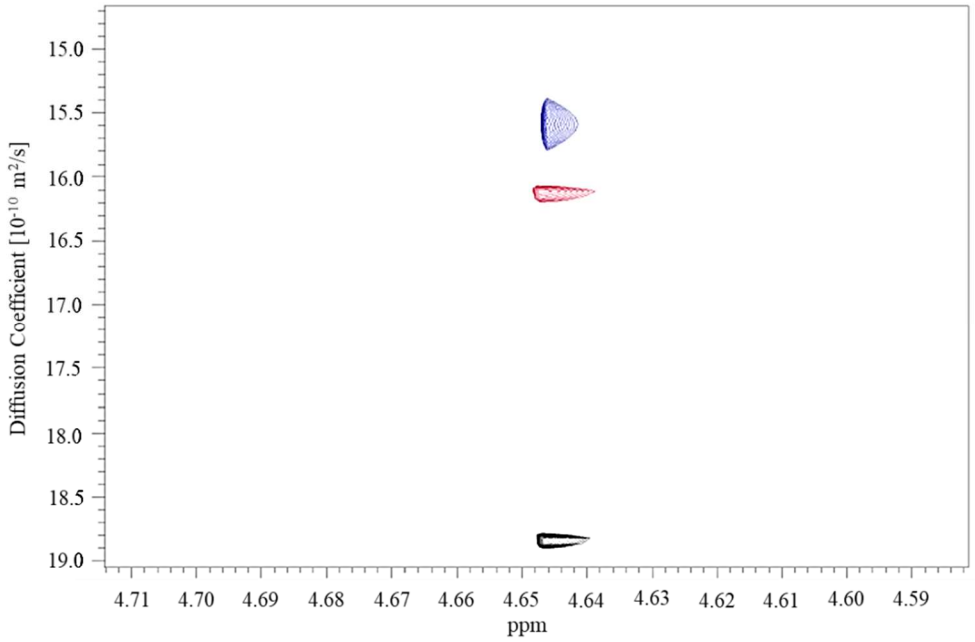

Figure 3.8: 2D DOSY of water (4.645 ppm) in hydrogels bulk with different PEGDA concentrations (20% in blue, 15% in red and 10% in black).

Finally, we evaluated the relation between diffusion coefficients and water content previously calculated. As reported in Figure 3.9, diffusion coefficients increased with increasing of $F_{water.}$ In particular, as the number of water molecules per unit mass of polymer increases, the ability of water molecules to diffuse increase, approximately linearly, toward that of free water (100% F_{water}). These results are comparable with data obtained by McConville et al.[27] In their work, was reported a measurements of the water self-diffusion coefficient for a set of nine commercially available contact lens hydrogels, both at equilibrium water content (EWC) and as a function of reduced water content, using the pulsed field gradient NMR method.

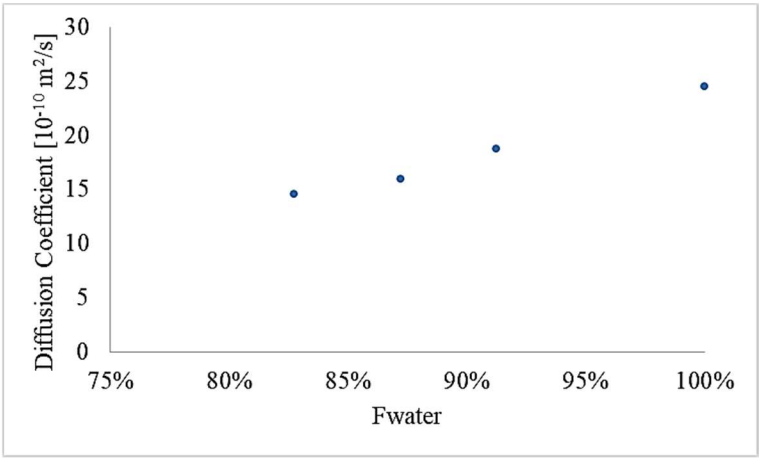

Figure 3.9: Diffusion coefficient versus water content for hydrogels sample.

3.3.2.3 Probes diffusion

Probes were properly chosen to simulate the behavior and diffusion of biological molecules. In particular, the smallest dextran (3 kDa) has hydrodynamic radius comparable with oligonucleotide (that represent molecule that we want to capture). On the other hand, 40 kDa dextran and blood proteins, such as albumin, have similar hydrodynamic radii and represent molecules that we want to exclude from our network. In order to validate our choice, hydrodynamic radii of sulforhodamine G and dextrans (3 kDa, 10 kDa, 40 kDa) were calculated using Einstein-Stokes equation (Equation 3.4), where K_B is the Boltzmann's constant, T is the absolute temperature and η is the viscosity of D_2O and D_0 is their diffusion coefficient in water, measured by DOSY-NMR.

$$R_h = \frac{1}{D_0}\frac{K_B T}{6\pi\eta} \qquad \text{Equation 3.4}$$

Results (Table 3.4) showed that probes diffusion coefficients in D_2O (D_0) were in the range of 0.5-3.7 [10^{-10} m^2/s] and their hydrodynamic radii had values between 3.9 and 0.6 nm. These results were comparable with the range size between small oligonucleotides and large molecules that we need to investigate for biological

studies. Our results are comparable with hydrodynamic radii and diffusion coefficients reported in literature, obtained both by NMR[31] and other different techniques such as diffusion measurement through microporous membrane filters,[32] fluorescence correlation spectroscopy (FCS)[33] and fluorescence recovery after photobleaching (FRAP).[34]

Table 3.4: Diffusion coefficient of different probes in D_2O and respective hydrodynamic radii.

	D_0 [10^{-10} m^2/s]	R_0 [nm]
Sulforhodamine G	3.67 ± 0.06	0.61 ± 0.01
Dextran 3kDa	1.60 ± 0.03	1.34 ± 0.01
Dextran 10kDa	0.91 ± 0.01	2.41 ± 0.01
Dextran 40kDa	0.557 ± 0.008	3.92 ± 0.03

In Figure 3.10 were reported, in double logarithmic plot, diffusion coefficients of these probes as function of their molecular weight. Our trend (black point) show a linearity in agreement with literature data of Callaghan et al (red triangle) which studied a self-diffusion of several dextrans both in water and in a polydisperse polymer system.[31] These results showed the effective relation between molecular weight and diffusion coefficient which strictly decrease with increasing of probe molecular weight.

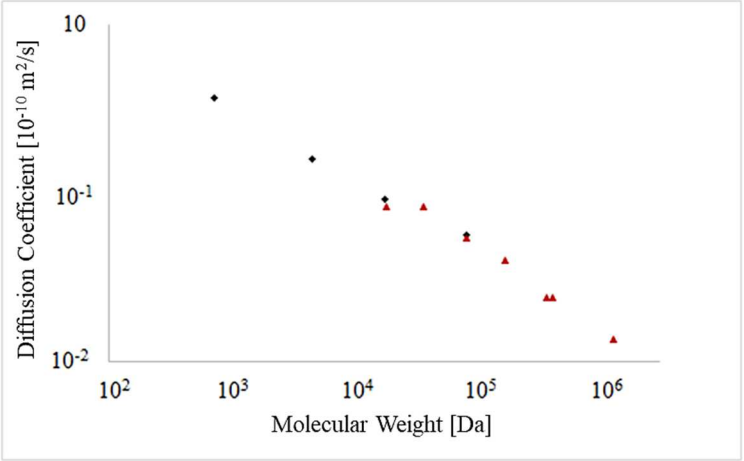

Figure 3.10: Probe diffusion coefficient as function of its molecular weight. Comparison between data obtained by this thesis (•) and literature data (▲).[31]

Afterwards, probes diffusion coefficients in bulk hydrogels (10%, 15%, 20% w/v) were calculated, as reported in Table 3.5.

Diffusion coefficient of small molecules, as sulforhodamine G (SR-G), should not be affected by a very large network structure and their values should be comparable with free diffusion of probe in water.[35] On the other hand, for bigger molecules as dextrans with different molecular weight, we expect a decreasing trend of diffusion coefficient values from the water solution to the highest polymer percentage hydrogel. Results, reported in Figure 3.11, confirmed those hypotheses.

Table 3.5: Diffusion coefficient ($\cdot 10^{-10}$ m^2/s) of water and different probes in both water and PEGDA hydrogels.

	WATER	**PEGDA 10%**	**PEGDA 15%**	**PEGDA 20%**
Water	24.55 ± 0.11	18.84 ± 0.03	16.05 ± 0.02	15.08 ± 0.13
Sulforhodamine G	3.67 ± 0.06	3.14 ± 0.15	3.11 ± 009	3.10 ± 0.24
Dextran 3kDa	1.60 ± 0.03	0.87 ± 0.12	0.63 ± 0.02	0.46 ± 0.04
Dextran 10kDa	0.91 ± 0.01	0.27 ± 0.02	0.234 ± 0.001	0.120 ± 0.005
Dextran 40kDa	0.557 ± 0.008	0.160 ± 0.001	0.140 ± 0.006	0.090 ± 0.003

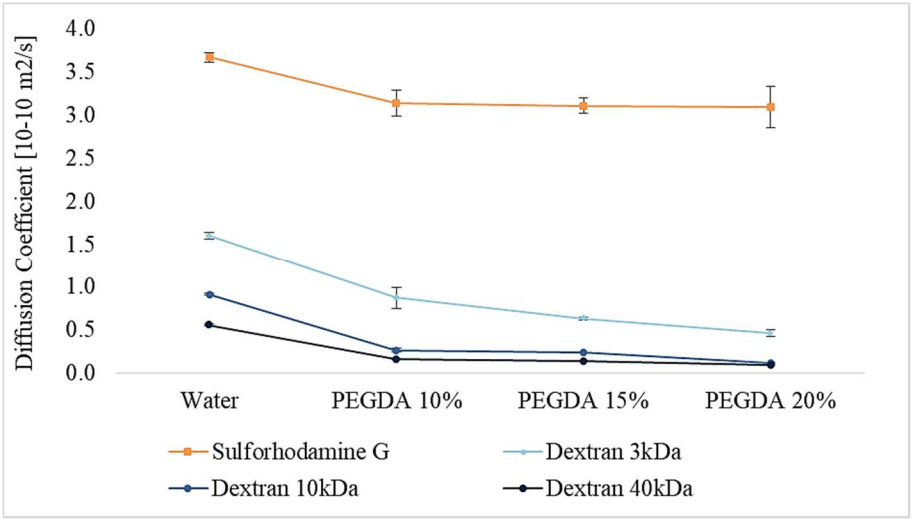

Figure 3.11: Diffusion coefficient of several probes in both water and hydrogels with different PEGDA concentrations.

Moreover, the effect of the polymer concentration on the reduction of diffusion coefficients was highlighted in Figure 3.12, where D/D_0 was plotted against polymer concentration.

D/D_0 values of water and sulforhodamine G, the smallest probe, resulted to be constant (~85%) for all PEGDA concentrations; by the contrast, dextrans probe showed a significant mobility reduction, related with the polymer concentrations.

In particular, for 3 kDa dextran, D/D_0 decreased from 55 % in the wider network up to 30% in the tighter one. Instead, both 10 kDa and 40 kDa had similar trend, between 30% and 15%, that confirms the mobility of these bigger molecules resulted to be deeply affected by the polymer network.

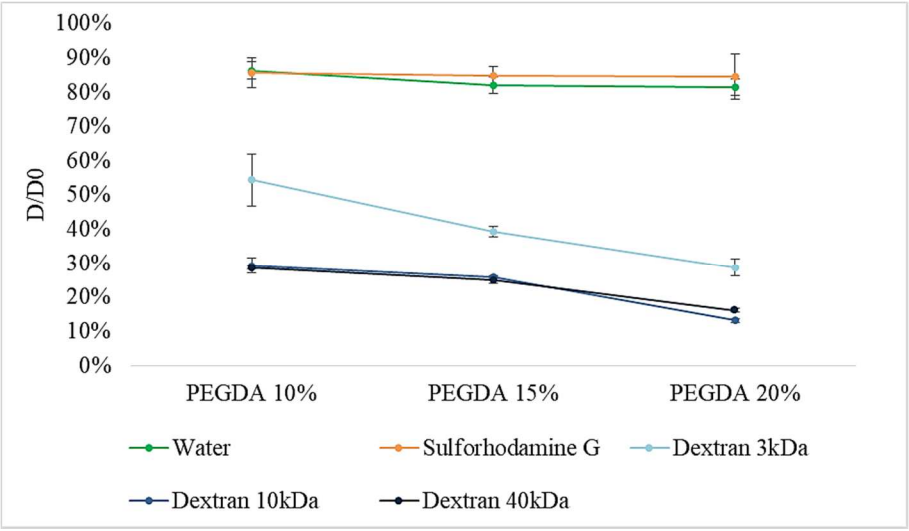

Figure 3.12: Effect of the polymer concentration on the reduction of diffusion coefficients (D/D_0).

Furthermore, in Figure 3.13 we plotted diffusion coefficients of dextrans probes as function of their hydrodynamic radius, in both water (D_0) and in three different polymer network ($D_{PEGDA10\%}$, $D_{PEGDA15\%}$, $D_{PEGDA20\%}$). For water solution and for 10-15% (w/v) of polymer concentrations, diffusion coefficients linearly decreased with hydrodynamic radii. Instead, probes diffusion coefficients in PEGDA 20%

(w/v) changed its trend showing that, in this network, diffusion of dextrans 10 kDa and 40 kDa was strictly hindered.

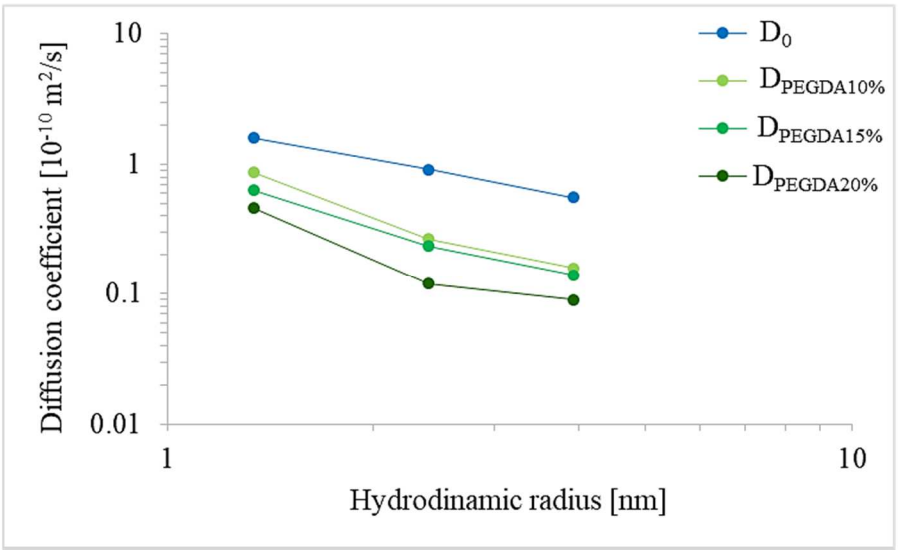

Figure 3.13: Diffusion coefficients of dextrans probes as function of their hydrodynamic radius obtained in water (•), PEGDA 10% (•), PEGDA 15% (•) and PEGDA 20% (•).

Pluen et al.[34] described in their work the diffusion of several macromolecules in agarose gels, applying different models to characterize the network.

With our studies, instead, we demonstrated the possibility to simplify their characterization combining DOSY diffusion measurement with swelling characterization, obtaining several information about our polymer network.

To sum up, NMR analysis show that hydrogels whit different PEGDA concentrations are able to exclude big molecules by their low diffusion coefficient.

Moreover, we can modulate the diffusion of the probe modifying the mesh size of the network, changing the PEGDA concentrations. In particular, dextran 3 kDa seems to be still able to pass through all the gels we made while dextrans 10 kDa and 40 kDa showed a very low diffusion also in the wide network.

As a matter of fact, our results indicate that it is possible to make a tunable PEGDA hydrogel with specific control of its network and use it as molecular filter.

3.3.3 Preliminary study for the assay

Preliminary studies for the detection assay optimization were fulfilled using a probe scheme already tested in previous work of our group.[36] The probe scheme was schematically reported in Figure 3.14

Figure 3.14: Scheme of oligonucleotide detection.

where fluorescent T-DNA is a short fluorescent DNA tail (12 nt), labelled at 5' end with ATTO 647N and modified at 3' with methacrylamide spacer to allow its covalent bound with polymer network. A Quencher strand (21 nt), internally modified with a Black Hole Quencher (BHQ), was used as probe diffusion.

When the tail hybridize, the BHQ comes in close proximity with the fluorophore and fluorescence quenching occurs.

For our studies, we used three DNA-sequences as reported in Table 3.6: fluorescent T-DNA that was covalently bounded with polymer network; complementary sequence (C) for the hybridization studies and non-complementary sequence (N) as control.

Table 3.6: Sequence and thermodynamic parameters of the DNA probes used in this study.

probe	sequence (5'-3')	length (nt)
Fluorescent T-DNA (F-DNA-Tail)	TG AAA TCG GTT A	12
Complementary sequence (C)	T AAC CGA TTT CG ATG GTG CTA	21
Non-complementary sequence (N)	GAG CUA CAG UGC UUC AUC UCA	21

In order to check the quenching efficiency of fluorescent tail with quencher strand, we firstly studied this system in 1M PBS solution. We tested different tail concentrations (5 µM - 0.1 µM) and BHQ-strand was added 1:1 respect to the tail. Results showed a quenching percentage from ~93% to 88% (Figure 3.15).

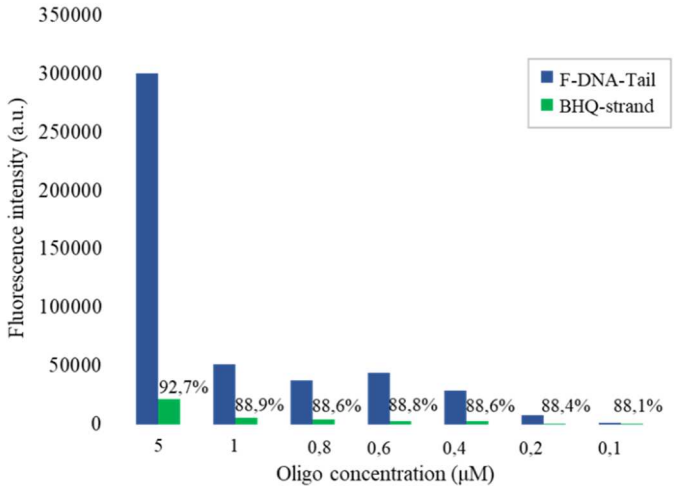

Figure 3.15: Quenching percentage in solution for different oligonucleotide concentrations.

Then, we studied the ATTO 647 response to UV treatment, measuring fluorescence pre and post polymerization, with and without photo-initiator. Results, schematized in Figure 3.16, showed that, in the presence of the darocur, fluorescence intensity significantly decrease post UV-treatment (~20% lower).

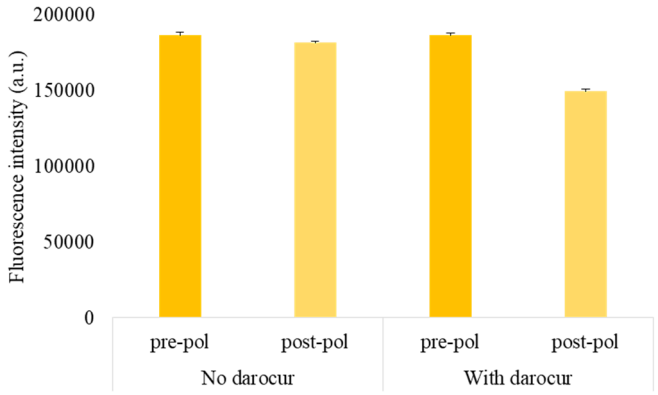

Figure 3.16: ATTO 647 response to UV treatment, with and without darocur in solution.

Then we tested the probe solution, 5 μM, within gels. Here, we reported the fluorescence intensity for the upper and lower polymer concentration (20% and 10% (w/v)). Firstly, we verified that, also in this case, UV-treatment produce a decrease of fluorescence intensity. Furthermore, we added BHQ strand and repeated the analysis. Comparing values of quenching percentage for the two different polymer concentrations, we attained a similar quenching percentage values (~75%). However, washing the bulk with PBS solution and re-analyzing the samples, we found that in PEGDA 20% bulk, the quenching was not effective (Figure 3.17-a).

In this case, in fact, the BHQ was near enough to collide with fluorophore with a consequent fluorescence decrement (dynamic quenching) but not enough to create a stable duplex and, therefore, after washing the fluorescence was recovered.

By the contrast, in PEGDA 10%, the network was sufficient wide to allow the formation of stable complex between oligonucleotide strands, so that the tail and quencher came in proximity and quenching occurred, even after several washes (Figure 3.17-b).

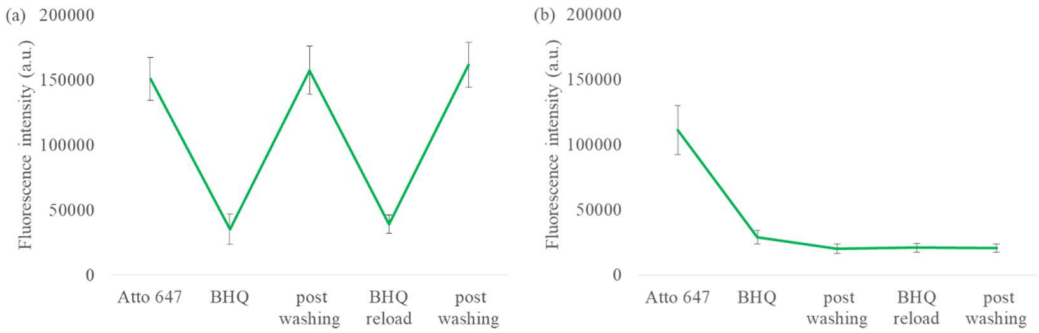

Figure 3.17: Fluorescence intensity of ATTO-BHQ in PEGDA 20% (a) and 10% (b).

In order to confirm that the narrow mesh size allowed only a dynamic quenching without the hybridization of duplex, we tasted a bulk with 50% PEGDA using both complementary (C) and non-complementary (N) BHQ-probes.

As reported in Figure 3.18, after the adding of C-BHQ we obtained a ~70% quenching that strongly decreased at ~3% after washing. Moreover, also adding an

N-BHQ we reached a high quenching percentage, proportional with the N-BHQ concentrations. Therefore, we can conclude that both narrow mesh size and high BHQ-strand concentrations do not allow an effective duplex hybridization.

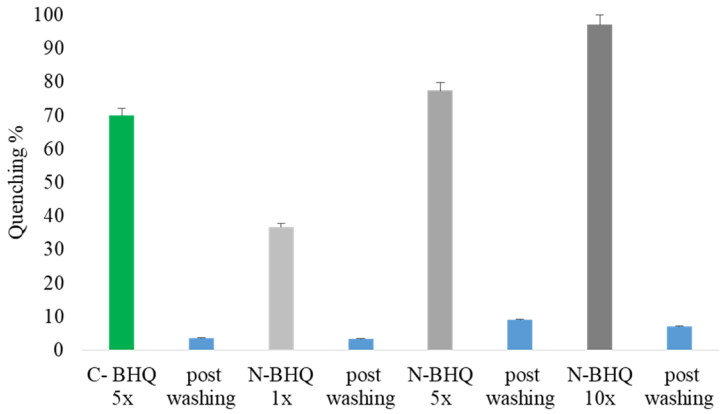

Figure 3.18: Quenching percentage with both complementary (C-BHQ) in green and several not complementary concentrations (N-BHQ) in grey.

Finally we studied the kinetic of quenching for three different PEGDA concentrations (10%-15%-20% w/v) analyzing the effect of both F-DNA-Tail and BHQ-strand concentrations.

In particular, all tests were carried out with 1 μM and 5 μM F-DNA-Tail with BHQ-strand 1x and 5x with respect of Tail. The three PEGDA samples showed different trend, confirming results previous described caused by the crowding of both polymer and oligonucleotides.

As regards PEGDA 10%, Figure 3.19 showed that quenching percentage increased with increasing of both F-DNA-Tail and BHQ concentrations. In particular, using F-DNA-Tail 1μM with BHQ in 1x (a), we reached an 80% of quenching after 120h. As expected, this quenching percentage was lower than that obtained in solution. Furthermore, adding BHQ 5x (b) we reached earlier, after 72h, the same 80 %. Finally, increasing both F-DNA-Tail and BHQ, we obtained 80% quenching in less than 48h (d).

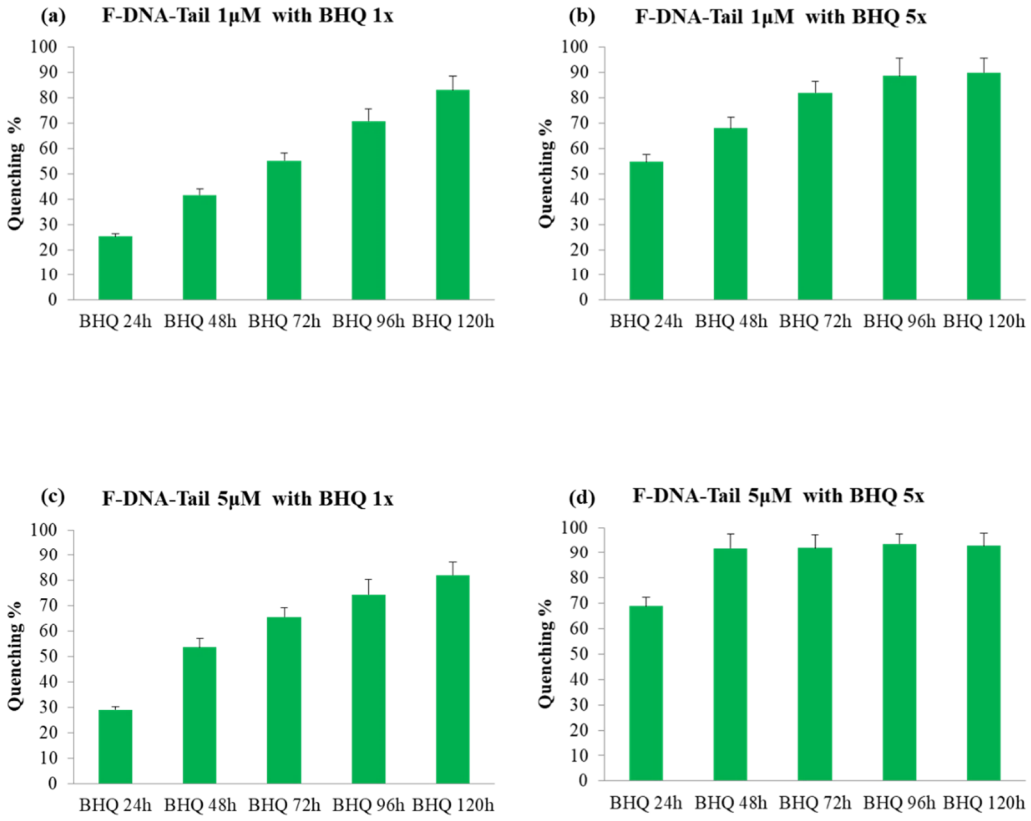

Figure 3.19: Quenching kinetic in PEGDA 10% with several oligonucleotides concentrations: (a) F-DNA-Tail 1µM- BHQ 1x; (b) F-DNA-Tail 1µM- BHQ 5x; (c) F-DNA-Tail 5µM- BHQ 1x; (b) F-DNA-Tail 5µM- BHQ 5x.

On the other hand for PEGDA 15%, only with F-DNA-Tail 5mM and BHQ 1x was possible to reach, after 96h, an 80% quenching (b).

In fact, with constant F-DNA-Tail, a lower BHQ concentration was not enough to provide a good quenching while an increase of F-DNA-Tail produced a crowding effect that obstacle the effective hybridization.

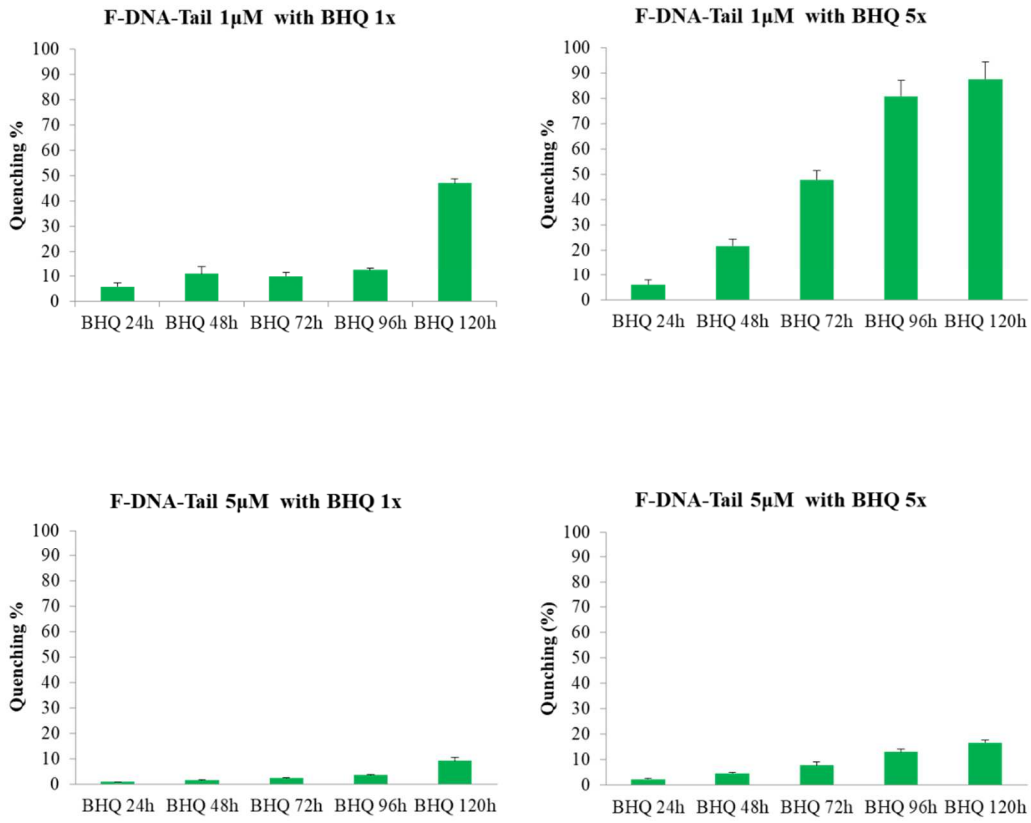

Figure 3.20: Quenching kinetic in PEGDA 15% with several oligonucleotides concentrations: (a) F-DNA-Tail 1µM- BHQ 1x; (b) F-DNA-Tail 1µM- BHQ 5x; (c) F-DNA-Tail 5µM- BHQ 1x; (b) F-DNA-Tail 5µM- BHQ 5x.

Finally, for PEGDA 20% we reached very low values of quenching for all sample preparations. Moreover, the decrease of quenching percentage post washing confirmed the not efficient hybridization.

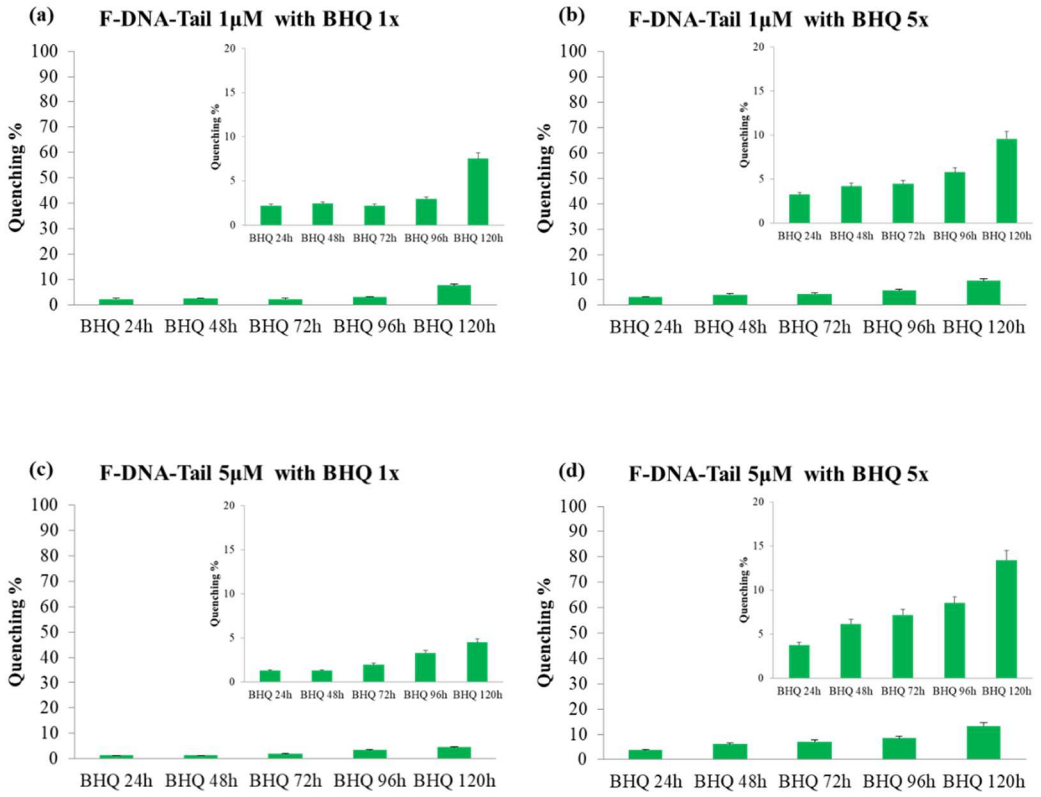

Figure 3.21: Quenching kinetic in PEGDA 20% with several oligonucleotides concentrations: (a) F-DNA-Tail 1µM- BHQ 1x; (b) F-DNA-Tail 1µM- BHQ 5x; (c) F-DNA-Tail 5µM- BHQ 1x; (b) F-DNA-Tail 5µM- BHQ 5x.

These preliminary studies gave us several information: firstly, polymer concentrations higher than 15% PEGDA were not suitable for probe diffusion that resulted to be hindered. Similarly, in order to reduce the crowding effect and permit the hybridization, we needed to use 1 µM Tail.

Finally, the significant fluorescence reduction caused by UV-treatment suggested changing the probe scheme (see chapter 4) using a not-fluorescent tail.

3.4 Conclusions

In this chapter, we focused on the synthesis and characterization of PEGDA-based bulk hydrogels. Swelling characterization showed the possibility of modulating mesh size and swelling parameters, changing the polymer concentration, in order to achieve different filter ability.

NMR analysis confirmed the opportunity to use hydrogels as molecular filter. In particular, 10% and 15% polymer concentrations resulted to be suitable for our purposes. In fact, these networks allowed the diffusion of molecules with size comparable with our probe (oligonucleotides) and excluded big molecules with size similar with proteins and antibody.

Moreover, fluorimetric analysis gave us important information regarding the ratio between polymer and oligonucleotides concentrations to let the efficient hybridization. In particular, 10% and 15% PEGDA concentrations showed a suitable network for both oligonucleotide diffusion and effective hybridization. In addition, results showed that for 10% of polymer we can obtain a good quenching percentage also for the highest oligo concentration tested. On the other hands, for 15% of polymer, we cannot use oligonucleotide concentration higher than 1 μM, because of crowding effect.

To sum up, our results showed the possibility to obtain functionalized and engineered materials, with a tunable network, that allow to combine both molecular filter and capture element capabilities. In this way, we can improve these materials to simplify the detection analysis of several target. These reported studies inspire us to scale-down this knowledge into micrometric-scale, in order to reduce sample volume and associated costs, as reported in the following chapter.

3.5 Appendix A

Here are reported and compared ^{1}H-NMR spectra of individual components darocur (IV) and PEGDA (III) and mixture pre (II) and post- polymerization (I).

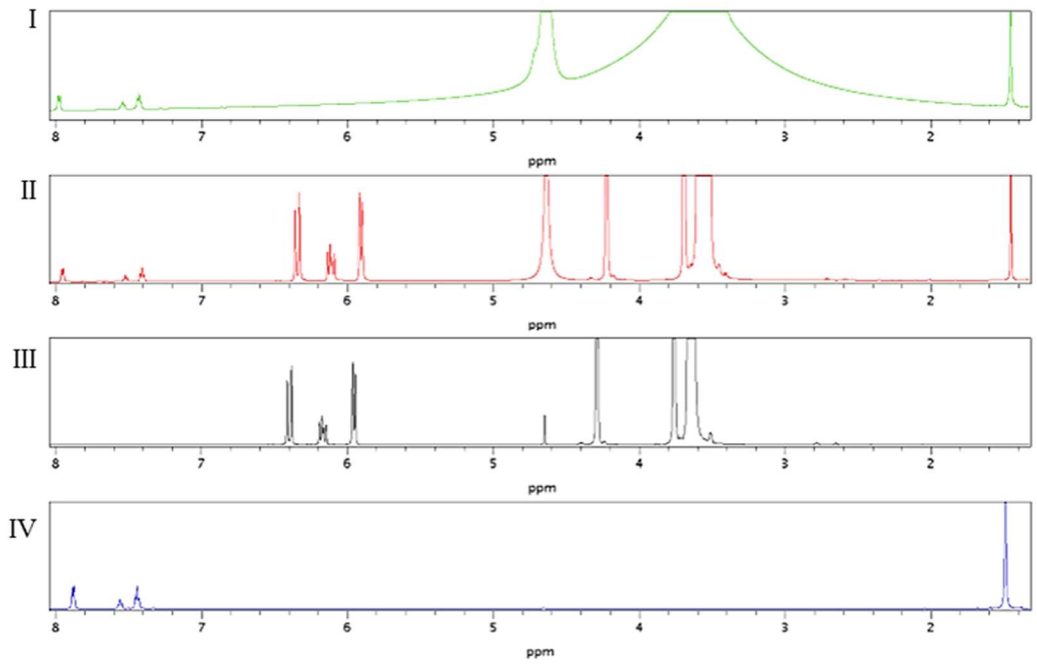

3.6 Appendix B

Interpolation curves fitting NMR- DOSY results fitted by Equation 3.3 for water diffusion in PEGDA 10-15-20% (w/v), respectively.

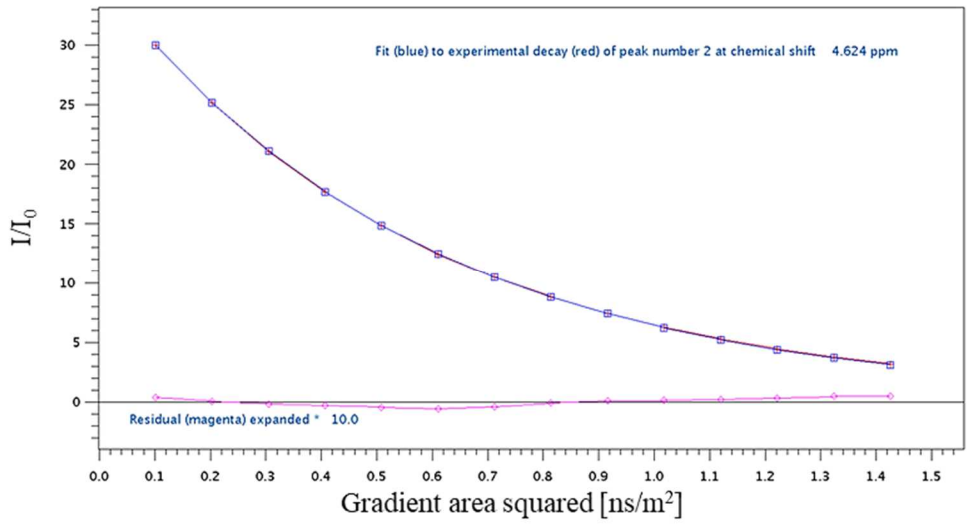

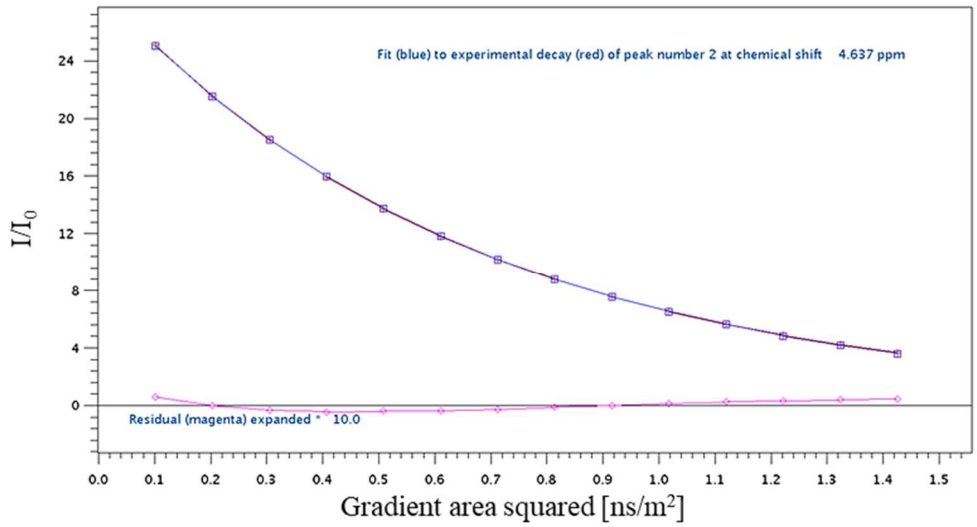

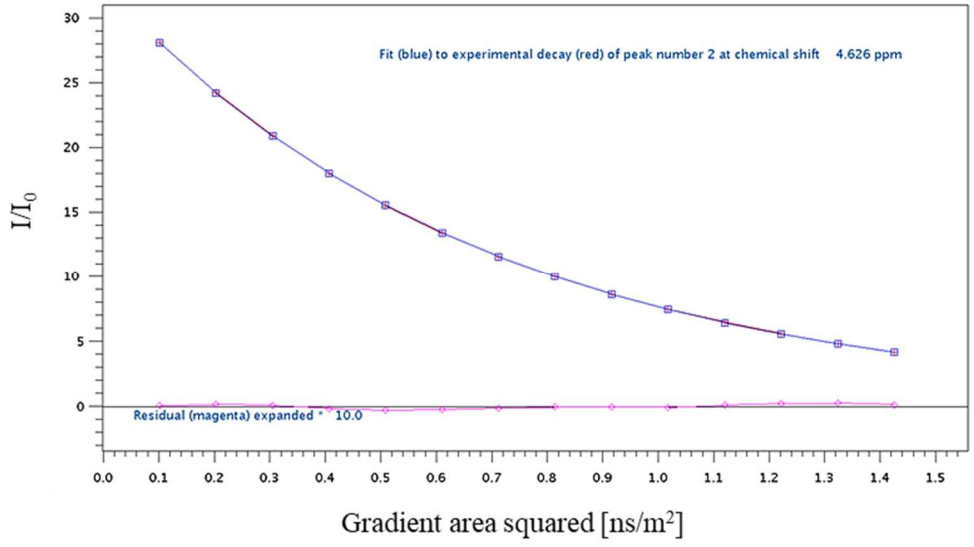
Fit (blue) to experimental decay (red) of peak number 2 at chemical shift 4.626 ppm
Residual (magenta) expanded * 10.0
I/I0
Gradient area squared [ns/m2]
30
25
20
15
10
5
0
0.0
0.1
0.2
0.3
0.4
0.5
0.6
0.7
0.8
0.9
1.0
1.1
1.2
1.3
1.4
1.5

3.7 References

1. Hoffman, A.; Schmer, G.; Harris, C.; Kraft, W., Covalent binding of biomolecules to radiation-grafted hydrogels on inert polymer surfaces. *ASAIO Journal* **1972,** *18* (1), 10-16.
2. Hoffman, A. S., Hydrogels for biomedical applications. *Advanced drug delivery reviews* **2012,** *64*, 18-23.
3. Zalipsky, S.; Harris, J. M., Introduction to chemistry and biological applications of poly (ethylene glycol). ACS Publications: 1997.
4. Peppas, N. A.; Merrill, E. W., Crosslinked poly (vinyl alcohol) hydrogels as swollen elastic networks. *Journal of Applied Polymer Science* **1977,** *21* (7), 1763-1770.
5. Peppas, N.; Huang, Y.; Torres-Lugo, M.; Ward, J.; Zhang, J., Physicochemical foundations and structural design of hydrogels in medicine and biology. *Annual review of biomedical engineering* **2000,** *2* (1), 9-29.
6. Peppas, N. A.; Keys, K. B.; Torres-Lugo, M.; Lowman, A. M., Poly (ethylene glycol)-containing hydrogels in drug delivery. *Journal of controlled release* **1999,** *62* (1), 81-87.
7. Peppas, N. A.; Hilt, J. Z.; Khademhosseini, A.; Langer, R., Hydrogels in biology and medicine: from molecular principles to bionanotechnology. *Advanced materials* **2006,** *18* (11), 1345-1360.
8. Kopecek, J., Hydrogels: From soft contact lenses and implants to self-assembled nanomaterials. *Journal of Polymer Science Part A: Polymer Chemistry* **2009,** *47* (22), 5929-5946.
9. Peppas, N.; Bures, P.; Leobandung, W.; Ichikawa, H., Hydrogels in pharmaceutical formulations. *European journal of pharmaceutics and biopharmaceutics* **2000,** *50* (1), 27-46.
10. Peppas, N. A.; Khare, A. R., Preparation, structure and diffusional behavior of hydrogels in controlled release. *Advanced drug delivery reviews* **1993,** *11* (1-2), 1-35.
11. Bryant, S. J.; Anseth, K. S., Hydrogel properties influence ECM production by chondrocytes photoencapsulated in poly (ethylene glycol) hydrogels. *Journal of Biomedical Materials Research Part A* **2002,** *59* (1), 63-72.
12. Flory, P. J., *Principles of polymer chemistry*. Cornell University Press: 1953.
13. Wallace, M.; Adams, D. J.; Iggo, J. A., Analysis of the mesh size in a supramolecular hydrogel by PFG-NMR spectroscopy. *Soft Matter* **2013,** *9* (22), 5483-5491.

14. Sun, J.; Lyles, B. F.; Yu, K. H.; Weddell, J.; Pople, J.; Hetzer, M.; Kee, D. D.; Russo, P. S., Diffusion of dextran probes in a self-assembled fibrous gel composed of two-dimensional arborols. *The Journal of Physical Chemistry B* **2008,** *112* (1), 29-35.
15. Branco, M. C.; Pochan, D. J.; Wagner, N. J.; Schneider, J. P., Macromolecular diffusion and release from self-assembled β-hairpin peptide hydrogels. *Biomaterials* **2009,** *30* (7), 1339-1347.
16. Cohen, Y.; Avram, L.; Frish, L., Diffusion NMR spectroscopy in supramolecular and combinatorial chemistry: an old parameter—new insights. *Angewandte Chemie International Edition* **2005,** *44* (4), 520-554.
17. Cao, S.; Fu, X.; Wang, N.; Wang, H.; Yang, Y., Release behavior of salicylic acid in supramolecular hydrogels formed by l-phenylalanine derivatives as hydrogelator. *International journal of pharmaceutics* **2008,** *357* (1), 95-99.
18. Scalettar, B. A.; Hearst, J. E.; Klein, M. P., FRAP and FCS studies of self-diffusion and mutual diffusion in entangled DNA solutions. *Macromolecules* **1989,** *22* (12), 4550-4559.
19. Colsenet, R.; Söderman, O.; Mariette, F., Pulsed field gradient NMR study of poly (ethylene glycol) diffusion in whey protein solutions and gels. *Macromolecules* **2006,** *39* (3), 1053-1059.
20. Gao, P.; Fagerness, P. E., Diffusion in HPMC gels. I. Determination of drug and water diffusivity by pulsed-field-gradient spin-echo NMR. *Pharmaceutical research* **1995,** *12* (7), 955-964.
21. Kwak, S.; Lafleur, M., Self-diffusion of macromolecules and macroassemblies in curdlan gels as examined by PFG-SE NMR technique. *Colloids and Surfaces A: Physicochemical and Engineering Aspects* **2003,** *221* (1), 231-242.
22. Gagnon, M.-A.; Lafleur, M., Comparison between nuclear magnetic resonance profiling and the source/sink approach for characterizing drug diffusion in hydrogel matrices. *Pharmaceutical development and technology* **2011,** *16* (6), 651-656.
23. Gagnon, M.-A.; Lafleur, M., Self-diffusion and mutual diffusion of small molecules in high-set curdlan hydrogels studied by 31P NMR. *The Journal of Physical Chemistry B* **2009,** *113* (27), 9084-9091.
24. Escuder, B.; LLusar, M.; Miravet, J. F., Insight on the NMR study of supramolecular gels and its application to monitor molecular recognition on self-assembled fibers. *The Journal of organic chemistry* **2006,** *71* (20), 7747-7752.
25. Shapiro, Y. E., Structure and dynamics of hydrogels and organogels: An NMR spectroscopy approach. *Progress in Polymer Science* **2011,** *36* (9), 1184-1253.
26. Kärger, J., NMR self-diffusion studies in heterogeneous systems. *Advances in Colloid and Interface Science* **1985,** *23*, 129-148.

27. McConville, P.; Pope, J., A comparison of water binding and mobility in contact lens hydrogels from NMR measurements of the water self-diffusion coefficient. *Polymer* **2000,** *41* (26), 9081-9088.
28. Litzenberger, A. L., A microfluidic method to measure diffusion in hydrogels. **2010**.
29. Johnson Jr, C. S., Diffusion ordered nuclear magnetic resonance spectroscopy: principles and applications. *Progress in Nuclear Magnetic Resonance Spectroscopy* **1999,** *34* (3-4), 203-256.
30. Holz, M.; Heil, S. R.; Sacco, A., Temperature-dependent self-diffusion coefficients of water and six selected molecular liquids for calibration in accurate 1H NMR PFG measurements. *Physical Chemistry Chemical Physics* **2000,** *2* (20), 4740-4742.
31. Callaghan, P. T.; Pinder, D., A pulsed field gradient NMR study of self-diffusion in a polydisperse polymer system: dextran in water. *Macromolecules* **1983,** *16* (6), 968-973.
32. Lebrun, L.; Junter, G.-A., Diffusion of dextran through microporous membrane filters. *Journal of membrane science* **1994,** *88* (2-3), 253-261.
33. Weiss, M.; Elsner, M.; Kartberg, F.; Nilsson, T., Anomalous subdiffusion is a measure for cytoplasmic crowding in living cells. *Biophysical journal* **2004,** *87* (5), 3518-3524.
34. Pluen, A.; Netti, P. A.; Jain, R. K.; Berk, D. A., Diffusion of macromolecules in agarose gels: comparison of linear and globular configurations. *Biophysical journal* **1999,** *77* (1), 542-552.
35. Cheng, Y.; Prud'Homme, R. K.; Thomas, J. L., Diffusion of mesoscopic probes in aqueous polymer solutions measured by fluorescence recovery after photobleaching. *Macromolecules* **2002,** *35* (21), 8111-8121.
36. Causa, F.; Aliberti, A.; Cusano, A. M.; Battista, E.; Netti, P. A., Supramolecular spectrally encoded microgels with double strand probes for absolute and direct miRNA fluorescence detection at high sensitivity. *Journal of the American Chemical Society* **2015,** *137* (5), 1758-1761.

Chapter 4

Engineered PEGDA-microparticles by microfluidics: oligonucleotide functionalization for selective miRNA 143-3p detection in serum

Abstract. Droplet microfluidics is the most powerful technology used to produce and manipulate monodisperse droplets. This technique addresses the need for lower costs, shorter times, and higher sensitivities. In such a way, we were able to synthesize high controlled microparticles, directly functionalized in flow, eliminating time-consuming labelling steps and their associated costs. Therefore, here we present a versatile and innovative assay that combine biomarker detection with engineered and functionalized microparticles obtained by microfluidic. In particular, firstly we report microfluidic optimization to achieve a high monodispersity and spherical shape. Then, both swelling characterization and diffusion studies, by CLSM, were carried out to reach a specific control of both network structure and probes diffusion. In particular, our studies were fulfilled using poly(ethyleneglycol) microparticles functionalized with DNA-Tail, properly designed for the direct detection of miRNA 143-3p (associated with several cardiovascular disease). The detection system is based on double-stranded displacement assay and do not require any sample manipulations. Therefore, we demonstrated the possibility to attain a high control of synthesized microparticles and the possibility to modulate both recipe and microfluidic parameters to obtain specific molecular filter ability and target recognition.

This Chapter is part of an article in preparation: **A. Mazzarotta,** T.M. Caputo, E. Battista, F. Causa, P.A. Netti.- ***"Engineered PEGDA-microparticles by microfluidics: oligonucleotide functionalization for selective miRNA 143-3p detection in serum."***

4.1 Introduction

In recent years, application of biosensor has rapidly increased and so there is a growing interest in the research of innovative tunable materials. Several studies of hydrogels-based technologies has been widely fulfilled with important improvement in their synthesis strategies. These materials are used for many different applications, in particular in biotechnology field for diagnostic,[1-4] drug delivery,[5-8] and tissue engineering.[9-12] In fact, due to the possibility of tune their size, shape and chemistry and for their biocompatibility, they represent ideal candidates for biosensing applications.

As demonstrated in chapter 3, it is possible to synthesize engineered hydrogels, with tunable network, to achieve a detection system for specific target. In this chapter, we scaled-down this knowledge into the micro-scale, producing high controlled microparticles for detection of biomolecules.

4.1.1 Microfluidic technique

Hydrogel microparticles for sensing purposes should be synthesized with high control in size, shape and chemical composition, trying to match the requirements of liquid bioassays as regard the encoding, the capturing system and mass transport. Conventional techniques for the syntheses of hydrogel microparticles are represented by dispersion, precipitation and emulsion polymerization procedures.[13-15] These methods have intrinsic limits, in fact the shape of such particles is restricted to spheres and often are not enough monodisperse. Moreover, biomolecules are incompatible toward organic solvents and high temperature conditions needed. Recently, with the improvement of microfabrication methods, hydrogel microparticles can be obtained using microfluidic device, achieving a tuned size and shape with a good chemical-physical properties control. In particular, droplet microfluidics facilitate large production of microparticles with a rate greater than 10^5 particles per hours and a narrow size monodispersity less than 5–6 %, not

possible with conventional methods, even though limited by the need of chemical mixtures of immiscible fluids and surface-compatible with microfluidic devices.[16] This approach represents the most promising methods for the production and the functionalization of monodisperse particles at low cost and reagent consumption, with higher reproducibility and saving time.[17]

Microfluidic techniques, based on droplet generation methods, have been wildly studied since 2005 as continuous on-chip production of water-in-oil emulsions based on the break-off of droplets in two-phases through different geometry: T-junction, flow focusing and co-flowing (Figure 4.1).[18-20]

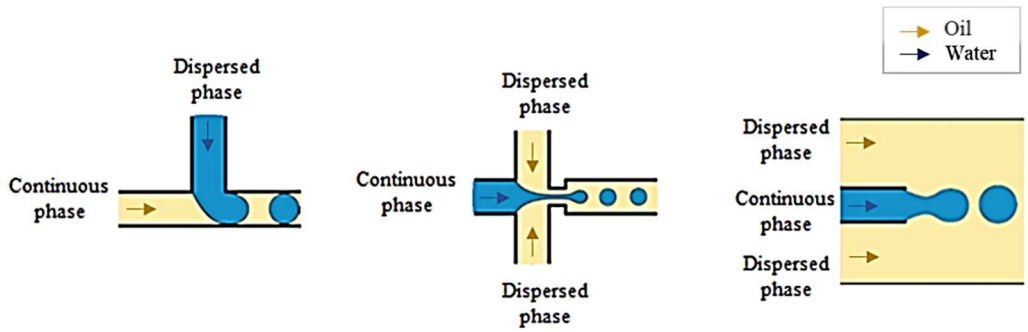

Figure 4.1: Droplet generation in three microfluidic devices: T-junction, flow focusing and co-flowing geometry.

Several variables such as flow rates, dimensions of geometry, viscosity of the fluid, surface tension and capillary number strongly affect the droplet formation.

The control of these parameters is fundamental to generate monodisperse and stable emulsion. In particular, the capillary number (Ca), that represents the relative effect of viscous forces versus surface tension acting across the interface between two immiscible fluids, is an adimensional number that can allow predicting the emulsion stability.

Many studies has been carried out to define critical values of Ca. Choi et al.[21] found a limited range of Ca (0.5×10^{-2} –0.5×10^{-1}) and a flow rate of disperse phase (0.2 - 1.1 μL/min) where stable and monodisperse emulsions can be generated. Celetti et al.[22] performed simulation in a flow-focusing droplet generator showing

that each of the parameters that influence Ca, affect the size of particles and the flow configurations after the junction. Nunes et al.[23] analyzed in detail the transition between dripping and jetting regimes (Figure 4.2). In their works,[24-29] was summarized that stable and monodisperse emulsions can be produced in T-junction device in Ca range of 10^{-3} – 10^{-1} and a flow rate ratio 10^{-2} – 10^{0}.

In the jetting regime, the droplets are generated not only due to the natural growth of an interfacial instability but also because of the viscous forces applied by the continuous phase fluid. In the dripping regime, instead, the combination of capillary instability and viscous drag is proposed to argue the mechanism of the generation of drops; in this case the size of the droplets is much smaller than the dimensions of the channel of the continuous phase fluid.[23] Surely, the dimension of geometry influence Ca optimal range.

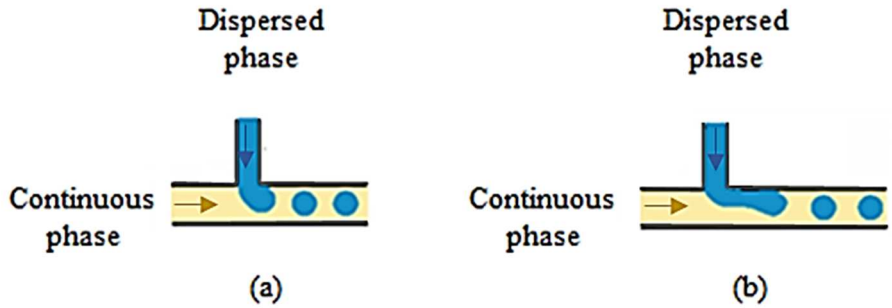

Figure 4.2: Schematic of flow regimes in T-junction microfluidic devices in both dripping (a) and jetting (b) regime.

Microparticles can be functionalized directly in flow or in a second step, employing strategies in droplet microfluidics. In fact, they can be engineered with several biological entities such as protein, peptide or nucleic acids[5] for the detection of biomarkers in complex fluids.[1] The possibility to functionalize hydrogels directly during synthesis step let us to find new strategies to eliminate time-consuming labelling steps and their associated costs (Figure 4.3).

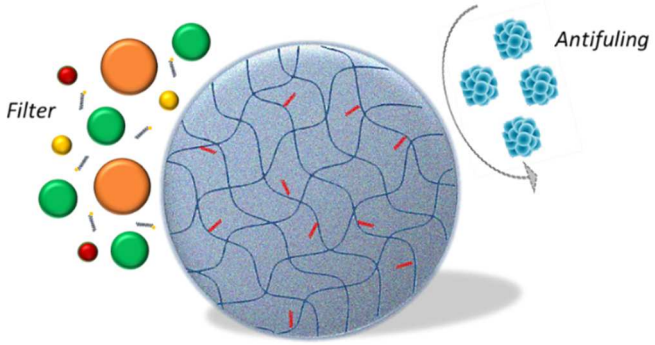

Figure 4.3: Engineered microparticles for specific target detection.

4.1.2 Biomarkers detection

Biomarkers cover a broad range of biochemical entities, such as proteins, nucleic acids, small metabolites, sugars and tumor cells found in the body fluid. They are widely used for risk assessment, diagnosis, prognosis, and for the prediction of treatment efficacy and toxicity.[30-31] In biomarkers context, miRNAs have attracted a growing attention as confirmed by the increasing of publication regarding micro RNA during the past 20 years (Figure 4.4). Due to their immense regulatory power, the variation of their levels can be utilized as potential biomarkers for the diagnosis and prognosis of a variety of diseases.[32-35]

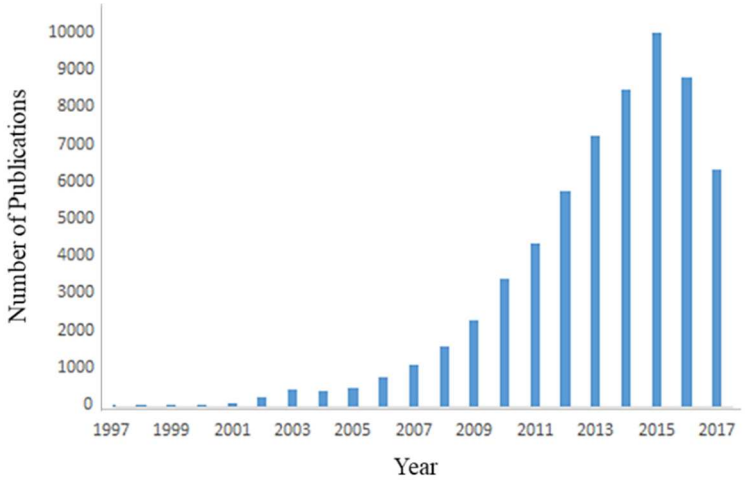

Figure 4.4: Histogram showing the increase in publications related to the keyword "*microRNA*" during the past 20 years. PubMed data.

In particular, several studies identified miRNA-143-3p as important transcriptional and post-transcriptional inhibitors of gene expression. The integrity of transcriptional and post-transcriptional regulatory circuit is essential for the maintenance of cardiac homeostasis. Nowadays, cardiovascular disease is the predominant cause of human morbidity and mortality in developed countries. miRNA-143-3p contribute to many cardiovascular processes such as embryonic stem cell differentiation, cardiomyocyte proliferation, endothelial responses to shear stress[36-44] and play an essential role in the function and formation of the cardiac chamber. Moreover, dysregulation of miRNA-143-3p physiological level is associated with many cardiovascular disease including heart failure, myocardial ischemia, congenital heart disease, atherosclerosis and hypertension.[45]

Conventional techniques for the detection of oligonucleotides, such as microarray analysis[46-47], polymerase chain reaction (PCR, qRT-PCR)[48] show several drawbacks due to preliminary steps needed (extraction and amplification) resulting in time-consuming analysis[49]. Due to high sequence homology, complex secondary structures, and low concentration levels, an accurate and robust quantification of circulating miRNA biomarkers in blood is still a major challenge for early stage, metastatic or recurrent diseases.

In this chapter, we propose an innovative bead-based assay, highly specific, which combine miRNA-143-3p detection with engineered and functionalized microparticles. Overcoming conventional techniques, our detection system is based on double-stranded displacement assay and do not require any sample manipulations. As concerns the assay, several experimental conditions can affect the final assay times.[50] Several studies have been conducted to optimize DNA hybridization. Ravan et al.[51] demonstrated that efficiency of hybridization could be influenced by many constraints such as electrostatic repulsion between oligonucleotide strands and the steric hindrance between neighboring DNA probes. All these interactions, in fact, reduce both the efficiency and the kinetic of DNA hybridization. Stevens et al.[52] focused on the determination of time required for particles

hybridization to reach equilibrium. They underlined that DNA hybridization on microparticles is temperature-dependent, with reactions coming to equilibrium faster at high temperatures than at low temperatures. In particular, in their work, was shown that, when all other parameters are equal, time required for reaction to reach equilibrium goes from 1 h at 50 °C to 24 h at 20 °C. Finally, Wong's group[50] examined both the ionic strength and probe sequences effects on the hybridization time. In their work, were reported the kinetics of the assay at different salt concentrations. Time required generally decreases with the salt concentration. In particular their results showed a rapid decrease in the range of 5-50 mM NaCl and a slowly decrease for NaCl concentrations over 100 mM. Moreover, also the length of two sequences that hybridize play an important role in the kinetics of the assay. It was evaluated the half-time of assay for different probe length. This time goes from 4 minutes for 10-base probe up to 3 h for the 23-base.

To sum up, nucleic acid hybridization kinetic is affected by surface probe density, surface charge, conformation and sequence of probe strands and by the curvature of the solid surface. Moreover, incubation temperature and ionic strength also sway the hybridization time. Therefore, several parameters have to be considered to evaluate the time required to reach hybridization equilibrium.

4.2 Experimental section

4.2.1 Materials

Poly(ethylene glycol) diacrylate (PEGDA-700 Da), Light mineral oil (LMO), Sorbitan monooleate (SPAN 80), Polyethylene glycol sorbitan monolaurate (TWEEN 20), Ethanol and Diethyl ether, Albumin-fluorescein isothiocyanate conjugate (BSA), Anti-Human IgG (whole molecule)-FITC antibody produced in goat (IgG) were purchased from Sigma-Aldrich (St. Gallen, CH) and used as

received. Crosslinking reagent 2-Hydroxy-2-methylpropiophenone (DAROCUR 1173) was supplied from Ciba. Phosphate Buffered Saline Tablets were purchased from MP Biomedicals. Texas Red labelled dextrans with different molecular weight (3 kDa, 10 kDa and 40 kDa) were supplied by Thermo Fisher Scientific. DNA and RNA oligonucleotides were provided from Metabion with HPLC purification. Human serum was supplied by Lonza. μ-Slide were provided by Ibidi. Tube and special DNA-LoBind tubes were provided by Eppendorf.

4.2.2 Synthesis of functionalized microparticles

Microparticles were synthesized using a microfluidic device bought from Dolomite. The chip is a glass microfluidic device with hydrophobic coating. It was designed for generating droplets, both with T-junction and Flow focusing geometry.

For our purpose, we used the first geometry that consists of two inputs for the continuous and disperse phase, a narrow orifice where the two opposite channels converge, and an output (Figure 4.5).

The dimensions of the device are 22.5 mm × 15.0 mm × 4 mm (length × width × thickness) with wide channels cross-section of 100μm × 300 μm (depth × width) and channels cross-section at junction of 100 μm × 105 μm (depth × width) (Figure 4.6).

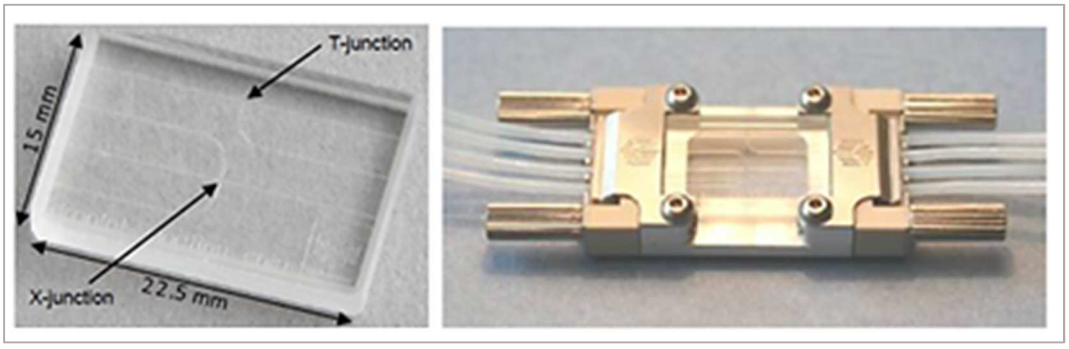

Figure 4.5: The Droplet Junction Chip and its Chip Interface H for fluidic connection.

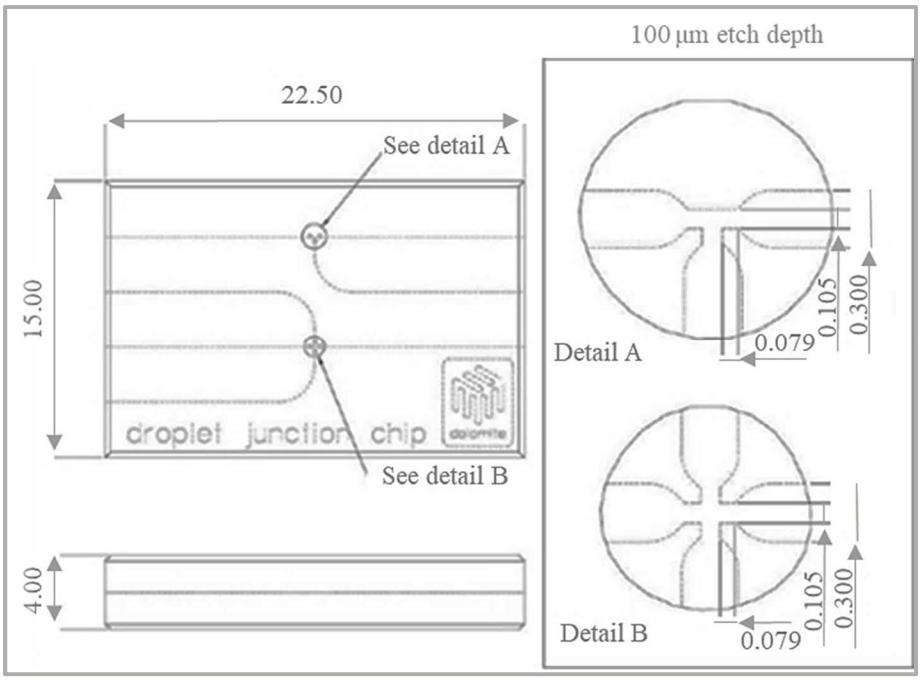

Figure 4.6: Dolomite chip: geometry and size.

Microparticles were synthesized using light mineral oil (LMO) containing non-ionic surfactant Span 80 (5 % v/v) as a continuous phase and a water solution of poly(ethylene glycol) diacrylate (PEGDA, MW 700 Da) (10-15-20 % w/v) with photoinitiator darocur (0.1-1% v/v with respect to the total volume) as dispersed phase. In order to functionalize microparticles, methacrylate oligonucleotide was added in the dispersed phase to reach final concentration of 1µM into the water solution. Similar UV free radical polymerization already described for bulk (chapter 3), occurred. In Figure 4.7. was reported our experimental set-up. Droplet emulsions were obtained adding in the first channel water solution and continuous phase in the other. Solutions were injected using high-precision syringe pumps (neMesys-low pressure) to ensure stable flow and reproducibility. This system was mounted on an inverted microscope (IX 71 Olympus). The droplets formation was monitored using an objective with 5x magnification and 0.12 numerical aperture and recorded with a CCD camera ImperxIGV-B0620M

that allow to record up to 259 frame per second. Once emulsion was formed, it was crosslinked outside the chip using an UV lamp at 365 nm wavelength at different power lamp (42-2000 mW) for ~ 2 minutes obtaining a complete polymerization. Thereafter, microparticles were collected in an eppendorf and exceeded oil phase was removed. Then particles were washed several times with different solvents (diethyl ether, ethanol and milliQ water-tween solution (0.05 % v/v)) to remove the residual oil. After washing, microgels were stored at room temperature in buffer solutions until further use. Our buffer was obtained mixing 1x PBS, NaCl 200 mM and tween-20 at 0.05% v/v in milliQ water.

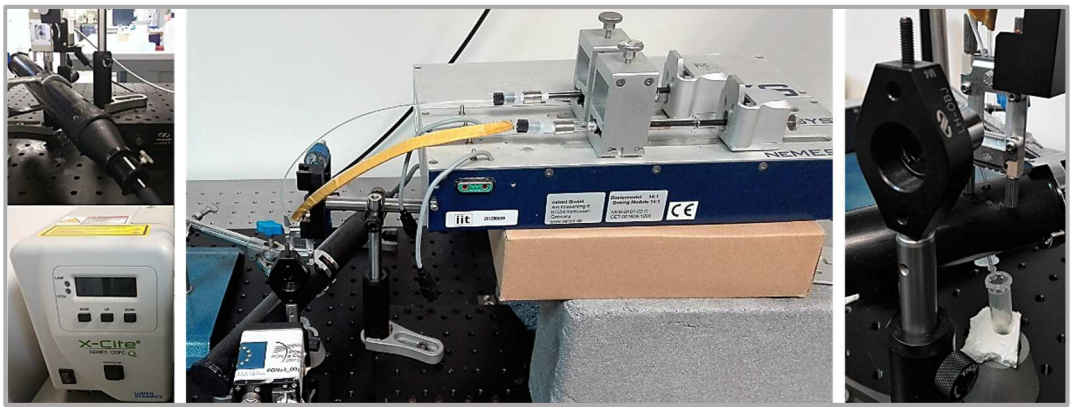

Figure 4.7: Set-up for functionalized microparticles generation.

4.2.3 Microparticles characterization

4.2.3.1 Swelling characterization

Approximately 100 microparticles diluted in 20 µL were loaded onto µ-slide 18 well-flat. Images in both swollen and dry conditions were collected with CLSM microscope (CLSM Leica SP5- with an Objective HC PL FLUOROTAR 20x0.5 DRY and a scan speed of 8000 Hz). Then, images were analyzed by ImageJ software to obtain diameter and calculate volume of microparticles in both conditions. Therefore, using equations described in chapter 1, polymer volume

fraction (Equation 1.6), molecular weight between crosslinks (Equation 1.3) and mesh size (Equation 1.11) were calculated.

4.2.3.2 Morphological characterization

Morphological characterization was done collecting images by SEM (scanning electron microscope) and CLSM (confocal laser scanning microscope). SEM measurements were performed on a FE-SEM Ultra Plus (Zeiss) microscope at 20 kV. For sample preparation, the microparticles solution was fixed on a microscope slide, air-dried and then sputtered with a 10 nm thin gold layer.

4.2.3.3 Diffusion characterization

Analysis were carried out following fluorescence intensity changes by CLSM. 10 μL of microparticles solution, containing approximately 100 microparticles, were loaded onto μ-slide 18 well-flat with 10 μL of probe solution (dextrans 3 kDa, 10 kDa, 40 kDa, Target143, BSA and IgG with final concentration 2 μM). Samples were illuminated at CLSM Leica SP5 using appropriate wavelength (λ_{ex} 543-488 nm) and fluorescence images of microparticles were collected.

4.2.3.4 Target detection

Fluorescence analysis, performed by CLSM with λex 633 nm, were also used for the target detection. All experimental steps were performed at room temperature in buffer phosphate solution (1x PBS, NaCl 200 mM and tween-20 at 0.05% v/v).
Non-fluorescent particles were analyzed adding in μ-Slide VI 0.4 a solution constituted by diluting 1 μL of DNA-Tail particles solution in 30 μL of buffer. As regard Tail hybridization step, 100 μL of microparticles-Tail solution (~$25 \cdot 10^3$ particles and ~6 pmol of Tail), were loaded in DNA-low binding tube with

F-DNA 10x (~60 pmol). Solution was kept under stirring until use for three days and then washed several times with our buffer.

Finally, for the CLSM experiment, 1 μL of this solution was diluted in 30 μL of buffer, added in μ-Slide VI 0.4 and therefore the fluorescence intensity was evaluated.

Concerning displacement step, several samples containing 2μL of microparticles-Tail-F solution (~330 particles and ~60 fmol of Tail), were loaded in DNA-low binding tubes with different Target concentrations (from 100 μM to 50 pM in buffer solution). Analogously to the previous step, solution was kept under stirring and washed several times with buffer. For the fluorescent analysis, 1 μL of this solution was diluted in 30 μL of buffer. To test the system in complex fluid, 2μL of microparticles-Tail-F solution were put in contact with Target-Human serum solution. The latest was prepared adding 200 μL of serum and 300μL of our buffer with Target 2 uM.

4.3 Results and discussion

4.3.1 Probe design

Probe used in this chapter was designed for selective and specific miRNA fluorescence detection according to a double strand (ds) displacement assay. In order to overcome problems connected with fluorescence reduction caused by UV-treatment, observed and described in chapter 3, we modified our scheme as reported in Figure 4.8. In particular, based on the miRNA 143-3p sequence (21 nt), we designed the ds probes formed by a tail (T-DNA, 12 nt), modified with methacrylamide spacer at the 3'end, for covalent bound with polymer network and a longer fluorescent DNA sequence (F-DNA, 21 nt), labelled with ATTO 647N

at 5' end. F-DNA sequence is partially complementary to T-DNA and totally complementary to the specific target.

The probe design implies that, when the F-DNA and T-DNA partially hybridize, the fluorescence occurs. In presence of the target, the F-DNA and the target hybridize so that low fluorescence background signal is registered.

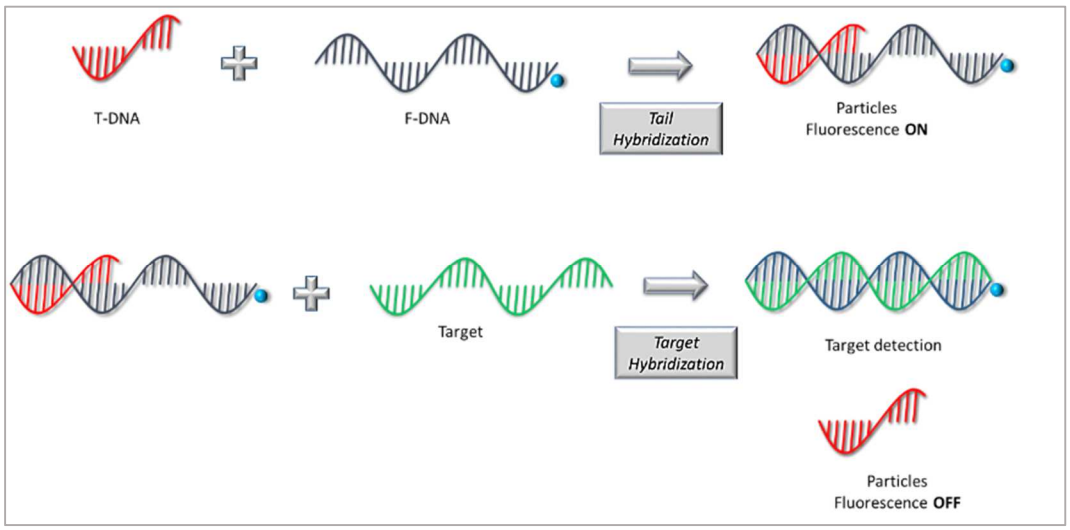

Figure 4.8: New scheme showing the mechanism of miRNA detection based on ds displacement assay.

Thermodynamic parameters such as melting temperature, stability at physiological ionic strength and folded fraction at assay condition were evaluated using appropriate tools (IDT-Integrated, D. N. A. "Technologies. OligoAnalyzer 3.1. Web." (2014)).

The length of the tail was optimized to obtain an appropriate difference in free energy. Thermodynamic parameters of the probes used for this work were reported in Table 4.1. TF_{hyb} represents the free energy gained from the partially complementary T-DNA/F-DNA duplex; $FTarget_{hyb}$ is the free energy gained from the fully complementary Target/F-DNA duplex; Δdisplacement is the free energy gained after T-DNA/F-DNA de-hybridization and Target/F-DNA hybridization.

Table 4.1: Sequence, length and thermodynamic parameters of the DNA probes and RNA targets.

miRNA 143-3p probe			
probe	**sequence (5'-3')**	**length (nt)**	**ΔG (Kcal/mol)**
T-DNA	GCA CTG TAG CTC	12	0
F-DNA	TGA GAT GAA GCA CTG TAG CTC	21	TF_{hyb} = -12.76
Target	GAG CUA CAG UGC UUC AUC UCA	21	$FTarget_{hyb}$ = -22.62 **Δdisplacement = 9.86**

4.3.2 Microparticles: optimization of microfluidic parameters

Several physical parameters such as geometry, flow rates, viscosity of the fluid, capillary number (Ca) and surface tension influence the droplet generation.[14] Hence, the control of these parameters is important for the production of monodisperse and stable emulsion. In particular, we focused on the effect of capillary number (Ca) on the emulsion stability. Ca represents the relative effect between the viscous stress and surface tension acting across an interface between two immiscible fluids.[18]

Firstly, we investigated the influence of Ca, modulated by varying flow rate of the continuous phase (Q_{oil}), on emulsion stability. As reported in Figure 4.9, fixed our geometry device, for Q_{oil} values higher than 15 μL/min unstable emulsion were generated and increasing more this value, the flow of polymer solution reversed into channels. When the value of Ca was in a limited range 0.05 ~ 0.20 and the value of Q_{oil} between 6 and 10 μL/min, the polymer phase broke into a stable emulsions. Precise control of particle size and monodispersity are fundamental for many applications of microparticles.Microfluidic device allows this control over a wide range of sizes. For this reason, we evaluated the influence of Q_{oil} on the droplet size. Different microgel sizes were reported in Figure 4.9 with a range of sizes from 20 to 100 μm. Droplets diameter were calculated in flow during the droplet production before and after polymerization showing similar results.

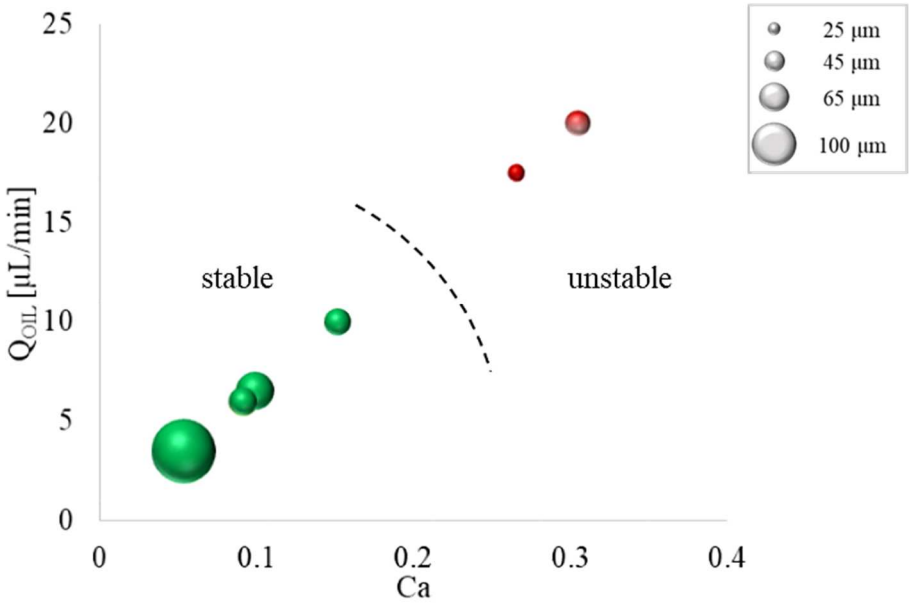

Figure 4.9: Diagram as a function of continuous phase flow rate (Qoil) and capillary number (Ca). Two different conditions are reported: stable (green) and unstable (red) emulsion.

Moreover, dripping and jetting regimes were investigated (Figure 4.10) changing flow rate ratio (Q_{oil}/Q_{PEGDA}), as reported in Figure 4.11.

Our results showed three different flow conditions after the junction: stable dripping, stable jetting and unstable emulsions. It was difficult to generate stable emulsion in dripping mode at high flow rates of polymer solution. In fact, W/O emulsion could not separate uniformly from the junction due to the unstable hydrodynamic pressure of PEGDA phase.

Figure 4.11 also show different emulsion size obtained for different flow rate ratio.

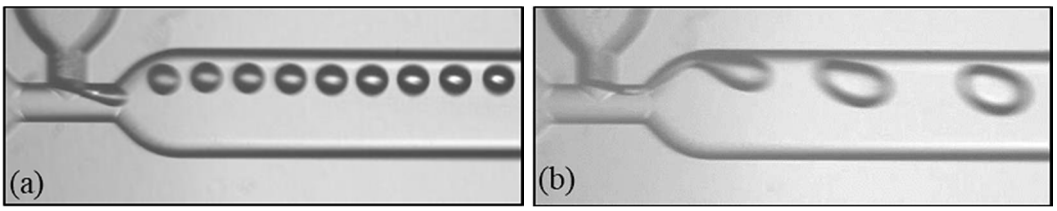

Figure 4.10: Droplet generation in dripping (a) and jetting (b) regimes.

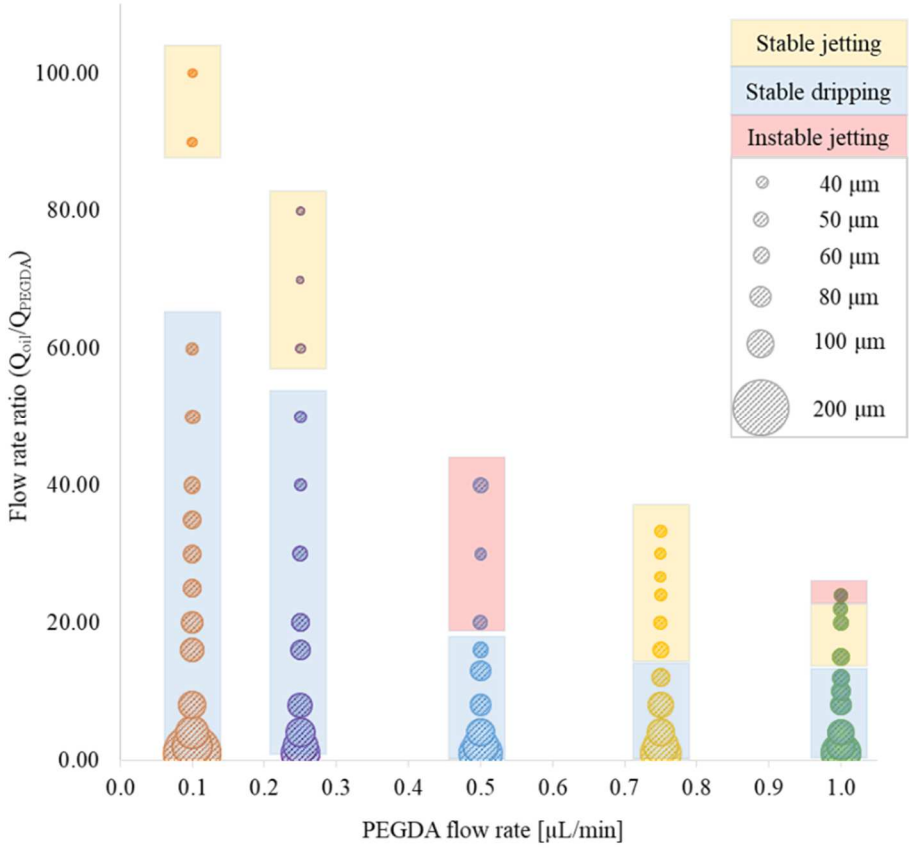

Figure 4.11: Diagram as a function of flow rate ratio (Q_{OIL}/Q_{PEGDA}) and dispersed phase flow rate (Q_{PEGDA}) operating in jetting (yellow rectangle), dripping (blue rectangle) and unstable regime (red rectangle).

In order to stabilize droplets against uncontrolled coalescence, the use of a surfactant was required. These molecules are often added on purpose in order to facilitate the creation and transport of drops and to prevent droplet coalescence. In the emulsification process, the value of interfacial tension displays a strong dependence on the local surface coverage with surfactant molecules and play an important role on droplet size and stability[53].

4.3.3 Microparticles: morphological characterization

Microparticles were constantly monitored during production step, images were recorded and their size was measured just after emulsion formation using Droplet

monitor software. It allowed obtaining several information about the droplet generation. In particular data analysis show the average droplet size and their distribution, the spacing between droplet and droplet rate.

For the final particles synthesis, specific flow rates were chosen: 0.5 μL/min for dispersed phase and 6.5 μL/min for continuous phase. In such a way, we were able to achieve a high throughput production of particles with a droplet rate of ~40 particles/sec.

Moreover, once polymerized, particles were collected, washed and characterized by optical and electronic microscope. Images so obtained (Figure 4.12a-c) confirmed that our microparticles were monodisperse and spherical, with a diameter of 79.2 ± 1.17 μm (Figure 4.12b).

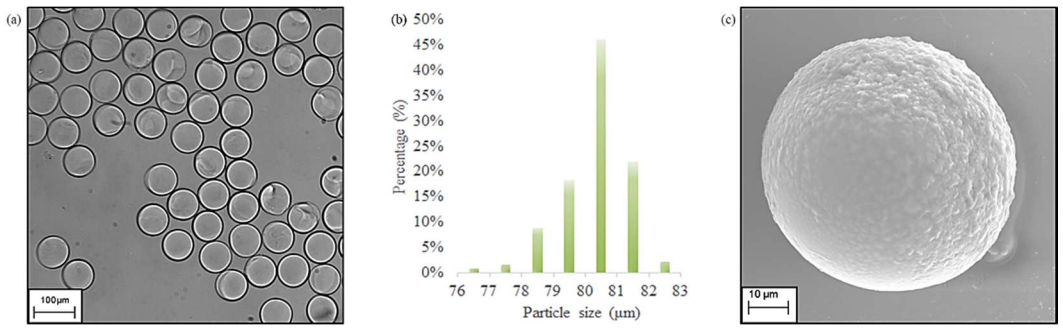

Figure 4.12: Optical image (a) of monodisperse microparticle and relative particle size distribution (b); (c) SEM image of microparticles.

4.3.4 Microparticles: swelling characterization

Firstly, in order to optimize experimental set-up and recipe, we evaluated the effect of lamp power and photo initiator concentration on the mesh size. For these studies, microparticles without oligonucleotide were prepared. Figure 4.13 show the mesh size values of PEGDA 15% microparticles, with three different darocur final concentrations (1-0.5-0.1% v/v), polymerized with several lamp power (from 42 to 2000 mW).

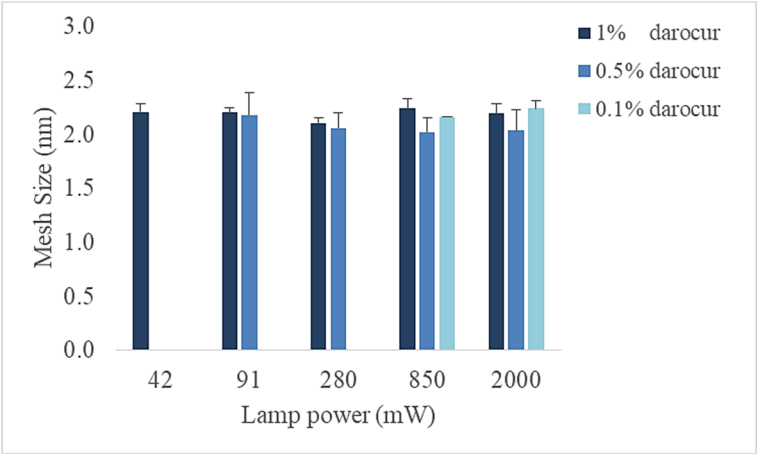

Figure 4.13: Effect of both lamp power and darocur concentration on mesh size of microparticles with PEGDA 15%.

Results showed that for lower darocur concentration (0.1%), particles polymerization occurred only with lamp power values higher than 850 mW. Increasing the photoinitiator concentration up to 1%, particles can be well polymerized also with lamp power of 42 mW.

All particles were characterized and mesh size values resulted to be comparable for all power lamp values and for all darocur concentrations. Therefore, both variables did not affect the final mesh size of microparticles. For subsequent characterizations and for microparticles production, we decided to use the lower darocur final concentration (0.1%) with power lamp of 850 mW.

As regards a complete swelling characterization, several samples obtained using polymer concentrations of 10-15-20 % w/v, were prepared in order to characterize different network structure and to compare these results with bulk one presented in chapter 3. In particular, swelling parameters ($v_{2,s}$, Q, $\bar{M}_c$, ξ) were calculated. (Table 4.1). As expected, same trend previously described was obtained also for microparticles. In particular, changing the PEGDA concentration, polymer volume fraction in the range of 0.008-0.206 was obtained. The equilibrium-swelling ratio decreased from 11.42 to 4.87 with PEGDA increasing. The molecular weight between crosslinks decreased from 338 to 283 Da as the crosslink density increased.

With these recipes, mesh size in the range of 2.55-1.77 nm was achieved (Figure 4.14), resulting between 4-11 % lower with respect to mesh calculated for bulk. This difference can be expected because of the difference in both synthesis procedure and in mesh size analysis.

Table 4.2: Properties of PEGDA microparticles.
All values were calculated from averaged measured values.

	PEGDA 10%	**PEGDA 15%**	**PEGDA 20%**
$\mathbf{V_{2,s}}$	0.088 ± 0.007	0.125 ± 0.007	0.206 ± 0.014
Q	11.42 ± 0.87	7.99 ± 0.46	4.87 ± 0.33
Mc (Da)	338 ± 2	325 ± 4	283 ± 12
ξ (nm)	2.55 ± 0.10	2.23 ± 0.07	1.77 ± 0.09

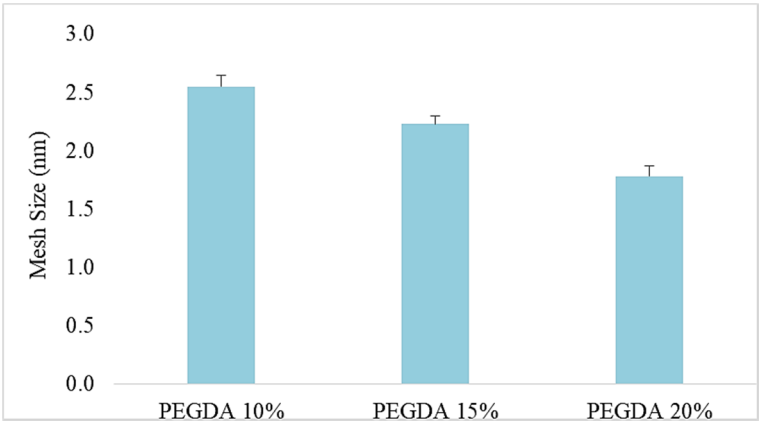

Figure 4.14: Mesh size values for different microparticles-PEGDA concentrations.

Then we added methacrylate DNA-Tail in the mixture reaction. In Table 4.3 were reported mesh size values (ξ) of 20% PEGDA with different oligonucleotide concentrations. Results showed that there was not significant effects.

Table 4.3: Mesh size of PEGDA (15%w/v) microparticles with different T-DNA concentrations.

	No Oligo	**T-DNA 400 nM**	**T-DNA 1 µM**	**T-DNA 10 µM**
ξ (nm)	2.23 ± 0.07	2.12 ± 0.05	2.18 ± 0.14	2.10 ± 0.07

For subsequent analysis, functionalized microparticles were synthesized using only 15% polymer concentration. In fact, results showed in chapter 3 demonstrated that higher PEGDA concentration were not suitable for an efficient hybridization, because of the narrow network. On the other hand, microparticles synthesized with 10% polymer resulted to be too soft and not enough resistant to washing procedure. Therefore, several recipes using 15% polymer and different methacrylate DNA-Tail concentrations (400nM- 1μM - 10μM) were prepared to evaluate the effect of oligonucleotide concentration on the network structure.

To sum up, this swelling characterization demonstrate that is possible to obtain different molecular filter capability regulating the polymer concentration.

For the specific purpose of selected miRNA, we decided to synthesized particles with 15% polymer concentration and T-DNA 1μM, which combine both network structure and stability required for the detection. As reported in chapter 3, higher T-DNA concentrations produced a crowding effect that obstacle the effective hybridization.

4.3.5 Diffusion studies: CLSM analysis

Diffusion studies were carried out using 15% PEGDA microparticles with and without 1μM DNA-Tail.

Diffusion percentage was evaluated following the fluorescence intensity changes by CLSM images. In particular, several probes were tested: dextrans 3 kDa, 10 kDa, 40 kDa, Target143, BSA and IgG all, of them with final concentration of 2μM. In correspondence of this concentration value, detected solute intensities inside the hydrogel and in the surrounding solution were proportional to dye concentration. Intensities values were reported in graph as ratio between the fluorescence intensity inside the microparticles (I_{IN}) and fluorescence in the surrounding gel (I_{OUT}).

As reported in Figure 4.15, we noticed that ~85% of both 3 kDa and 10 kDa dextrans were able to spread into microparticles. A smaller percentage, ~40%, of 40 kDa and oligonucleotide are capable to go into the hydrogel.

Finally, only a 10% of proteins (BSA and IgG) were detected into the network. These results were reported for functionalized microparticles; the same results were obtained also for microparticles not functionalized, with not significant differences in fluorescence values.

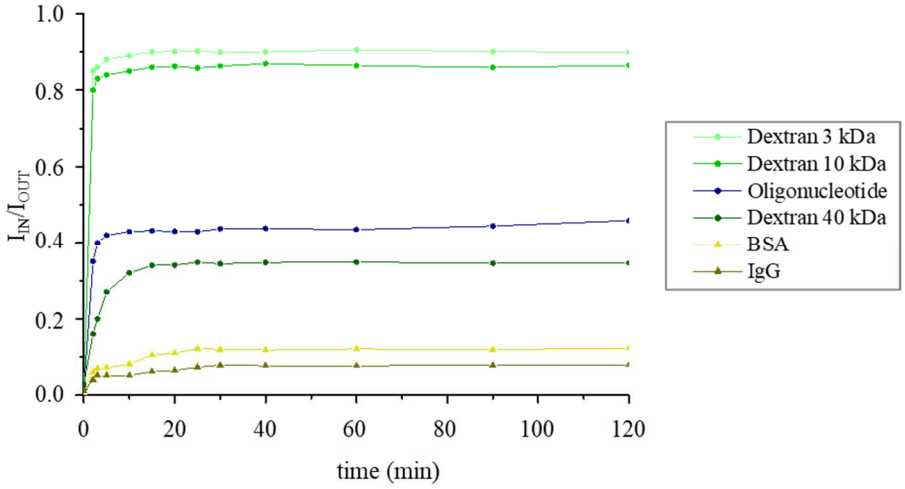

Figure 4.15: Time lapse of fluorescence intensity (I_{IN}/I_{OUT}) of several probes. All values reported show a standard deviation of 10%.

Then fractal dimension (d_f) was evaluated for dextrans probes used for this work. This parameter gave us information about their rigidity, in particular for a rigid sphere, d_f=3.0, for a linear Gaussian polymer coil (random walk) d_f=2.0, and df < 2 for polymers with excluded-volume interactions.[54] Fractal dimension was defined by the scaling law (Equation 4.1)[55]:

$$M \propto r^{d_f} \qquad \text{Equation 4.1}$$

where M represents their molecular weight and r their size, expressed as hydrodynamic radius. Figure 4.16 showed a double logarithmic plot of the probe molecular weight versus their hydrodynamic radius.

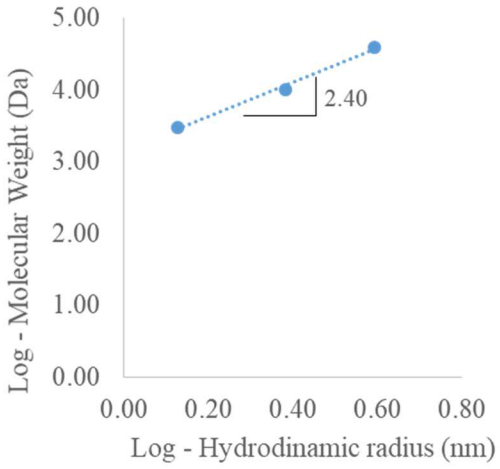

Figure 4.16: Dextrans molecular weight as function of its hydrodynamic radii.

The fractal dimension calculated for our dextrans was d_f ~2.4 and it was in agreement with previously published results.[54, 56] The $d_f > 2$ is thought to arise from partial branching of dextrans. Our results suggested that dextran probes were not rigid particles and therefore they can spread into a narrow network, as occurred in our microparticles.

Moreover, we calculated partition coefficient (k) as the ratio between the concentration of the solute in the external aqueous solution equilibrated with the gel (C_{OUT}) and the concentration of solute in the gel (C_{IN}) per unit volume of gel.[57]

In correspondence of our probes concentrations, detected solute intensities inside the hydrogel and in the surrounding solution were proportional to dye concentration. Consequently, the partition coefficient was given by the ratio of solute intensity in the microparticles to that in the loading solution. In Figure 4.17 are reported partition coefficient of dextrans as function of their hydrodynamic radii.

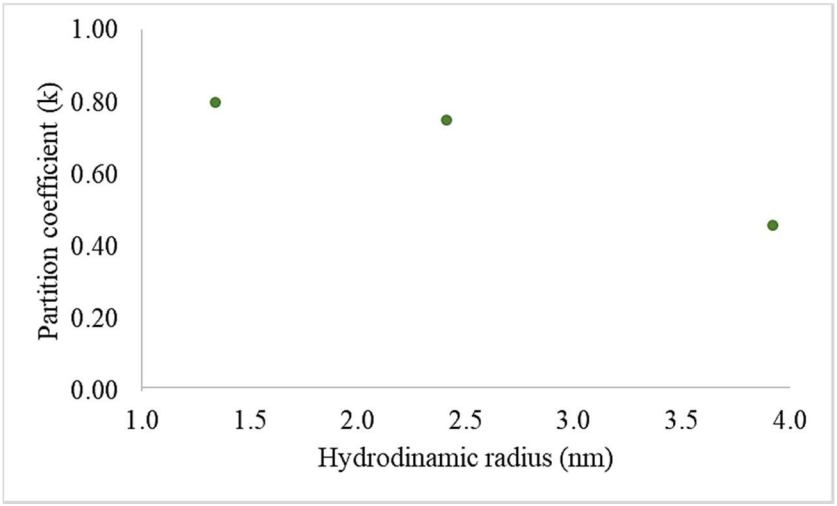

Figure 4.17: Dextrans partition coefficient as function of hydrodynamic radius.

Plotted values showed that larger solutes exhibit progressively smaller partition coefficients, indicative of size exclusion from the water domain of our microparticles.

Finally, we reported I/I_{MAX} versus time in order to compare diffusion behavior of all probes inside the microparticles. Experimental points were fitted with Equation 4.2, and reported in Figure 4.18.

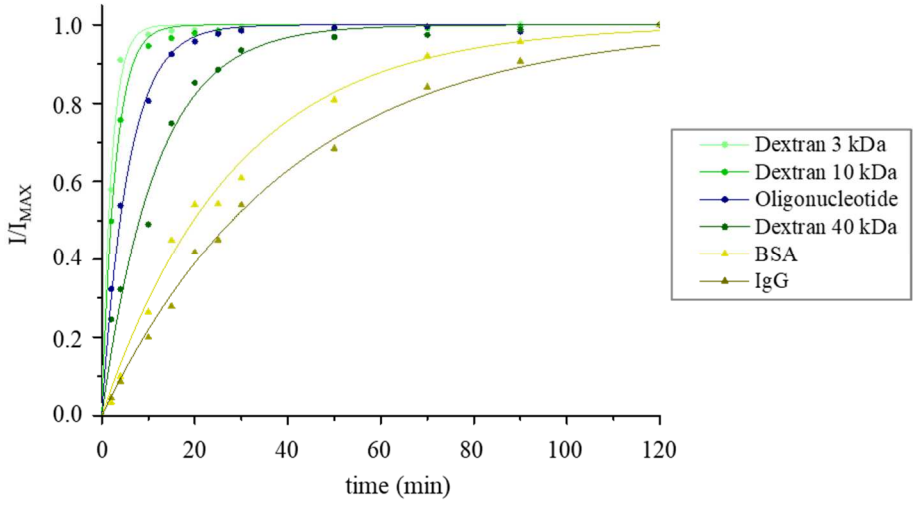

Figure 4.18: Time lapse of fluorescence intensity (I/I_{max}) of several probes. All values reported show a standard deviation of 10%.

$$\frac{I}{I_{MAX}} = 1 - e^{-\frac{t}{\tau}}$$ Equation 4.2

where τ is the extrapolated value that represent time required to achieve 63% of maximum intensity. In such a way, we were able to determine τ for each curve, as reported in Table 4.4.

Table 4.4: Extrapolated values of τ for each probes.

Probes	τ (min)
Dextran 3 kDa	2.1 ± 0.1
Dextran 10 kDa	2.9 ± 0.1
Oligonucleotide	5.7 ± 0.3
Dextran 40 kDa	11.6 ± 0.7
BSA	28.4 ± 1.2
IgG	40.4 ± 2.0

Results showed that smaller probes such as dextrans 3 kDa and 10 kDa required about 2-3 minutes to accomplish 63% of maximum value. Oligonucleotide needed ~6 minutes while dextrans 40 kDa required twice the time of the latter. Finally, both proteins needed longer times, approximately 30-40 minutes.

Because of τ is inversely proportional to the diffusion coefficient, these data confirmed the molecular size exclusion of our polymer network.

To sum up, our results showed that it is possible to use our engineered microparticles as molecular filter that allow the target to go in and exclude the majority of big molecules as proteins.

4.3.6 miRNA 143-3p detection

As reported in paragraph 4.3.1, our double strand probe consisted of a short methacrylate DNA-Tail (T-DNA, 12 nt), covalently bound to the polymer networks, and a longer fluorescent DNA sequence (F-DNA, 21 nt). The latter was partially complementary to DNA-Tail and totally complementary to a specific target. Target identification occurred by double strand displacement assay (Figure 4.19).

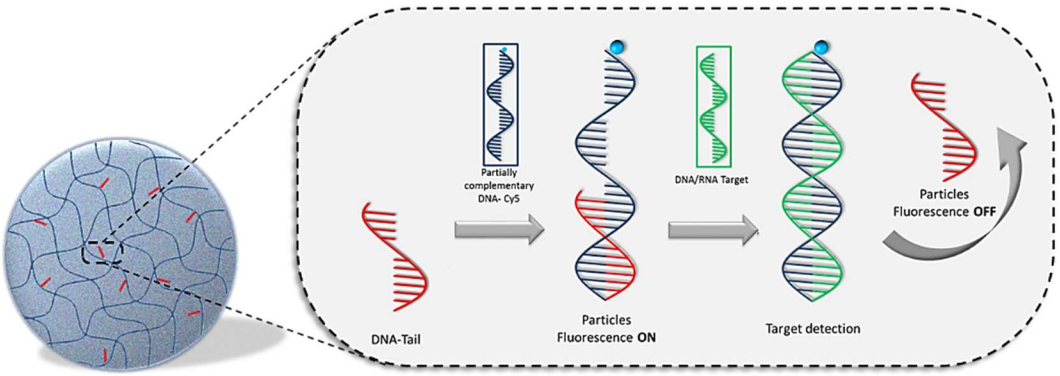

Figure 4.19: Mechanism of Target detection.

In particular, results reported below were referred to large excess of Target concentration (2 μM). 1μl of T-DNA particles solution was loaded into μ-Slide, analyzing by CLSM their fluorescence intensity.

As showed in Figure 4.20a-Figure 4.21a, only a low background fluorescent signal is registered. Then 100 μL of T-DNA particles solution were used for tail hybridization. The longer F-DNA (10x with respect to the tail concentration) was added toT-DNA particles solution. This was stirred until used and washed with buffer solution before next measurement.

Hybridization efficiency was monitored for three days until the equilibrium was reached. Then 1μL of the washed solution was diluted in 30 μL of buffer solution and loaded in μ-Slide for fluorescence intensity analysis.

Images showed a significant increase in microgels fluorescence and, therefore, hybridization between DNA-Tail and F-DNA has occurred (Figure 4.20b and Figure 4.21b).

The required time needed to reach equilibrium is not unusual considering our experimental conditions. In fact, even if Stevens et al.[52] demonstrated that was possible to reduce time required for hybridization increasing both temperature and tail concentration, we suffer of some limitations. Indeed, due to the low melting temperature of our hetero-duplex (Tm= 45°C), we can not raise the temperature to enhance hybridization efficiency. Moreover, regarding the oligonucleotide concentration, as showed in chapter 3, we can not use more than 1 μM of methacrylate tail for PEGDA 15% (w/v) because of the crowding effect observed. Finally, another parameter that can be modified to enhance the hybridization time, is the ionic strength[50]. However, ore buffer was already optimized, with the addiction of 200 mM of NaCl, to reach the best assay conditions.

In order to evaluate the displacement, 2 μL of the Tail/F solution were added to the solution that was constantly stirred until equilibrium was reached. Then washing steps were done to remove F-DNA/target complex.

Analogously to the previous procedure, 1μL of the washed solution was diluted in 30 μL of buffer solution and loaded in μ-Slide. Figure 4.20c-Figure 4.21c showed that, in the presence of target, fluorescence strongly decrease confirming that displacement occurred.

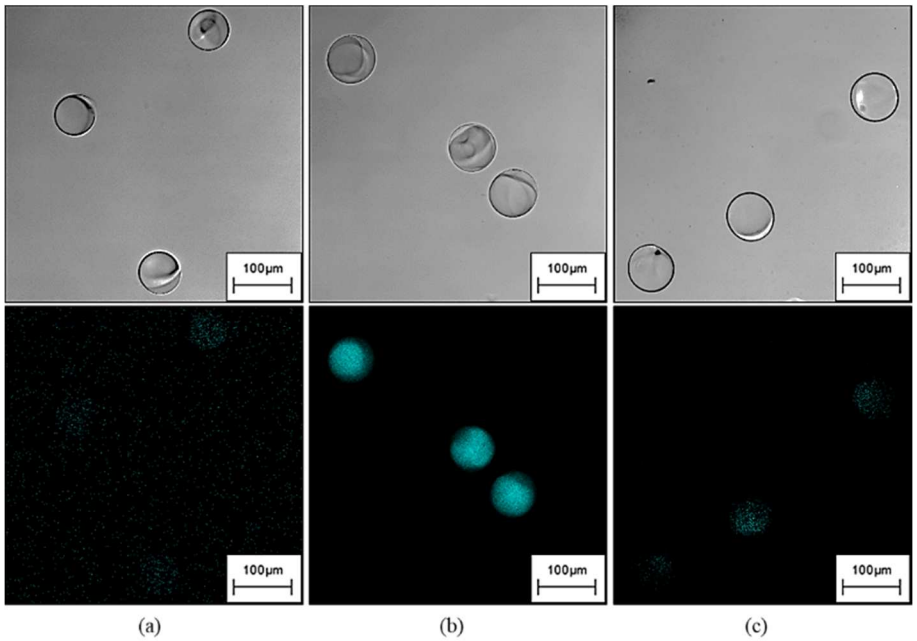

Figure 4.20: CLSM images of the three fundamental steps of target identification: (a) T-DNA, (b) adding F-DNA, (c) displacement in presence of the Target.

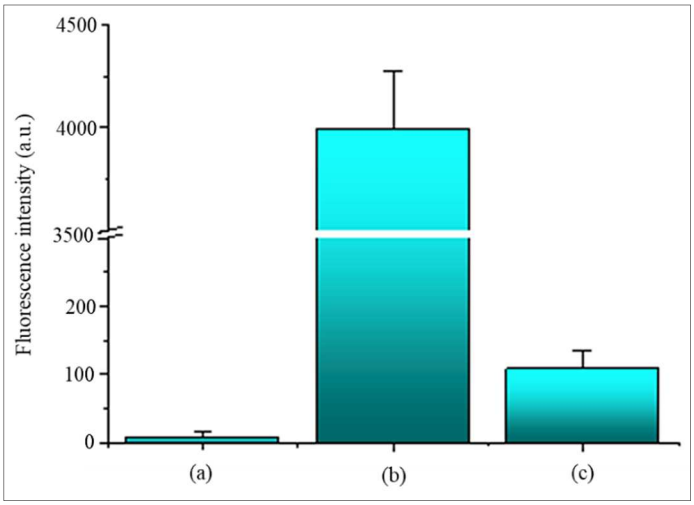

Figure 4.21: Fluorescence intensity of (a) T-DNA, (b) adding F-DNA, (c) displacement in presence of the Target in buffer solution.

Moreover, we tested several target concentrations from 100 µM to 50 pM. Results, reported in Figure 4.22, showed that for the highest concentration tested, ~97% of displacement was obtained. For Target 2 µM, used for our analysis, the displacement

is ~93%. Decreasing target concentrations up to 500 pM, we reach ~73% of displacement. Between 400-325 pM displacement decrease at ~40% and for lower concentrations, no significant displacement were obtained.

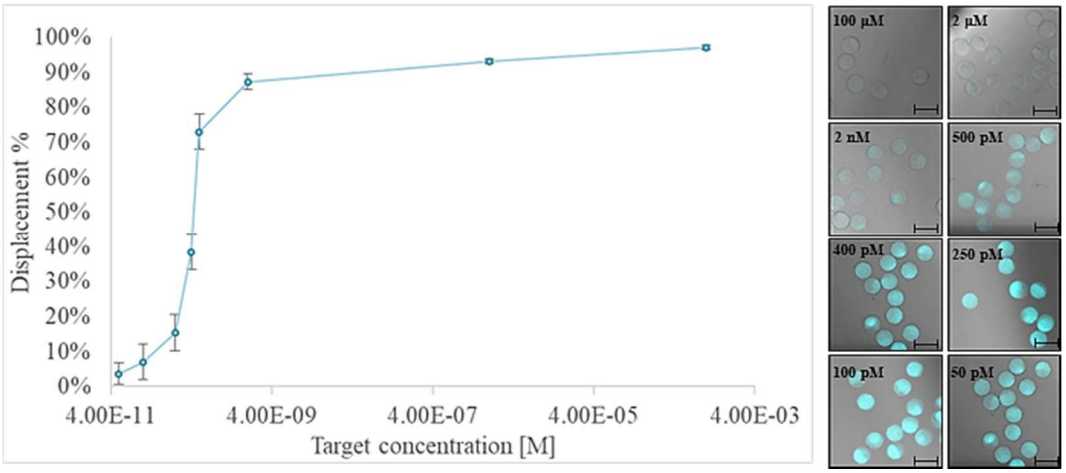

Figure 4.22: Displacement percentage for different Target concentrations. CLSM images of microgels. Scale bars: 100 µm.

To test the assay performance in complex fluids, ds displacement assay was carried out spiking 2 µM of the target in defined volumes of human serum sample. Results confirmed an efficient displacement of ~90% also in this case.

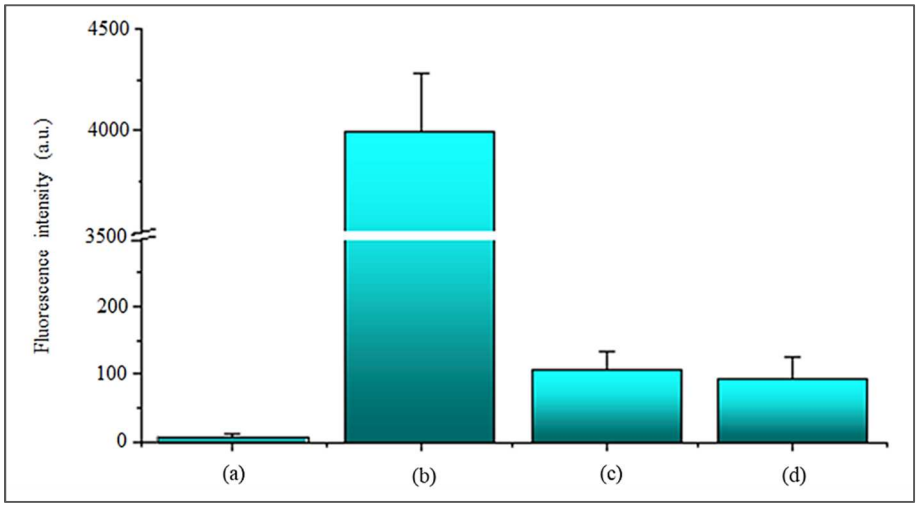

Figure 4.23: Fluorescence intensity of (a) T-DNA, (b) adding F-DNA, (c) displacement in presence of the Target in buffer solution and (d) in human serum.

To sum up these CLSM analysis confirm the efficiency of our detection system in both PBS buffer and Human Serum. Furthermore, preliminarily tests were fulfilled using a bead-based microfluidic assays. This system showed an edge over normal fluidic systems, as it employs microbeads as a solid support. In such way, it was possible to increase the sensitivity of the assay due to higher efficiency of interactions between samples and reagents. Moreover, the analytes attached onto the microparticles can be easily transported in a fluidic system using pressure-driven flow. Microfluidic chip consist of a set of pillars which define a chamber where the beads are confined for both washing and subsequent analysis steps (Figure 4.24 a). A thickest set of pillars were arranged before the outlet in order to trap the microparticles (Figure 4.24 b).

This preliminary test foresee the possibility of using our assay for point-of-care tasting.

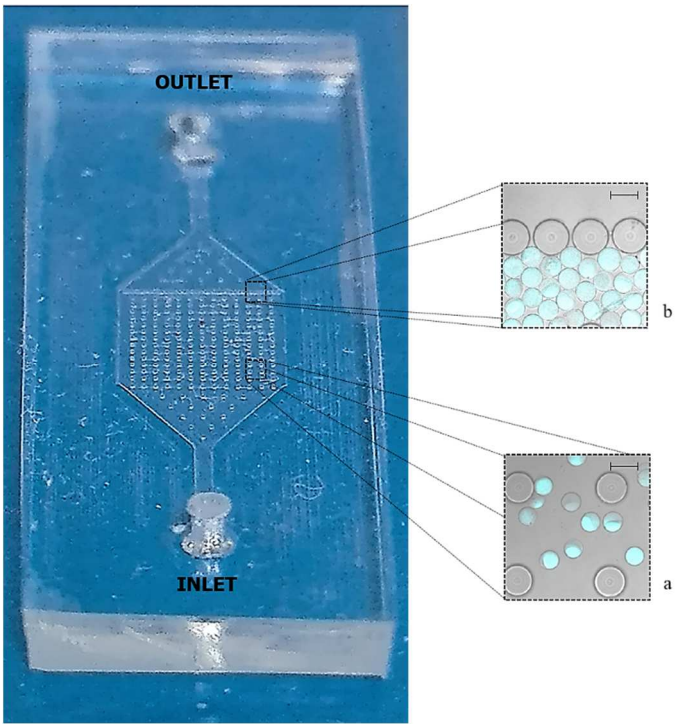

Figure 4.24: Bead-based microfluidic assays with fluorescent microparticles. Scale bars 100 µm.

4.4 Conclusions

In this chapter, we focused on the synthesis, characterization and functionalization of PEGDA-based microparticles. Probe was properly designed for detection of miRNA-143-3p, responsible of several cardiovascular diseases.

Swelling characterization confirmed results already obtained for bulk hydrogels in chapter 3. In order to obtain different molecular filter capability, it was possible to modulate both microfluidic parameters and recipes to generate stable and monodisperse microparticles, with high control of both size, shape, chemistry and swelling parameters. In particular, our results pointed out that microparticles synthesized with PEGDA 15% and T-DNA 1μM best combined both stability and network structure ability for an efficient hybridization. In particular, highest polymer concentration show a too narrow network while 10% PEGDA let us to produce too soft microparticles that are not enough resistant to washing procedure.

Diffusion studies, fulfilled with CLSM, demonstrated the capability of our microparticles to be used as molecular filter letting target go in and excluding the majority of big molecules. Finally, our detection system resulted to be very efficient also in complex fluids as human serum, with a displacement percentage of ~90%. Preliminary experiments, carried out using a bead-based microfluidic assay, showed the opportunity to improve our system achieving a point-of-care device.

To sum up, our results confirmed the possibility to synthesize engineered and functionalized hydrogel-based microparticles, with a tunable network, that allow to combine both molecular filter and detection capability. In this way, we achieve a new system to simplify the detection of miRNA 143-3p in complex fluids.

4.5 References

1. Helgeson, M. E.; Chapin, S. C.; Doyle, P. S., Hydrogel microparticles from lithographic processes: Novel materials for fundamental and applied colloid science. *Current opinion in colloid & interface science* **2011,** *16* (2), 106-117.
2. Langer, R.; Tirrell, D. A., Designing materials for biology and medicine. *Nature* **2004,** *428* (6982), 487-492.
3. Russell, R. J.; Pishko, M. V.; Gefrides, C. C.; McShane, M. J.; Cote, G. L., A fluorescence-based glucose biosensor using concanavalin A and dextran encapsulated in a poly (ethylene glycol) hydrogel. *Analytical Chemistry* **1999,** *71* (15), 3126-3132.
4. <(New Directions in Organic & Biological Chemistry) Julie Fisher-Modern NMR Techniques for Synthetic Chemistry-CRC Press (2014).pdf>.
5. Peppas, N. A.; Hilt, J. Z.; Khademhosseini, A.; Langer, R., Hydrogels in biology and medicine: from molecular principles to bionanotechnology. *Advanced materials* **2006,** *18* (11), 1345-1360.
6. Peppas, N. A.; Keys, K. B.; Torres-Lugo, M.; Lowman, A. M., Poly (ethylene glycol)-containing hydrogels in drug delivery. *Journal of controlled release* **1999,** *62* (1), 81-87.
7. Saxena, A. K., Synthetic biodegradable hydrogel (PleuraSeal) sealant for sealing of lung tissue after thoracoscopic resection. *The Journal of thoracic and cardiovascular surgery* **2010,** *139* (2), 496-497.
8. Hamidi, M.; Azadi, A.; Rafiei, P., Hydrogel nanoparticles in drug delivery. *Advanced drug delivery reviews* **2008,** *60* (15), 1638-1649.
9. Lee, K. Y.; Mooney, D. J., Hydrogels for tissue engineering. *Chemical reviews* **2001,** *101* (7), 1869-1880.
10. Zhang, L.; Li, K.; Xiao, W.; Zheng, L.; Xiao, Y.; Fan, H.; Zhang, X., Preparation of collagen–chondroitin sulfate–hyaluronic acid hybrid hydrogel scaffolds and cell compatibility in vitro. *Carbohydrate polymers* **2011,** *84* (1), 118-125.
11. Slaughter, B. V.; Khurshid, S. S.; Fisher, O. Z.; Khademhosseini, A.; Peppas, N. A., Hydrogels in regenerative medicine. *Advanced materials* **2009,** *21* (32-33), 3307-3329.
12. Nguyen, K. T.; West, J. L., Photopolymerizable hydrogels for tissue engineering applications. *Biomaterials* **2002,** *23* (22), 4307-4314.
13. Serra, C. A.; Chang, Z., Microfluidic-assisted synthesis of polymer particles. *Chemical engineering & technology* **2008,** *31* (8), 1099-1115.
14. Dendukuri, D.; Doyle, P. S., The synthesis and assembly of polymeric microparticles using microfluidics. *Advanced Materials* **2009,** *21* (41), 4071-4086.

15. Ahmed, E. M., Hydrogel: Preparation, characterization, and applications: A review. *Journal of advanced research* **2015,** *6* (2), 105-121.
16. Battista, E.; Causa, F.; Netti, P. A., Bioengineering Microgels and Hydrogel Microparticles for Sensing Biomolecular Targets. *Gels* **2017,** *3* (2), 20.
17. Wang, J. T.; Wang, J.; Han, J. J., Fabrication of Advanced Particles and Particle-Based Materials Assisted by Droplet-Based Microfluidics. *small* **2011,** *7* (13), 1728-1754.
18. Baroud, C. N.; Gallaire, F.; Dangla, R., Dynamics of microfluidic droplets. *Lab on a Chip* **2010,** *10* (16), 2032-2045.
19. Zhu, P.; Wang, L., Passive and active droplet generation with microfluidics: a review. *Lab on a Chip* **2017,** *17* (1), 34-75.
20. Heida, T.; Neubauer, J. W.; Seuss, M.; Hauck, N.; Thiele, J.; Fery, A., Mechanically defined microgels by droplet microfluidics. *Macromolecular Chemistry and Physics* **2017,** *218* (2).
21. Choi, C.-H.; Jung, J.-H.; Hwang, T.-S.; Lee, C.-S., In situ microfluidic synthesis of monodisperse PEG microspheres. *Macromolecular research* **2009,** *17* (3), 163-167.
22. Celetti, G.; Di Natale, C.; Causa, F.; Battista, E.; Netti, P. A., Functionalized poly (ethylene glycol) diacrylate microgels by microfluidics: In situ peptide encapsulation for in serum selective protein detection. *Colloids and Surfaces B: Biointerfaces* **2016,** *145*, 21-29.
23. Nunes, J.; Tsai, S.; Wan, J.; Stone, H., Dripping and jetting in microfluidic multiphase flows applied to particle and fibre synthesis. *Journal of physics D: Applied physics* **2013,** *46* (11), 114002.
24. Abate, A.; Poitzsch, A.; Hwang, Y.; Lee, J.; Czerwinska, J.; Weitz, D., Impact of inlet channel geometry on microfluidic drop formation. *Physical Review E* **2009,** *80* (2), 026310.
25. Christopher, G. F.; Noharuddin, N. N.; Taylor, J. A.; Anna, S. L., Experimental observations of the squeezing-to-dripping transition in T-shaped microfluidic junctions. *Physical Review E* **2008,** *78* (3), 036317.
26. Herrada, M. A.; Ganan-Calvo, A. M.; Guillot, P., Spatiotemporal instability of a confined capillary jet. *Physical Review E* **2008,** *78* (4), 046312.
27. Husny, J.; Cooper-White, J. J., The effect of elasticity on drop creation in T-shaped microchannels. *Journal of non-newtonian fluid mechanics* **2006,** *137* (1), 121-136.
28. Li, X.-B.; Li, F.-C.; Yang, J.-C.; Kinoshita, H.; Oishi, M.; Oshima, M., Study on the mechanism of droplet formation in T-junction microchannel. *Chemical engineering science* **2012,** *69* (1), 340-351.

29. Wang, K.; Lu, Y.; Xu, J.; Luo, G., Determination of dynamic interfacial tension and its effect on droplet formation in the T-shaped microdispersion process. *Langmuir* **2009,** *25* (4), 2153-2158.

30. Wu, L.; Qu, X., Cancer biomarker detection: recent achievements and challenges. *Chemical Society Reviews* **2015,** *44* (10), 2963-2997.

31. Kosaka, N.; Iguchi, H.; Ochiya, T., Circulating microRNA in body fluid: a new potential biomarker for cancer diagnosis and prognosis. *Cancer science* **2010,** *101* (10), 2087-2092.

32. Condorelli, G.; Latronico, M. V.; Cavarretta, E., microRNAs in cardiovascular diseases: current knowledge and the road ahead. *Journal of the American College of Cardiology* **2014,** *63* (21), 2177-2187.

33. Hébert, S. S.; Horré, K.; Nicolaï, L.; Bergmans, B.; Papadopoulou, A. S.; Delacourte, A.; De Strooper, B., MicroRNA regulation of Alzheimer's Amyloid precursor protein expression. *Neurobiology of disease* **2009,** *33* (3), 422-428.

34. Hitachi, K.; Nakatani, M.; Tsuchida, K., Myostatin signaling regulates Akt activity via the regulation of miR-486 expression. *The international journal of biochemistry & cell biology* **2014,** *47*, 93-103.

35. Kjaer-Frifeldt, S.; Hansen, T.; Nielsen, B.; Joergensen, S.; Lindebjerg, J.; Soerensen, F.; dePont Christensen, R.; Jakobsen, A., The prognostic importance of miR-21 in stage II colon cancer: a population-based study. *British journal of cancer* **2012,** *107* (7), 1169.

36. Zhao, W.; Zhao, S.-P.; Zhao, Y.-H., MicroRNA-143/-145 in cardiovascular diseases. *BioMed research international* **2015,** *2015*.

37. Parmacek, M. S., MicroRNA-modulated targeting of vascular smooth muscle cells. *The Journal of clinical investigation* **2009,** *119* (9), 2526.

38. Marin, T.; Gongol, B.; Chen, Z.; Woo, B.; Subramaniam, S.; Chien, S.; Shyy, J. Y.-J., Mechanosensitive microRNAs—role in endothelial responses to shear stress and redox state. *Free Radical Biology and Medicine* **2013,** *64*, 61-68.

39. Listowski, M. A.; Heger, E.; Bogusławska, D. M.; Machnicka, B.; Kuliczkowski, K.; Leluk, J.; Sikorski, A. F., microRNAs: fine tuning of erythropoiesis. *Cellular & molecular biology letters* **2012,** *18* (1), 34.

40. Kumar, S.; Kim, C. W.; Simmons, R. D.; Jo, H., Role of flow-sensitive microRNAs in endothelial dysfunction and atherosclerosis. *Arteriosclerosis, thrombosis, and vascular biology* **2014,** *34* (10), 2206-2216.

41. Jakob, P.; Landmesser, U., Role of microRNAs in stem/progenitor cells and cardiovascular repair. *Cardiovascular research* **2011,** *93* (4), 614-622.

42. Rangrez, A. Y.; Massy, Z. A.; Metzinger-Le Meuth, V.; Metzinger, L., MiR-143 and MiR-145. *Circulation: Cardiovascular Genetics* **2011,** *4* (2), 197-205.

43. Small, E. M.; Frost, R. J.; Olson, E. N., MicroRNAs add a new dimension to cardiovascular disease. *Circulation* **2010,** *121* (8), 1022-1032.

44. Small, E. M.; Olson, E. N., Pervasive roles of microRNAs in cardiovascular biology. *Nature* **2011,** *469* (7330), 336.

45. Meder, B.; Keller, A.; Vogel, B.; Haas, J.; Sedaghat-Hamedani, F.; Kayvanpour, E.; Just, S.; Borries, A.; Rudloff, J.; Leidinger, P., MicroRNA signatures in total peripheral blood as novel biomarkers for acute myocardial infarction. *Basic research in cardiology* **2011,** *106* (1), 13-23.

46. Garcia-Schwarz, G.; Santiago, J. G., Integration of on-chip isotachophoresis and functionalized hydrogels for enhanced-sensitivity nucleic acid detection. *Analytical chemistry* **2012,** *84* (15), 6366-6369.

47. Wark, A. W.; Lee, H. J.; Corn, R. M., Multiplexed detection methods for profiling microRNA expression in biological samples. *Angewandte Chemie International Edition* **2008,** *47* (4), 644-652.

48. Chen, C.; Tan, R.; Wong, L.; Fekete, R.; Halsey, J., Quantitation of microRNAs by real-time RT-qPCR. *PCR Protocols* **2011**, 113-134.

49. Tothill, I. E. In *Biosensors for cancer markers diagnosis*, Seminars in cell & developmental biology, Elsevier: 2009; pp 55-62.

50. Gidwani, V.; Riahi, R.; Zhang, D. D.; Wong, P. K., Hybridization kinetics of double-stranded DNA probes for rapid molecular analysis. *Analyst* **2009,** *134* (8), 1675-1681.

51. Ravan, H.; Kashanian, S.; Sanadgol, N.; Badoei-Dalfard, A.; Karami, Z., Strategies for optimizing DNA hybridization on surfaces. *Analytical biochemistry* **2014,** *444*, 41-46.

52. Stevens, P. W.; Henry, M. R.; Kelso, D. M., DNA hybridization on microparticles: determining capture-probe density and equilibrium dissociation constants. *Nucleic acids research* **1999,** *27* (7), 1719-1727.

53. Baret, J.-C., Surfactants in droplet-based microfluidics. *Lab on a Chip* **2012,** *12* (3), 422-433.

54. Cheng, Y.; Prud'Homme, R. K.; Thomas, J. L., Diffusion of mesoscopic probes in aqueous polymer solutions measured by fluorescence recovery after photobleaching. *Macromolecules* **2002,** *35* (21), 8111-8121.

55. Chaikin, P. M.; Lubensky, T. C., *Principles of condensed matter physics*. Cambridge university press: 2000.

56. Bu, Z.; Russo, P., Diffusion of dextran in aqueous (hydroxypropyl) cellulose. *Macromolecules* **1994,** *27* (5), 1187-1194.

57. Kotsmar, C.; Sells, T.; Taylor, N.; Liu, D. E.; Prausnitz, J.; Radke, C., Aqueous solute partitioning and mesh size in HEMA/MAA hydrogels. *Macromolecules* **2012,** *45* (22), 9177-9187.

Chapter 5

Conclusions and future perspectives

The work described in this thesis intends to show the combined effect of materials knowledge and biosensing to produce engineered device for detection. In particular, we achieved a versatile and innovative assay, which successfully combine biomarker miRNA detection with molecular filter capability of engineered and functionalized hydrogels with several architectures.

PEG-based hydrogels resulted to be ideal materials for this purpose combining broad range of molecular weight and chemical functionalities with biocompatibility and antifouling properties.

Nowadays the detection of biomarkers such as nucleic acids, in particular of miRNAs, have attracted high attention due to their immense regulatory power so that the variation of their levels can be used as potential biomarkers for the diagnosis and prognosis of a variety of diseases.

Firstly, we synthesized and characterized microgels with complex architecture core-shell. The flexibility in synthesis steps of these fluorescent encoded microgels, make them suitable for multiplex analysis. Moreover, our results showed the possibility to attain a high control of size and structural parameters, characterizing each shell combining both AFM images and equilibrium-swelling theory.

Then, the possibility to functionalize hydrogels directly during synthesis step let us to find new strategies to eliminate time-consuming labelling steps and their associated costs.

In particular, we synthesized bulk hydrogels properly functionalized with methacrylate oligonucleotide. We demonstrated the possibility to achieve a specific control of both network structure and efficiency of the capture element, using both NMR technique and fluorimetric analysis. Moreover, scaling-down this knowledge into micrometric scale, we produced in a single step, by microfluidic, monodisperse, spherical and engineered microparticles able for specific detection.

This approach represents the most promising methods for the production and the functionalization of monodisperse particles at low cost and reagent consumption, with higher reproducibility and saving time.

In particular, we added directly in flow a probe, properly designed for the detection of miRNA143-3p (responsible of cardiovascular diseases) and, in such a way, we were able to detect the specific target also in complex fluids.

In conclusion, we demonstrated the possibility to obtain hydrogels with different architecture and shape, with high control of both network structure and position of capture element.

This approach promises to be useful to achieve a novel, efficient and sensitive hydrogel-based no-wash assay, combining molecular filter capability and biomarkers detection to simplify the miRNA detection in complex fluids.

The final goal of this project is the production of a microfluidic lab-on-a-chip (LoC) platform for in vitro, direct measurement of miRNAs present in biological fluids. In particular, foresee the possibility to accomplish a miniaturized system that combine both filter system and optical device for fluorescence signal transduction.

The integrated optical device, appropriately optimized, allow merging the purification, extraction, detection and analysis procedures all inside the device. In such a way, we can directly analyze a single blood drop overcoming time-consuming manipulations. As in fact, our major challenge is pointed towards the production of a device for point-of-care (POC) diagnostics.

Traditional system do not address the needs of the majority of the world's people afflicted with infectious diseases, who have, at best, access to poorly resourced health care facilities with almost no supporting clinical laboratory infrastructure.

The versatility of our system exhibited the possibility to use our engineered microparticles for the detection of several diseases.

Preliminaries studies showed the potentiality of the system also for the detection of tuberculosis infection. In such a way, our system may provide some improving in the actual research on several diseases, improving the quality of life.